Aging viscoelastic properties of cement paste

by

Poornima Patil

B.E., Visvesvaraya Technological University, 2013
MTech., Visvesvaraya Technological University, 2015

AN ABSTRACT OF A DISSERTATION

submitted in partial fulfillment of the requirements for the degree

DOCTOR OF PHILOSOPHY

Department of Civil Engineering
Carl R. Ice College of Engineering

KANSAS STATE UNIVERSITY
Manhattan, Kansas

2023

Abstract

This work is focused on assessing the aging viscoelasticity of cement paste using nanoindentation. First, sources of uncertainty in nanoindentation experiments for cementitious materials are identified. Results from this study indicate that a "critical indentation depth" exists such that individual indentations shallower than the critical depth demonstrate greater variability for all measured properties than deeper indentations. Surface roughness and the polishing method profoundly influence measured properties. Second, feedback controlled statistical based nanoindentation creep and stress relaxation tests are performed on cementitious material and polycarbonate to characterize the viscoelastic properties. A closed form linear viscoelastic analytical solutions are derived based on the elastic-viscoelastic correspondence principle to study the creep and stress relaxation response. The viscoelastic properties obtained from testing hardened cement paste and standard polycarbonate indicate strong agreement between the measured and the fit data. Additionally, nanoindentation based stress relaxation test appears to provide more converged data compared to creep tests, hence the study proposes nanoindentation as an additional and efficient tool to characterize the stress relaxation of cementitious materials. Third, investigation of the effect of combined neutron–gamma irradiation on cement paste is conducted to understand the viscoelastic behaviour of irradiated concrete in nuclear safety structures. The reduced modulus, relaxation modulus, and creep compliance of irradiated and the control samples obtained from reference creep nanoindentation test at various locations are presented and explained in detail in this study. The results demonstrate a considerable drop in reduced modulus and relaxation modulus of irradiated samples and a significant increase in the creep compared to the control samples. Lastly in the present study, the aging viscoelastic response of cement paste is measured and modeled using time shift approach and solidification method. The hydration of the cement paste is arrested at different ages (6hr., 12hr., 1day, 2day, 3day, 7day and 28 day) using solvent exchange and freeze dry method. The results emphasize that the time shift approach appears to be promising model to predict the aging viscoelasticity of cement paste at later (after 3 days) ages and solidification theory can effectively predict the aging viscoelastic behavior at early (less than 3 days) ages.

Aging viscoelastic properties of cement paste

by

Poornima Patil

B.E., Visvesvaraya Technological University, 2013
MTech., Visvesvaraya Technological University, 2015

A DISSERTATION

submitted in partial fulfillment of the requirements for the degree

DOCTOR OF PHILOSOPHY

Department of Civil Engineering
Carl R. Ice College of Engineering

KANSAS STATE UNIVERSITY
Manhattan, Kansas

2023

Approved by:

Major Professor
Christopher A. Jones

Copyright

© Poornima Patil 2023.

Abstract

This work is focused on assessing the aging viscoelasticity of cement paste using nanoindentation. First, sources of uncertainty in nanoindentation experiments for cementitious materials are identified. Results from this study indicate that a "critical indentation depth" exists such that individual indentations shallower than the critical depth demonstrate greater variability for all measured properties than deeper indentations. Surface roughness and the polishing method profoundly influence measured properties. Second, feedback controlled statistical based nanoindentation creep and stress relaxation tests are performed on cementitious material and polycarbonate to characterize the viscoelastic properties. A closed form linear viscoelastic analytical solutions are derived based on the elastic-viscoelastic correspondence principle to study the creep and stress relaxation response. The viscoelastic properties obtained from testing hardened cement paste and standard polycarbonate indicate strong agreement between the measured and the fit data. Additionally, nanoindentation based stress relaxation test appears to provide more converged data compared to creep tests, hence the study proposes nanoindentation as an additional and efficient tool to characterize the stress relaxation of cementitious materials. Third, investigation of the effect of combined neutron–gamma irradiation on cement paste is conducted to understand the viscoelastic behaviour of irradiated concrete in nuclear safety structures. The reduced modulus, relaxation modulus, and creep compliance of irradiated and the control samples obtained from reference creep nanoindentation test at various locations are presented and explained in detail in this study. The results demonstrate a considerable drop in reduced modulus and relaxation modulus of irradiated samples and a significant increase in the creep compared to the control samples. Lastly in the present study, the aging viscoelastic response of cement paste is measured and modeled using time shift approach and solidification method. The hydration of the cement paste is arrested at different ages (6hr., 12hr., 1day, 2day, 3day, 7day and 28 day) using solvent exchange and freeze dry method. The results emphasize that the time shift approach appears to be promising model to predict the aging viscoelasticity of cement paste at later (after 3 days) ages and solidification theory can effectively predict the aging viscoelastic behavior at early (less than 3 days) ages.

Table of Contents

List of Figures viii
List of Tables xiii
Acknowledgements xiv
Dedication xv
Chapter 1 - Introduction to Nanoindentation 1
1.1 Research Significance 2
1.1.1 Objectives 3
1.2 Structure of the Thesis 4
Chapter 2 - Reducing Uncertainties in Nanoindentation Experiments for Cementitious Materials. 6
2.1 Introduction 6
2.2 Methodology 9
2.2.1 Materials and Sample Preparation 9
2.2.2 Polishing 9
2.2.3 Nanoindentation and Atomic Force Microscopy Imaging 10
2.2.4 Basic Elastic Nanoindentation 13
2.3 Results and Discussions 14
2.3.1 Indentation Depth and Load 14
2.3.2 Grid Size and Spacing 18
2.3.3 Surface Roughness 21
2.3.3.1 Atomic Force Microscope vs Nanoindentation 21
2.3.3.2 Polishing Methods 22
2.4 Conclusions and Recommendations 25
Chapter 3 - Stress Relaxation and Creep Nanoindentation for Cement Paste 27
3.1 Introduction 27
3.2 Theory 28
3.2.1 Background Theory 29
3.2.1.1 Closed Form Analytical Solution 29
3.3 Experimental 33

3.3.1 Sample Preparation 34
3.3.2 Nanoindentation Based Creep and Relaxation Test 34
3.4 Results and Discussion 35
3.5 Conclusions 42
Chapter 4 - Investigation of Viscoelastic Properties of Irradiated Cement Paste Using Statistical Nanoindentation 43
4.1 Introduction 43
4.2 Materials and Sample Preparation 44
4.3 Neutron and Gamma Irradiation 45
4.4 Nanoindentation Testing 47
4.5 Results and Discussions 47
4.6 Conclusions 60
Chapter 5 - A Study of Aging Viscoelasticity of Cement Paste Using Nanoindentation 62
5.1 Introduction 62
5.2 Constitutive Theories for Aging Viscoelastic Materials 63
5.2.1 Solidification Theory 63
5.2.2 Time–Shift Approach 65
5.3 Methodology 66
5.3.1 Solvent Exchange Method 67
5.3.2 Freeze Drying Method 67
5.3.3 Nanoindentation Based Creep Tests 68
5.3.4 Constitutive Modeling of Aging Creep Using Solidification Theory 69
5.3.5 Constitutive Modeling of Aging Creep Using Time-Shift Approach 69
5.4 Results and Discussions 72
5.4.1 Solidification Theory 72
5.4.2 Time Shift Approach 82
5.5 Conclusions 94
Chapter 6 - Conclusions 96
References 100
Appendix A - Load Functions and Fit Parameters 108
Appendix B - Raw Data for Nanoindentation Based Creep and Stress Relaxation Test 111

List of Figures

Figure 1.1 Representative individual *P-h* indentation curve [17]..... 2
Figure 2.1 NI images from three polishing methods with RMS (nm) (A) PM1 – 117,..... 11
Figure 2.2 AFM images from three polishing methods with RMS (nm) (A) PM1 – 213, ... 12
Figure 2.3 AFM image of 0.35 w/c showing the subdomains of 2 x 2 μm2 scan area extracted from a 10 x 10 μm^2 13
Figure 2.4 Plot of reduced modulus, load and indentation depth of samples with 0.35 w/c, red circles represent E_r and blue squares represent Load (*P*). 15
Figure 2.5 Plot of reduced modulus, load and indentation depth of samples with 0.40 w/c, red circles represent E_r and blue squares represent Load (*P)* 16
Figure 2.6 Plot of reduced modulus, load and indentation depth of samples with 0.45 w/c, red circles represent E_r and blue squares represent Load (*P*). 16
Figure 2.7 Plot of reduced modulus, load and indentation depth of samples with 0.50 w/c, red circles represent E_r and blue squares represent Load (*P*). 17
Figure 2.8 Plot of mean reduced modulus v/s grid size of 0.35 w/c at critical load. 19
Figure 2.9 Plot of mean reduced modulus v/s grid spacing of 0.35 w/c at critical load. 20
Figure 2.10 The dependence of the RMS roughness obtained from PM1 on the porosity of the sample. 21
Figure 2.11 Plot of RMS roughness of 0.35 w/c sample obtained from three polishing methods using NI. 23
Figure 2.12 Plot of RMS roughness of 0.35 w/c sample obtained from three polishing methods using AFM. 24
Figure 2.13 Plots of reduced Modulus and contact depth of 0.35 w/c sample by three polishing methods. 25
Figure 3.1 Schematic of Berkovich nanoindentation at load P. 30
Figure 3.2 Flowchart for Mathematica code to fit the creep data. 31
Figure 3.3 Flowchart for Mathematica code to fit the relaxation data..... 33
Figure 3.4 Flowchart for Mathematica code to obtain $J_C(t)$ and $J_R(t)$ vs time plot. 33

Figure 3.5 Plot of nanoindentation depth vs time for a typical 30 s experiment of cement paste, with the fit function included for comparison. 36
Figure 3.6 Plot of nanoindentation depth vs time for a typical 30 s experiment of polycarbonate, with the fit function included for comparison. 36
Figure 3.7 Plot of nanoindentation load vs time for a typical 30 s experiment of cement paste, with the fit function included for comparison. 37
Figure 3.8 Plot of nanoindentation load vs time for a typical 30 s experiment of polycarbonate, with the fit function included for comparison. 37
Figure 3.9 Experimentally obtained $J(t)$-$J(0)$ versus approximation as the inverse of an experimentally obtained relaxation function for cement paste. 38
Figure 3.10 Experimentally obtained $J(t)$-$J(0)$ versus approximation as the inverse of an experimentally obtained relaxation function for polycarbonate. 39
Figure 3.11 Rate of stress decay in creep and relaxation test of cement paste. 40
Figure 3.12 Rate of stress decay in creep and relaxation test of polycarbonate. 41
Figure 4.1 Arrangement of cement samples and iron wires within sample holder. Assembly placed in central thimble of reactor for irradiation. 46
Figure 4.2 The box and whisker plot for mean E_r of 0.35 w/c irradiated and control cement paste sample obtained from creep nanoindentation test. 48
Figure 4.3 The box and whisker plot for mean E_r of 0.40 w/c irradiated and control cement paste sample obtained from creep nanoindentation test. 49
Figure 4.4 The box and whisker plot for mean E_r of 0.50 w/c irradiated and control cement paste sample obtained from creep nanoindentation test. 49
Figure 4.5 The box and whisker plot for mean E_r of 0.35 w/c irradiated and control cement paste sample obtained from relaxation nanoindentation test. 50
Figure 4.6 The box and whisker plot for mean E_r of 0.40 w/c irradiated and control cement paste sample obtained from relaxation nanoindentation test. 50
Figure 4.7 The box and whisker plot for mean E_r of 0.50 w/c irradiated and control cement paste sample obtained from relaxation nanoindentation test. 51
Figure 4.8 Box and whisker plot of creep compliance 0.35 w/c for irradiated and control cement paste samples at 30 seconds. 52

Figure 4.9 Box and whisker plot of creep compliance for 0.40 w/c irradiated and control cement paste samples at 30 seconds. 53
Figure 4.10 Box and whisker plot of creep compliance for 0.50 w/c irradiated and control cement paste samples at 30 seconds. 53
Figure 4.11 Box and whisker plot of relaxation modulus for 0.35 w/c irradiated and control cement paste samples at 30 seconds. 54
Figure 4.12 Box and whisker plot of relaxation modulus for 0.40 w/c irradiated and control cement paste samples at 30 seconds. 54
Figure 4.13 Box and whisker plot of relaxation modulus for 0.50 w/c irradiated and control cement paste samples at 30 seconds. 55
Figure 4.14 Normalized creep compliance of 0.35 w/c irradiated and control cement paste. 56
Figure 4.15 Normalized creep compliance of 0.40 w/c irradiated and control cement paste. 56
Figure 4.16 Normalized creep compliance of 0.50 w/c irradiated and control cement paste. 57
Figure 4.17 Normalized relaxation modulus of 0.35 w/c irradiated and control cement paste. ... 58
Figure 4.18 Normalized relaxation modulus of 0.40 w/c irradiated and control cement paste. ... 58
Figure 4.19 Normalized relaxation modulus of 0.50 w/c irradiated and control cement paste. ... 59
Figure 5.1 Conceptual diagram of solidifying material subjected to applied stress, σ. Carol and Bazant (1993). 64
Figure 5.2 Images of 0.35 w/c whose hydration was arrested using solvent exchange method at (A) 0.25D (B) 28D (C) Polished 0.35 w/c sample disc of approximately 16 mm dia. 67
Figure 5.3 Step load function with a constant maximum load P_{max} = 1695 μN. 68
Figure 5.4 Flowchart of the process for obtaining age shift factor and pseudo time. 71
Figure 5.5 Flowchart of the process for applying the time-shift approach to model aging creep. 71
Figure 5.6 Normalized aging elastic compliance fit to the aging function of cement paste: hydration arrested using solvent exchange. 73
Figure 5.7 Normalized aging elastic compliance fit to the aging function of cement paste: hydration arrested using freeze-drying. 73
Figure 5.8 Measured and predicted normalized creep compliance of 0.25D cement paste using solidification theory: hydration arrested by solvent exchange method. 74
Figure 5.9 Measured and predicted normalized creep compliance of 0.5D cement paste using solidification theory: hydration arrested by solvent exchange method. 75

Figure 5.10 Measured and predicted normalized creep compliance of 1D cement paste using solidification theory: hydration arrested by solvent exchange method..... 75
Figure 5.11 Measured and predicted normalized creep compliance of 2D cement paste using solidification theory: hydration arrested by solvent exchange method..... 76
Figure 5.12 Measured and predicted normalized creep compliance of 3D cement paste using solidification theory: hydration arrested by solvent exchange method..... 76
Figure 5.13 Measured and predicted normalized creep compliance of 7D cement paste using solidification theory: hydration arrested by solvent exchange method..... 77
Figure 5.14 Measured and predicted normalized creep compliance of 28D cement paste using solidification theory: hydration arrested by solvent exchange method..... 77
Figure 5.15 Measured and predicted normalized creep compliance of 0.25D cement paste using solidification theory: hydration arrested by freeze drying method. 79
Figure 5.16 Measured and predicted normalized creep compliance of 0.5D cement paste using solidification theory: hydration arrested by freeze drying method. 79
Figure 5.17 Measured and predicted normalized creep compliance of 1D cement paste using solidification theory: hydration arrested by freeze drying method. 80
Figure 5.18 Measured and predicted normalized creep compliance of 2D cement paste using solidification theory: hydration arrested by freeze drying method. 80
Figure 5.19 Measured and predicted normalized creep compliance of 3D cement paste using solidification theory: hydration arrested by freeze drying method. 81
Figure 5.20 Measured and predicted normalized creep compliance of 7D cement paste using solidification theory: hydration arrested by freeze drying method. 81
Figure 5.21 Measured and predicted normalized creep compliance of 28D cement paste using solidification theory: hydration arrested by freeze drying method. 82
Figure 5.22 Shifted compliance of all age cement paste samples using age factor μ: hydration arrested using solvent exchange method..... 83
Figure 5.23 Shifted compliance of all age cement paste samples using age factor μ: hydration arrested using freeze-drying method..... 83
Figure 5.24 Measured and predicted normalized creep compliance of 0.25D cement paste using time shift approach: hydration arrested by solvent exchange method. 84

Figure 5.25 Measured and predicted normalized creep compliance of 0.25D cement paste using time shift approach: hydration arrested by solvent exchange method. 85
Figure 5.26 Measured and predicted normalized creep compliance of 1D cement paste using time shift approach: hydration arrested by solvent exchange method. 85
Figure 5.27 Measured and predicted normalized creep compliance of 2D cement paste using time shift approach: hydration arrested by solvent exchange method. 86
Figure 5.28 Measured and predicted normalized creep compliance of 3D cement paste using time shift approach: hydration arrested by solvent exchange method. 86
Figure 5.29 Measured and predicted normalized creep compliance of 7D cement paste using time shift approach: hydration arrested by solvent exchange method. 87
Figure 5.30 Measured and predicted normalized creep compliance of 28D cement paste using time shift approach: hydration arrested by solvent exchange method. 87
Figure 5.31 Measured and predicted normalized creep compliance of 0.25D cement paste using time shift approach: hydration arrested by freeze drying method. 89
Figure 5.32 Measured and predicted normalized creep compliance of 0.5D cement paste using time shift approach: hydration arrested by freeze drying method. 89
Figure 5.33 Measured and predicted normalized creep compliance of 1D cement paste using time shift approach: hydration arrested by freeze drying method..... 90
Figure 5.34 Measured and predicted normalized creep compliance of 2D cement paste using time shift approach: hydration arrested by freeze drying method..... 90
Figure 5.35 Measured and predicted normalized creep compliance of 3D cement paste using time shift approach: hydration arrested by freeze drying method..... 91
Figure 5.36 Measured and predicted normalized creep compliance of 7D cement paste using time shift approach: hydration arrested by freeze drying method..... 91
Figure 5.37 Measured and predicted normalized creep compliance of 28D cement paste using time shift approach: hydration arrested by freeze drying method. 92

List of Tables

Table 2.1 Metanalysis of cementitious composites corresponding to different load cases, grid nanoindentation parameters and roughness. 8
Table 2.2 Summary of polishing methods. 10
Table 2.3 Summary of testing procedure used. 14
Table 2.4 Critical indentation depth, critical load, and minimum feature size. 15
Table 2.5 Mean E_r at varying, corresponding variance from F test and E_r at critical load. 18
Table 2.6 Mean and Variance for RMS roughness of 0.35 w/c with three polishing methods. ... 22
Table 2.7 Summary of descriptive statistics of roughness data from three polishing methods. ... 23
Table 3.1: Description of polishing process adopted. 34
Table 3.2 Summary of nanoindentation based creep and relaxation test. 35
Table 3.3 Average fit parameters and reduced modulus. 41
Table 4.1 Summary of nanoindentation based creep and relaxation test. 47
Table 4.2 Reduced Modulus (E_r) of irradiated and control cement paste sample. 48
Table 4.3 Mean depth/load observed for irradiated and control cement paste samples. 60
Table 5.1 Comparision of solvent exchange and freeze drying method with respect to reduced modulus and maximum displacement. 93

Acknowledgements

I would not have successfully executed this research work without the support and guidance of various people at the Kansas State University.

First and foremost, I am extremely grateful to my supervisor, Dr. Christopher A. Jones for his invaluable advice, continuous support, and patience during my PhD study. Your immense knowledge and plentiful experience have encouraged me in all the time of my academic research and daily life. I acknowledge your role in creating various opportunities for me, believing in my potentials, and giving me adequate preparation in completing my research. I could not have imagined having a better advisor and mentor for my doctoral study. I thank you for providing me an opportunity to fulfill my most cherished dream.

My thesis committee guided me through all these years. I would like to thank Dr. Mustaque Hossain, Dr. Robert J. Peterman, and Dr. Gurpreet Singh for agreeing to serve on the committee and encouragement, but also, for generously taking time out of their schedules to participate in my research and make this work possible.

I would like to thank my friends, colleagues and research team here at civil engineering department for a cherished time spent together in the lab, and in social settings. I am also grateful to all my friends from my pre-K-State days for their support and encouragement.

Nobody has been more important to me in the pursuit of this project than the members of my family. I would like to thank my parents and in-laws, whose love and guidance are with me in whatever I pursue. They are the ultimate role models. I also like to thank my sister Varsha and Madhu, as well as my brother Andanagouda. Thank you for supporting me for everything, and especially I can't thank you enough for encouraging me throughout this experience.

Most importantly, I wish to thank my loving and supportive husband, Pavan, without whom I wouldn't have started, continued, or finished. Your dedication, unqualified love, sustenance, sense of humor, tolerance, hopefulness, and guidance were more valuable than you can ever imagine.

Dedication

This thesis is dedicated to my Father **Dr. Shantagouda Patil** and Mother **Indrani Patil.**

For their endless love, support and encouragement

Chapter 1 - Introduction to Nanoindentation

Nanotechnology is generally defined as the understanding, control, and restructuring of matter on the order of nanometers [1]. As discussed by K.L. Scrivener [2] nanotechnology consists of two main components: (i) the ‘‘top-down” approach, this refers to successive cutting of bulk material to get nano sized structures and (ii) the “bottom-up” approach, where the structure is created from smaller building blocks. Nanotechnology is a highly interdisciplinary field; its widespread use has created new opportunities for research involving cementitious materials.

Portland cement is the second most used material on the earth after water [3]. Hydrated cementitious products age over time and exist in multiple scale lengths (nano to micro to macro), and multiple phases, each phase with different mechanical properties [4]. Calcium silicate hydrate (C-S-H) is a nano-porous, nanostructured material on which most of the mechanical and transport properties of concrete depended. It is well-known that properties and processes occurring at nanoscale define the engineering properties and performance of the bulk material with the cement-based composites. Hence, much research effort has been applied to understanding the properties of C-S-H and other cement phases at the nanometer scale in turn to enhance and tailor the properties at macroscale [5].

Various sophisticated instruments with high spatial resolution have enabled the study of concrete at the nanoscale and assess the physical, chemical and mechanical properties at different length scales [6]. Many enhanced instruments like scanning electron microscopy (SEM), atomic force microscopy (AFM), and transmission electron microscopy (TEM) are in use to investigate the various phases in the cement paste. However, most of these techniques only characterize the properties at the surface level [5]. Nanoindentation has been widely used and is considered a powerful tool for characterizing the mechanical properties in cementitious composites [7]. To date nanoindentation has been increasingly used to assess the mechanical properties of cementitious materials such as elastic parameters, strength, ductility, creep, shrinkage, and fracture behavior [8-14]. Nanoindentation ensures that contact is established between the specimen and the indenter whose properties and geometry are known. The load (P) acting on the indenter is applied as the control variable and the corresponding penetration depth h is recorded [15]. The instantaneous mechanical properties of the material are usually evaluated from the

unloading part of the load–displacement curve obtained from nanoindentation (Figure 1.1). According to the Oliver-Pharr method [16] used for the analysis of nanoindentation testing, assuming the deformation upon unloading is purely elastic, the reduced elastic modulus (E_r), contact stiffness (S) and hardness (H) are expressed as:

$$E_r = \left(\frac{\sqrt{\pi}}{2}\right)\left(\frac{S}{\sqrt{A_c}}\right) \quad \text{Equation 1.1}$$

$$S = \frac{dP}{dh} = \left(\frac{2}{\sqrt{\pi}}\right)\left(\frac{E_r}{\sqrt{A_c}}\right) \quad \text{Equation 1.2}$$

$$H = \left(\frac{P_{max}}{A_c}\right) \quad \text{Equation 1.3}$$

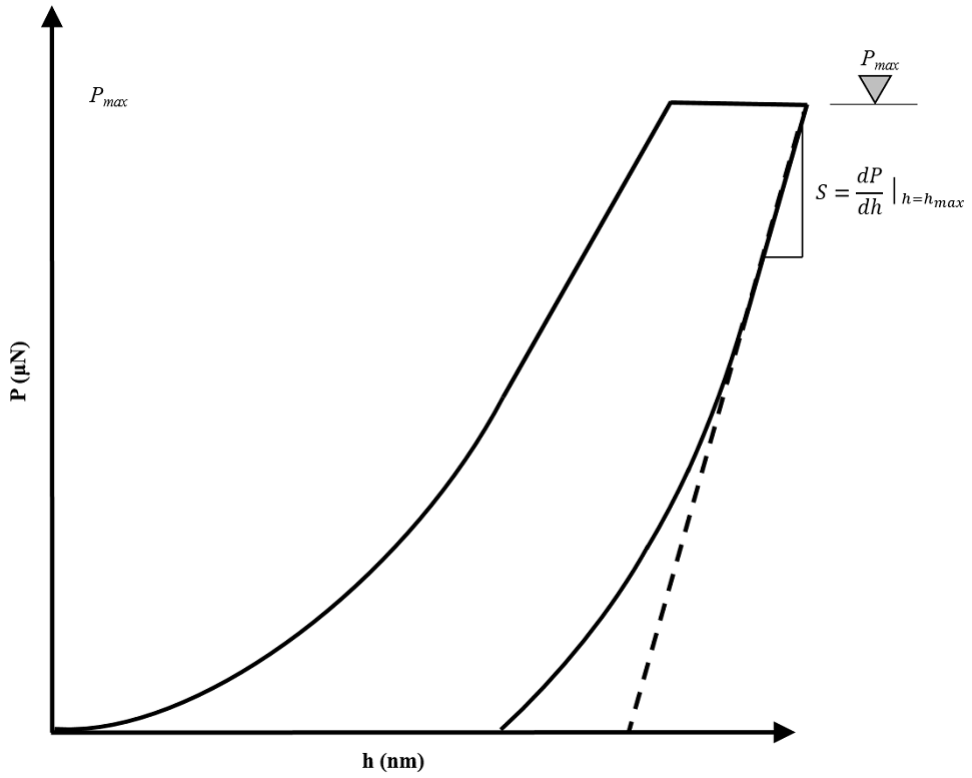

Figure 1.1 Representative individual *P-h* indentation curve [17]

1.1 Research Significance

Cementitious composites are extensively used in the construction industry due to their high compressive strength, low cost of maintenance, simple manufacturing process, and ease of use [15]. The mechanical properties of cement-based materials have been studied extensively for

a long time. Studies have been mainly focused on developing numerical computational methods to predict their linear elastic properties [18]. However, cementitious materials are viscoelastic, thus, it's important to understand stress relaxation and creep behavior to estimate the long-term performance of cementitious materials effectively. Cement paste consisting of hydration products such as calcium silicate hydrate, and calcium hydroxide, along with unhydrated cement grains, pores, and water is the primary contributor to the viscoelasticity of concrete. Considering this heterogeneous and aging microstructure of cement paste, it is vital to investigate and characterize the cement paste at a short length scale (micro and nanoscale) to gain considerable insight into the intrinsic structure and fundamental properties of construction materials.

Nanotechnology is a highly interdisciplinary field; its widespread use has created new opportunities for research involving cementitious materials [5]. the present study utilizes statistical nanoindentation to perform multiscale characterization of time-dependent properties, as only few researchers attempted to study aging viscoelasticity of cement pastes at micro/nano scale length. The research work, which uses nanoindentation coupled with nanoscale composite modeling to study the creep of cement-based materials, combines the various nanoscale properties to predict meso and macro scale properties. The aging viscoelastic properties profoundly affect long-span concrete girders [19], thus measuring creep on the micro to nanoscale enhances the understanding of concrete deformation mechanisms at the macro scale. By understanding and predicting phenomenological behavior, improved design methodologies can also be developed. The overarching goal of this type of research is to be able to predict the long-term time-dependent behavior of concrete from the nanoscale. The study will serve as the necessary first step toward accomplishing this goal.

1.1.1 Objectives

Combined experimental and analytical approaches form the basis of this study. The primary objectives of the study are:

1. to reduce uncertainties associated with the application of nanoindentation technique on cementitious materials;
2. to construct and validate a closed-form analytical solution to extract the time-dependent constitutive features of cementitious materials;

3. to investigate the influence of nuclear radiation on viscoelastic properties of cement paste using statistical nanoindentation;
4. to characterize the aging creep of cement paste at the nanoscale using microstructure dependent constitutive models.

1.2 Structure of the Thesis

The present study is branched into five chapters. Nanotechnology and the nanoindentation method are presented in Chapter 1. The chapter also provides a concise overview of the research's goals and motivations. Chapter 2 to 5 individually presents the methodology adopted to achieve each objective, in detail discusses the results, and outlines the most important conclusions.

Chapter 2 presents a detailed review of the use of the nanoindentation technique on concrete and cementitious composites to determine time-dependent and time-independent properties. Nanoindentation is often used on flat, homogeneous samples, but extending its use to heterogeneous and composite materials requires certain assumptions. The chapter provides a discussion on the polishing method to adopt in order to ensure a reasonably flat surface without disturbing the microstructure of the cement paste sample. The discussion on surface roughness studied using atomic force microscopy and nanoindentation is also presented. This chapter meticulously examines the uncertainties and proposes an experimentally and statistically validated approach, acknowledging the absence of standards for designing the statistical nanoindentation experiments and for preparing the cementitious materials for nanoindentation.

The particular nanoindenter is capable of performing both relaxation and creep tests by applying continuous indentation depth and load, respectively. These test results allow for the extraction of time-dependent parameters such as relaxation modulus and creep compliance. Chapter 3 discusses the importance of studying the stress relaxation of concrete and the advantages of analyzing nanoindentation data to quantify the long-term time-dependent properties of cementitious composites. A closed-form analytical solution is derived based on the correspondence principle. The chapter presents the reliability of the analytical solution to interrelate the nanoindentation displacement, and time data to the contact creep and relaxation functions of the material (cement paste and polycarbonate).

Concrete is well recognized for its radiation-shielding capacity in nuclear safety structures. Chapter 4 focuses on understanding the effect of radiations on the mechanical viscoelastic properties of concrete and cementitious materials. The chapter in detail discusses the procedure of subjecting cement paste samples to combined neutron and gamma radiations. In addition, nanoindentation creep and stress relaxation data for irradiated and controlled cement paste samples are analyzed and presented.

Nanoscale characterization paired with multi-scale composite modeling combines the various nanoscale properties to predict properties at the macro scale. For a comprehensive understanding of the time-dependent behavior of concrete, it is necessary to model the aging viscoelastic characteristics of cement pastes. In Chapter 5, the aging viscoelasticity of cement paste is measured and modeled based on the time–shift approach and the solidification theory. The chapter describes the solvent exchange and freeze-drying methods adopted to stop the hydration of cement paste at different ages. Lastly in Chapter 6, the main conclusions of the thesis are outlined.

Chapter 2 - Reducing Uncertainties in Nanoindentation Experiments for Cementitious Materials.

2.1 Introduction

The fundamental equations used in the computations of generalized indentation solutions involves certain assumptions such as an infinite, homogeneous, and isotropic ideally smooth surface; the indenter also has a perfect geometrical form [7, 20, 21]. Cement paste, on the other hand, violates assumption of infinite half space and homogeneity owing to its complicated composition, pore structure, and presence of multiple hydration phases. Thus, utilization of nanoindentation on cementitious composites with such mechanics solutions introduces uncertainty to the data obtained. Different hydration phases exist in cementitious materials at various small length scales, and testing the distinct phases is of interest. Measuring individual phases using single indentations is difficult [22]. Grid indentation is a method for characterization of the mechanical properties of individual hydration phases by statistically analyzing the data obtained from a large number of single indentation tests in a grid without any a priori knowledge of the microstructure at the location of indentation [23, 24]. The precision of the mechanical mapping of the indented surface is restricted by various parameters like grid spacing, grid size, indentation depth, peak load and surface roughness. The maximum penetration depth of the indentation, h, should fulfil the scale separation, that is, for small indentation depths, $h < D/10$ and for deep indentations, $h/D > 6$, where D is the characteristic size of the microstructure [25]. However, D is complex and difficult to determine as it depends on mix proportions, hydration degree, type of cement, etc. The minimum spacing (l) between indentation points should be $l\sqrt{N} \gg D$ to avoid interference from the neighboring indentation points, where N is the total number of indentation points [26]. The choice of grid spacing and grid size in many literature (Table 2.1) is not justified [10, 12-14, 21, 24, 27-31].

Mechanics solutions require an ideally smooth sample surface. For cement paste, roughness should be a small fraction of the maximum indentation depth. Attaining a smooth surface is challenging for cement paste due to its weak, porous, brittle, and heterogeneous microstructure that can facilely damage during preparation [32]. Surface smoothness has been shown to impact test results [33]. In spite of its importance there are no standards available for

sample preparation for nanoindentation on cement paste. It was suggested that if the sample surface roughness is below 100 nm over a scan area of 50 mm × 50 mm [34] or less than approximately 1/20 of indentation depth [33] should be sufficient to satisfy the assumption of optimally smooth surface. But these studies disregard the influence of porosity and the age of the sample on surface roughness. Many researchers attempted to address the surface roughness through different sample preparation procedures [21, 32, 34, 35], and generally the root mean square (RMS) roughness which is 5 times less than the average indentation depth is proposed as a roughness target [34]. However, rigorously forcing this criterion is difficult provided the material under study [34] had extremely low porosity and the reliability of reported roughness is questioned [35]. Uniform polishing is difficult to obtain, and excessive polishing can damage the pore structure as well as local micro and nano structure of the material. Hence, the question of how to minimize RMS roughness for cement paste without disturbing the microstructure is yet be answered.

To the best of the author's knowledge there has been very limited work on understanding the uncertainties and errors involved with using nanoindentation on cementitious composites. The literature provides limited evidence to support selection of a critical load based on the porosity of the material. This chapter aims to address these uncertainties and recommend experimentally and statistically verified processes to design nanoindentation tests on cementitious materials.

Table 2.1 Metanalysis of cementitious composites corresponding to different load cases, grid nanoindentation parameters and roughness.

Cement Type	w/c ratio	Load (mN)	Indentation Depth (nm)	Grid Details		Surface Roughness (nm)	Reference
				Size (μm)	Spacing (nm)		
White Portland cement	0.5	0.5	167 ± 53	10×10	10	10 - 30	[36]
OPC	0.2	4	310	20×12	20	NA	[37]
OPC	0.53	2	80 & 600	15×15	20	NA	[38]
OPC	0.28	1.2	60 - 180	11×3	3 and 5	59 - 12	[39]
UHP FR CC with nano silica	NA	0.2	200	10×10	15	NA	[40]
OPC	0.2	2	100 & 400	20×15	20	50 - 20	[34]
Alite rich CEM 1	0.15 to 0.4	2 and 8	200 & 20000	NA	NA	20	[41]
AALBORG white cement	0.4	1,2,4,5	150 - 600	10×10	30	30 - 40	[24]
OPC	0.45	0.55	200	5×10	200	NA	[42]
OPC	0.3, 0.4 & 0.5	1.25	NA	NA	NA	NA	[43]
HPCC	NA	12mN/min	200	16×18	8	< 60	[30]
OPC	0.4	2	200 - 400	NA	NA	NA	[44]
OPC	0.4	NA	NA	NA	NA	133	[21]
Type I/II	0.28	2	150 - 450	20×10	10	NA	[14]
OPC	0.4	1.5	NA	20×20	10	NA	[5]
CEM1 42.5N	0.4	1	NA	NA	NA	NA	[17]
Type I OPC	0.45	0.5 – 1.5	250 -500	NA	NA	NA	[15]
42N OPC	0.35	NA	300 - 400	NA	10	NA	[45]
Type 1 OPC	0.5	NA	NA	NA	NA	NA	[46]
Type I/II	0.4	1.5	NA	NA	NA	NA	[10]
42.5N OPC	0.4	NA	100 - 300	12×16	10	NA	[32]

Where UHP FR CC: Ultra high-performance fiber reinforced cementitious composite with nano silica, OPC: ordinary Portland cement, HPCC: High performance cementitious composite.

2.2 Methodology

Nanoindentation experiments should strictly adhere to a sample preparation process. Furthermore, methodological parameters should also be identified and controlled. Thus, the purpose of this study is to investigate the effect of sample preparation by addressing the RMS roughness, lubricant, and polishing method. The influence of experimental setup is studied by considering indentation depth, and load; and the parameters of grid indentation which includes grid size and spacing. Each of these factors are discussed in detail in the following sections.

2.2.1 Materials and Sample Preparation

For the present study four samples were cast from TYPE I/II cement with 0.35, 0.40, 0.45 and 0.50 water to cement ratio (w/c). The paste was filled in cylindrical plastic molds 45 mm long and 17 mm diameter. All the samples were cured for 28 days in a 100% relative humidity environment and samples were not extruded prior to placement in the moist room. The specimens were extracted from the cured cement paste samples by cutting small coin size discs with a thickness of approximately 3 mm with a diamond blade saw at medium speed using water as lubricant. The discs were allowed to dry in room condition.

2.2.2 Polishing

The finished samples of size 3 mm thick and 17 mm diameter were prepared for grinding and polishing by embedding them in epoxy resin. The exposed flat surface of the samples was polished using three different methods. During first method (PM1) all the specimens were polished manually using silicon-carbide abrasive discs. Additional polishing was done using diamond lapping discs. During this polishing process specimens were constantly wetted with isopropyl alcohol to lubricate the polishing media and to avoid any dissolution of water-soluble hydration products, principally calcium hydroxide. In the second method (PM2) 0.35 w/c sample which was polished manually (PM1) was again polished with the FEMTO 1100S automated polishing machine (Pace Technologies) capable of polishing multiple specimens individually and independent of the other specimens allowing for easy removal and inspection of the specimen in-between each polishing step. The time of polishing on each abrasive size was varied in this method and isopropyl alcohol was used as lubricant. For the third method (PM3) of polishing a fresh 0.35 w/c sample was cut and was polished using the same machine with water as lubricant.

Table 2.2 summarizes the polishing methods. In the methods PM2 and PM3 the wheel and the specimen rotated in the same direction at a speed of 200 RPM, at a downforce of 18 to 22 N. The individual down force required was calculated in accordance with ASTM E3-11 based on the diameter of the sample and the piston [47]. After polishing, the specimens were placed in the nanoindentation environmental enclosure which maintained an average temperature of 76° F and relative humidity of 22.6 %.

Table 2.2 Summary of polishing methods.

Abrasive type (grit)/ Size	Time (min)		
	PM1	PM2	PM3
180	5	0.5	0.5
240	5	0.5	1
320	5	1	1
400	5	1	10
600	5	30	40
800	5	30	40
1200	5	120	180
3 µm	5	45	60
1.5 µm	5	-	-
1 µm	5	45	60
0.5 µm	5	45	60

2.2.3 Nanoindentation and Atomic Force Microscopy Imaging

Hysitron Triboindenter model TI Premier (NI) and TT-2 atomic force microscope (AFM) were employed to obtain topographic information on the polished surfaces of the specimen obtained from three methods of polishing. Four images were obtained at various random locations of sample surfaces. Scans were performed using contact/non-vibrating mode. A scan size of 10 x 10 μm^2 with a scan rate of 0.5 Hz, setpoint of 2 µN and a resolution of 256 x 256 pixels was adopted for both devices and all images. The images obtained by NI and AFM were analyzed digitally and the corresponding RMS and average roughness were recorded. The images of sample 0.35

w/c scanned using NI and AFM using all three polishing methods are displayed in Figure 2.1 and Figure 2.2 below.

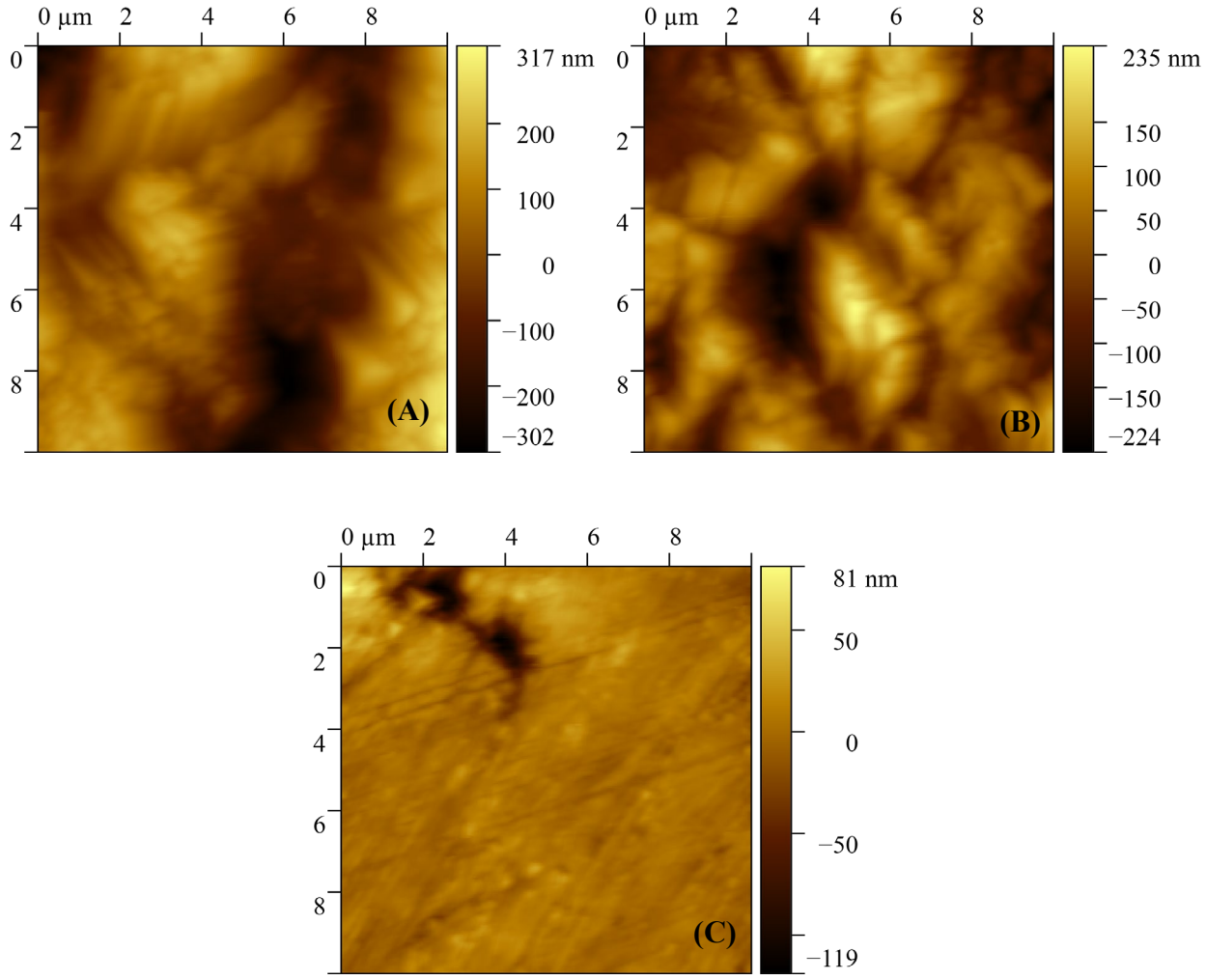

Figure 2.1 NI images from three polishing methods with RMS (nm) (A) PM1 – 117, (B) PM2 – 81, (C) PM3 – 17

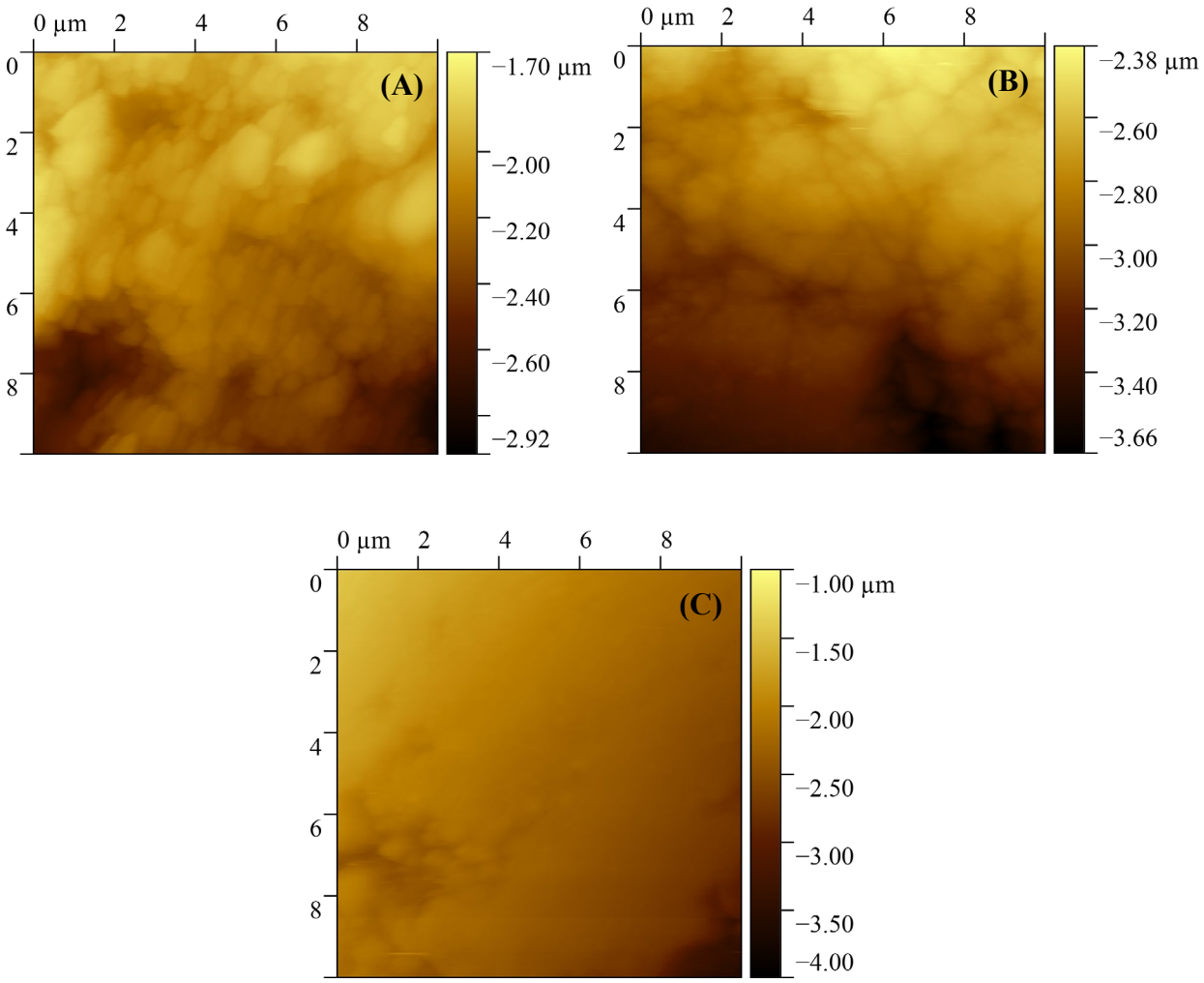

Figure 2.2 AFM images from three polishing methods with RMS (nm) (A) PM1 – 213, (B) PM2 – 291, (C) PM3 – 331

To investigate the significant spatial variability of RMS roughness, post processing of the SPM and AFM surface data was performed to obtain smaller subdomains that correspond to the area associated with the single indentation. Gwyddion and Tribo View software was used to analyze the AFM and NI scans. 25 subdomains with a scan area of 2 x 2 μm^2 were obtained from each image of 10 x 10 μm^2 scan area (Figure 2.3). RMS roughness was computed for each subdomain totaling 100 independent observations for roughness parameter. The average indent size was 1.3 μm^2 and the 95th percentile was 2.9 μm^2. Hence, the choice of 4 μm^2 subdomain scan corresponds to the individual indent and is also large enough to reasonably homogenize the roughness statistic. The subdomain RMS roughness from 4 scans obtained using NI and AFM on

random location of the sample for 3 polishing methods was tested using one way ANOVA test. The p-value was less than α (0.05), suggesting the difference between the averages of groups is large enough to be statistically significant.

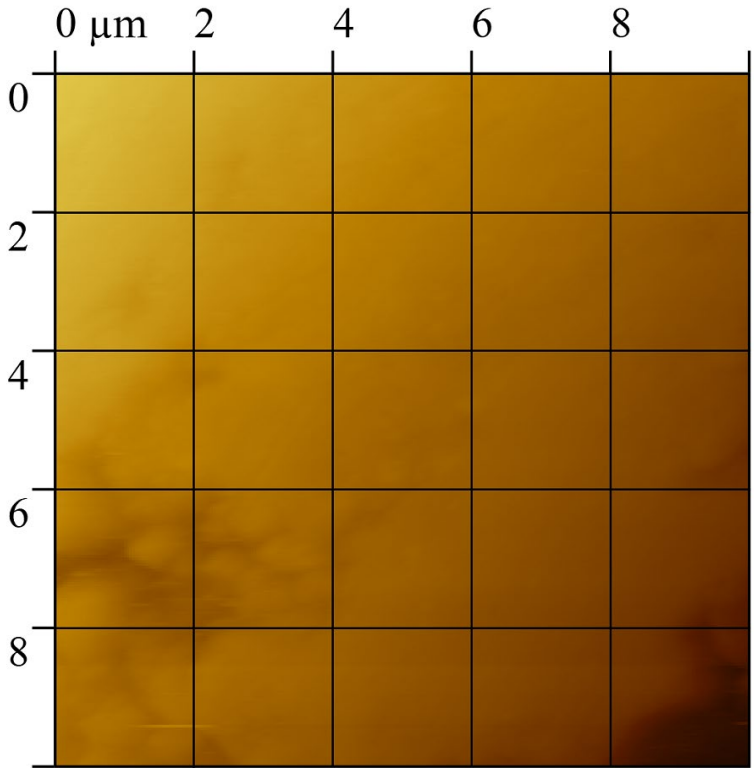

Figure 2.3 AFM image of 0.35 w/c showing the subdomains of 2 x 2 μm2 scan area extracted from a 10 x 10 μm^2

2.2.4 Basic Elastic Nanoindentation

The nanoindentation tests were performed using a Hysitron Triboindenter model TI Premier. Basic elastic indents were performed using a standard Berkovich probe with total included angle of 142.35°. The optic-probe tip offset calibration was performed on polycarbonate sample and the tip area function was calibrated periodically on standard quartz sample using the standard procedure [48]. The indenter was air calibrated before and after each grid indentation test. The basic elastic indentation test consisting of a trapezoidal shape load history with 5s loading segment, 2s holding segment and 5s unloading segment was used. The basic elastic nanoindentation tests conducted in this study were performed with different grid spacing, grid size and load levels at two different areas of each specimen. All four samples were tested with

respect to each of these variables mentioned using load control feedback mode, in order to understand and reduce the uncertainties associated with the testing procedure and sample. After AFM imaging all specimens remained in the enclosure for the duration of the experimental research to assure the identical environment for all the specimens throughout the testing. Table 2.3 details the experimental procedure used for the study.

Table 2.3 Summary of testing procedure used.

Parameters	w/c ratio	Load (μN)	Grid Spacing (μm)	Grid Size
Indentation load/depth	0.35, 0.40, 0.45 & 0.50	200 to 4000	3	10 × 10
Grid Size	0.35	1695	3	3 × 3, 5 × 5, 7 × 7 & 10 × 10
Grid Spacing	0.35	1695	1, 2, 3, 10, 20, 30 & 40	10 × 10

2.3 Results and Discussions

There is no decent correlation between the present calculation methods of E_r and H due to the complexity of cement paste's composition and the limits of existing calculation techniques. As a result, the influence of uncertainty parameters discussed in the methodology section was assessed using E_r.

2.3.1 Indentation Depth and Load

The graph of E_r vs. h obtained from the nanoindentation test on 0.35, 0.40, 0.45 and 0.50 w/c sample indicates higher variability of data below a particular contact depth called as “critical indentation depth” [26] (Figure 2.4, 2.5, 2.6, and 2.7). This critical indentation depth varies for each sample, and it increases with increase in w/c from the data obtained (Figure 2.4, 2.5, 2.6, and 2.7). As the w/c ratio increases, the porosity of the sample will increase. A sample with low w/c ratio will have relatively higher fraction of unhydrated cement grains and the resultant C-S-H tends to form in a space-constrained fashion [49] both of which are less compliant. Hence, it is expected to see increase in the critical indentation depth as w/c increases. Accurate determination of the critical indentation depth is important for estimating the minimum feature size that may be resolved via nanoindentation.

Table 2.4 Critical indentation depth, critical load, and minimum feature size.

w/c ratio	Critical indentation depth (nm)		Critical Load (μN)		Minimum feature size (μm) ($h_{crit}/D>6$)	
	F test	Graphically observed	F test	Graphically observed	F test	Graphically observed
0.35	120	250	1040	1695	0.02	0.04
0.40	220	300	1255	1800	0.04	0.05
0.45	130	350	901	2174	0.02	0.06
0.50	200	375	1504	2692	0.03	0.06

Table 2.4 above shows the critical indentation depth and the corresponding critical load obtained from F test and the plots of load v/s depth. Applicability of critical indentation depth to indent the smallest feature is tested against the condition $h_{crit}/D>6$. The resulted minimum feature size being significantly lower than 1 μm (characteristic size of C-S-H) justifies that h_{crit} is large enough to assess the homogenized material property (Table 2.4).

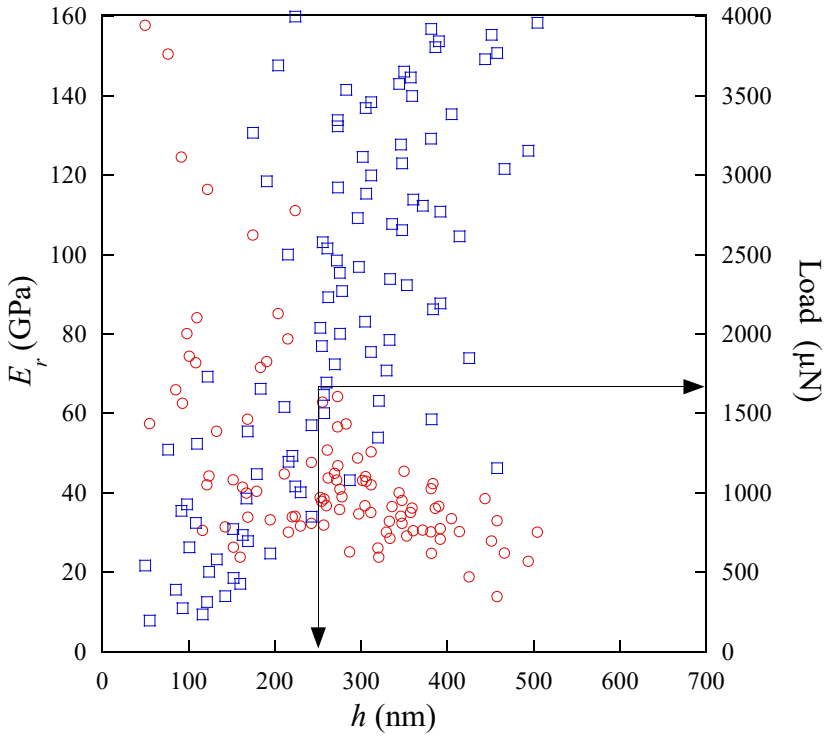

Figure 2.4 Plot of reduced modulus, load and indentation depth of samples with 0.35 w/c, red circles represent E_r and blue squares represent Load (P).

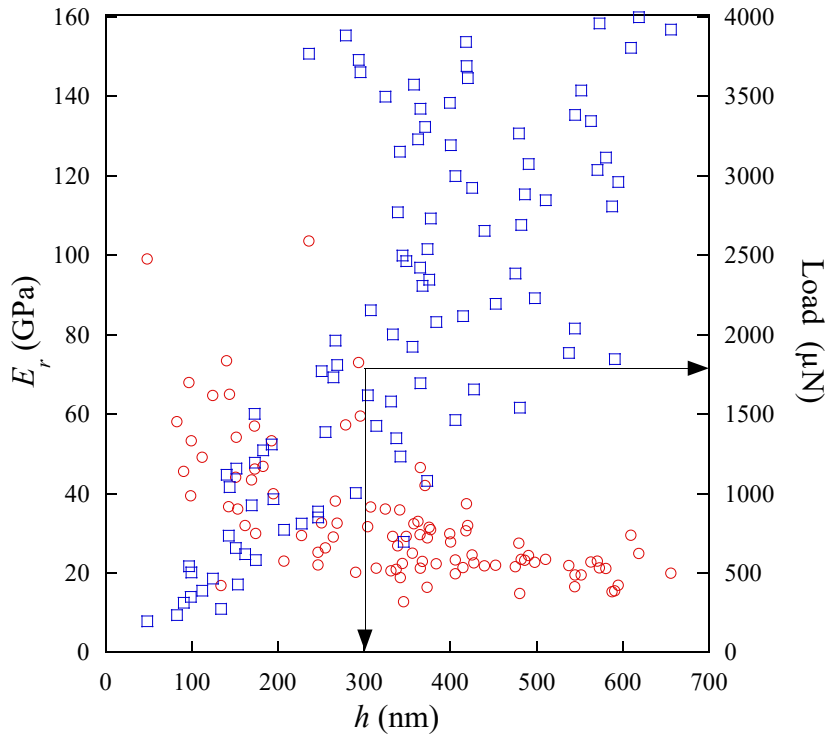

Figure 2.5 Plot of reduced modulus, load and indentation depth of samples with 0.40 w/c, red circles represent E_r and blue squares represent Load (P)

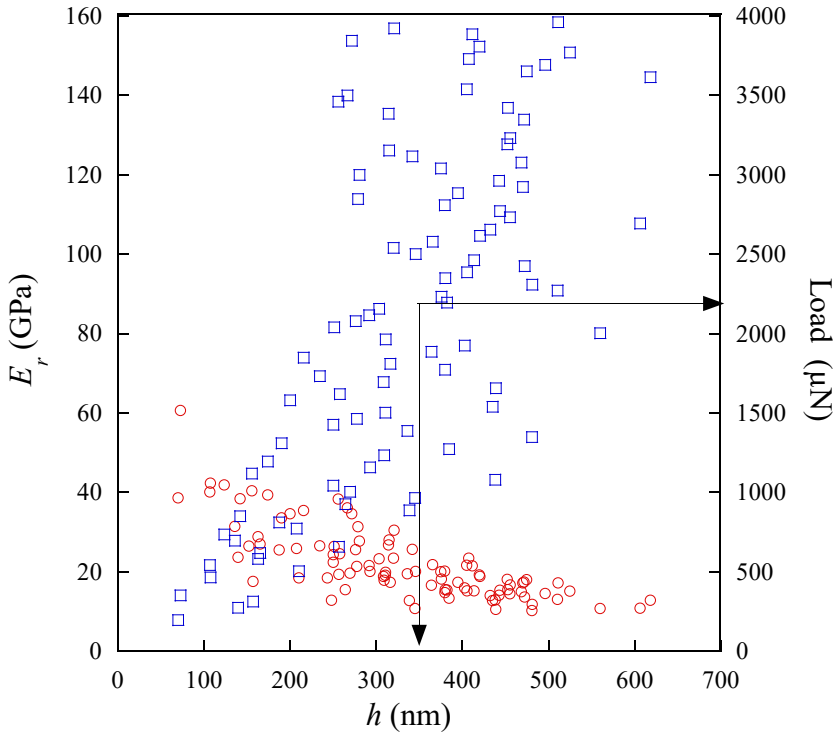

Figure 2.6 Plot of reduced modulus, load and indentation depth of samples with 0.45 w/c, red circles represent E_r and blue squares represent Load (P).

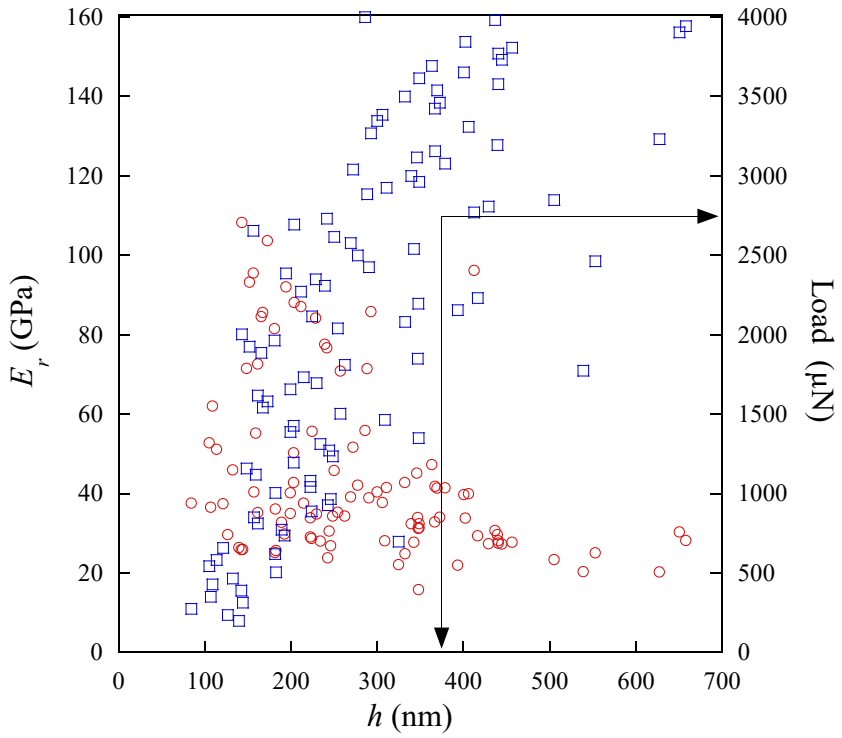

Figure 2.7 Plot of reduced modulus, load and indentation depth of samples with 0.50 w/c, red circles represent E_r and blue squares represent Load (P).

Most commercial nanoindentation equipment is load controlled, so careful load selection is important for ensuring that the critical indentation depth is reached. In order to determine the critical indentation depth,

1. Loads varying from 200 – 4000 μN were applied with an increase of 38.38 μN for each additional indent keeping the loading rate constant.
2. Critical indentation depth was identified through the plot of measured E_r versus h (Figure 2.4, 2.5, 2.6, and 2.7) by visually identifying the depth (h) at which the E_r appears to be converged.
3. The critical indentation depth identified as a baseline and its reliability was statistically analyzed by employing F test. The split data of depth was iteratively scaled down until the F test fails to reject the null hypothesis and the corresponding critical indentation depth was recorded (Table 2.4).
4. The critical load corresponding to the critical indentation depth was determined from graphical representation (Figure 2.4) and F test.

The critical indentation depth and load obtained from the data set of the plot (Table 2.4) indicated the requirement of higher load with increase in w/c and a similar trend is observed even for F test except for 0.45 w/c and the reason for this is not clear. Also, the mean E_r data below critical indentation depth is scattered far from the mean and indicates greater variability (Table 2.5). The mean of modulus of elasticity for bulk cement paste below the critical indentation depth does not agree with actual value of 30-45 GPa [50]. The critical indentation depth ranges from 100 nm to 400 nm, enclosing the majority of the various phases present in the cement paste, with the smallest being C-S-H in the range 1 to 3 μm [21].

Table 2.5 Mean E_r at varying, corresponding variance from F test and E_r at critical load.

	Below critical indentation depth		**Above critical indentation depth**		**E_r (GPa) for critical load**
Sample	Mean E_r (GPa)	Variance	Mean E_r (GPa)	Variance	
0.35	64.2	2070	36.4	93.5	44.3
0.40	45.9	407	26.8	112	38.3
0.45	26.5	85.9	15.4	9.77	38.6
0.50	48.5	543	33.7	204	33.1

Good agreement of the mean E_r with actual value of 30-45 GPa [50] can be seen in Table 2.5 for critical load. Under loads below critical load, surface forces and adhesion between the indenter and sample will be significant, and can dramatically change the load-depth curves, and under loads above critical can damage the pore structure and increases the variability [20].

The present study recommends that for cement paste samples with Type I/II cement indented with Berkovitch tip, the critical load corresponding depth should be arrived at by performing indents using a wide range of load levels (200 to 4000 μN). Figure 2.4, 2.5, 2.6, and 2.7 provides the critical load and depth for all four-sample tested, for 0.35 w/c sample, a critical load of 1695 μN was selected to obtain the critical depth of 250 nm **(**Figure 2.4). Again, these critical values are unique to material porosity, surface roughness and microstructural details under study.

2.3.2 Grid Size and Spacing

The interaction and response from nanoindentation depend on the indent size and on the difference of properties of the phases. In the design of nanoindentation experiments, deciding the

grid size and grid spacing controls may also influence the uncertainty in the measured properties. From Figure 2.5 it can be observed that choosing grid size and grid spacing randomly can affect the mean E_r and hence, needs to be experimentally justified. For a continuum representation of a heterogeneous multiphase material, it is important to interrogate a sufficiently large sample area. As shown in Figure 2.8 when the grid size was increased from 3 x 3 to 10 x 10 the mean E_r remained approximately constant while the standard deviation of measured mean E_r increased. This is due to interaction with more heterogeneous phases. Based on the convergence of the mean E_r, a larger grid size of 10 x 10 was selected to capture the influence of multiple cement paste phases.

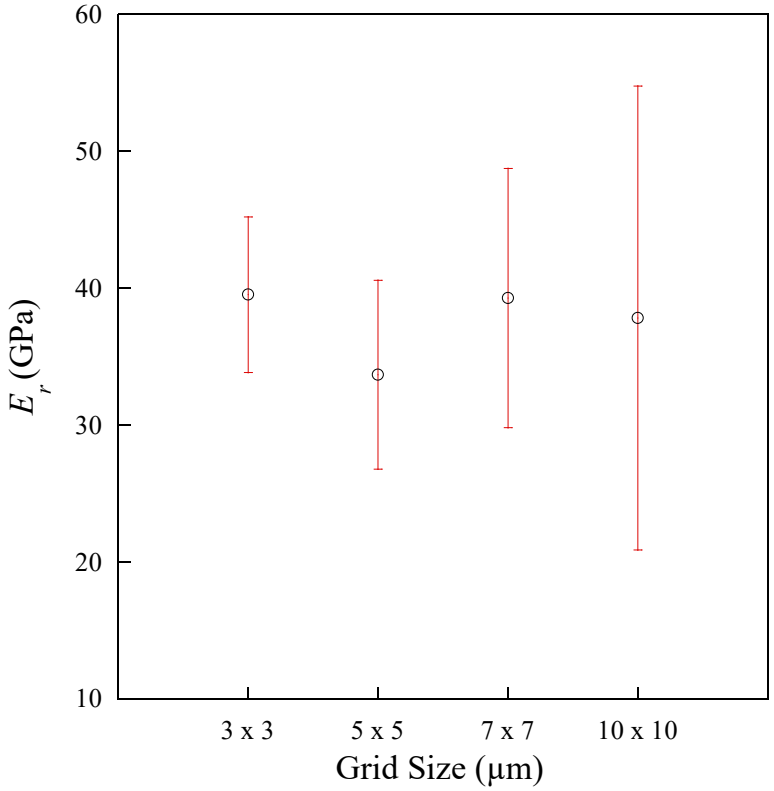

Figure 2.8 Plot of mean reduced modulus v/s grid size of 0.35 w/c at critical load.

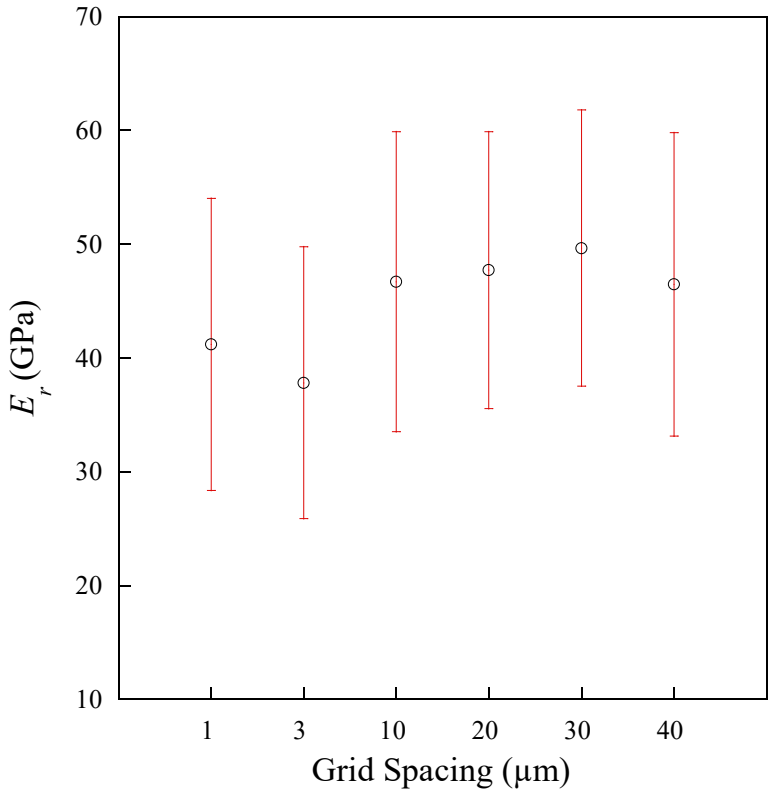

Figure 2.9 Plot of mean reduced modulus v/s grid spacing of 0.35 w/c at critical load.

The mean E_r deviated more from mean value of 40 GPa for bulk cement paste with spacing more than 3 μm (Figure 2.9) and indicates that standard deviation of individual spacing are within the standard deviation of one another. Increasing the spacing beyond 3 μm raises the potential of incorporating additional pores, which substantially alters the critical depth required to homogenize the sample. Also, it appears that 3 μm spacing is sufficiently large to avoid any interference of individual indents with the neighboring indents.

A grid spacing of 3 μm satisfies the condition $l \gg D/\sqrt{N}$ where N is the total number of indentation points and D is characteristic size of the phases [25]. Increasing the grid spacing and grid size increase the test time. Thus, a grid spacing of 3 μm and a grid size of 10 x 10 to evaluate the bulk properties of all the samples in the study appears to be a good compromise for the design of experiment.

2.3.3 Surface Roughness

It is now a well-known fact that sample preparation is a crucial step to characterize the cement paste properties at nano scale using nanoindentation [28, 34, 35, 45, 51]. The following subsections discuss the influence of using AFM and NI imagining techniques and different polishing methods on the RMS roughness.

2.3.3.1 Atomic Force Microscope vs Nanoindentation

NI and AFM were used to scan the sample surfaces and to highlight the advantage of using the same probe to scan and indent the surface of the sample. Figure 2.10 shows the dependence of RMS roughness on the porosity of the sample polished using method PM1, the plot clearly points out the increase in the RMS roughness obtained from both NI and AFM as the w/c increases. Critical indentation depth is related to surface roughness [34], and shows a similar trend with higher porosity (Table 2.4).

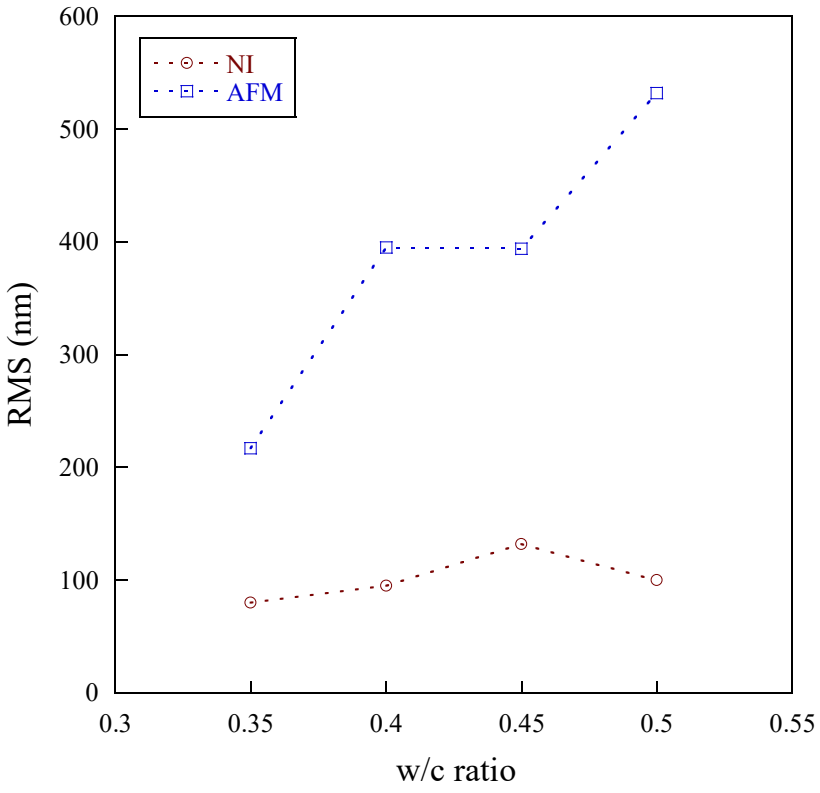

Figure 2.10 The dependence of the RMS roughness obtained from PM1 on the porosity of the sample.

The significantly higher AFM RMS roughness compared to the NI RMS roughness (Figure 2.10 and Table 2.6) is due to the tip shape and aspect ratio of the probes used to scan the samples. Regardless of measurement technique, the RMS roughness varies significantly at different points on the same sample due to the polished surface's intrinsic heterogeneity (Figure 2.10). AFM clearly offers higher resolution because of the high aspect ratio of tip, but AFM nanoindentation is not a widely utilized device as nanoindenter for the study of mechanical characteristics of materials at the nanoscale, because the latter is more precise and standardized [52]. It was therefore concluded that there is a significant advantage to measuring the roughness of the sample with the nanoindentation probe. Namely that the roughness measurement is taken at precisely the same location on the sample that the subsequent indentation test will occur.

2.3.3.2 Polishing Methods

Owing to the importance of surface roughness and unavailability of a widely accepted standard method, three different polishing methods were adopted in this study. Table 2.6 highlights the influence of three different polishing methods on the RMS roughness obtained from subdomains of 2 x 2 μm^2 scan area.

Table 2.6 Mean and Variance for RMS roughness of 0.35 w/c with three polishing methods.

Polishing Methods	**RMS Roughness (nm)**				**E_r (Gpa) of 0.35 w/c**	
	NI		**AFM**			
	Mean	Variance	Mean	Variance	Mean	Variance
PM1	54	799	78	835	39	71
PM2	53	466	81	830	34	82
PM3	27	403	72	1121	19	6

The variance of RMS roughness obtained from NI decreases from PM1 to PM3, but the same is not seen with RMS roughness obtained from AFM, this inconsistency in variance can be again explained by the aforementioned AFM tip sharpness and high aspect ratio. There was a statistically significant difference between PM1 and PM3, PM2 and PM3 as tested by ANOVA where the p-value was vanishingly small ($p<0.05$) in case of RMS roughness from NI. This shows that the more time spent on the polishing discs will evidently improves the surface roughness irrespective of the heterogeneity in terms of porosity and multiple hydration phases. For RMS roughness obtained from AFM, ANOVA showed no statistical difference ($p>0.05$) in

the means among three methods, which strengthens the argument of high resolution, but defies the effect of rigorous polishing (Table 2.6).

Table 2.7 Summary of descriptive statistics of roughness data from three polishing methods.

	PM1		PM2		PM3	
	NI	AFM	NI	AFM	NI	AFM
Standard Error	2.85	3.34	2.16	2.88	2.01	3.34
Median	48.1	75.7	50.5	80.5	21.1	73.5
Mode	41.2	82.2	43.6	89.0	46.4	72.0
Standard Deviation	28.4	28.9	21.6	28.8	20.1	33.5
Kurtosis	1.46	2.06	1.82	0.724	-0.907	6.29
Skewness	1.08	1.03	1.11	0.711	0.564	1.26
Range	146.2	155.2	117.9	141.0	70.1	228.0
Sample size	100	75	100	100	100	100
Test statistic (K)	1.19	0.644	1.11	0.812	1.78	1.14
P-value	0.106	0.772	0.155	0.499	0.003	0.135

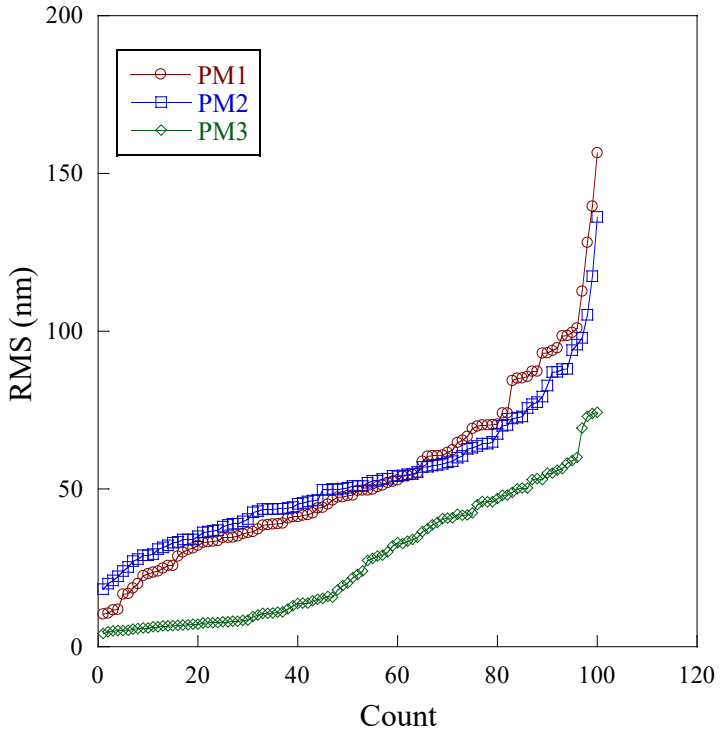

Figure 2.11 Plot of RMS roughness of 0.35 w/c sample obtained from three polishing methods using NI.

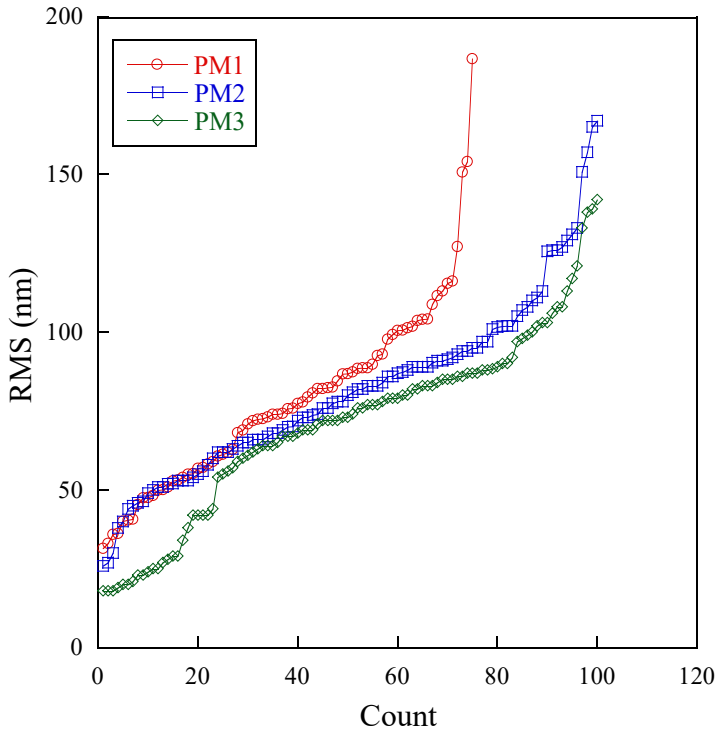

Figure 2.12 Plot of RMS roughness of 0.35 w/c sample obtained from three polishing methods using AFM.

Figure 2.11and 2.12 shows the RMS roughness of individual subdomains ranked from smallest to largest for each of the polishing techniques recorded using NI and AFM (total 100 reference observations). It can be seen that overall RMS roughness of PM3 is lower than PM1 and PM2 which are approximately same indicating that on the NI length scale polishing fluid appears to be influencing factor, but the AFM does not show any such obvious sensitivity.

Figure 2.13 depicts almost identical ranges of indentation depth for 0.35 w/c polished with three different methods, this indicates the approach of determining the critical indentation depth appears reliable irrespective of the polishing method. The low average modulus value of 19 GPa for method PM3 is due to the use of water as the lubricant during the polishing process. Using water enhances the further hydration and possible dissolution of hydrates mainly calcium hydroxide and forces additional C-S-H to grow, making the sample unrepresentative of its original microstructure. The E_r value of 19 GPa, agrees well with the previous results on C-S-H [21, 25, 36] and justifies the above explanation. The low modulus value can also be explained by the more rigorous polishing method (PM3) which may disturb the microstructure by possibly increasing the effect of large capillary pores and leading to variability in measured response.

Based on the preceding discussion it appears that PM2 is the most suitable method to polish the samples. The lubricant (isopropyl alcohol) ensures no dissolution or formation of additional hydration products, and the machine provides uniform pressure and speed throughout polishing, resulting in a sufficiently smooth surface.

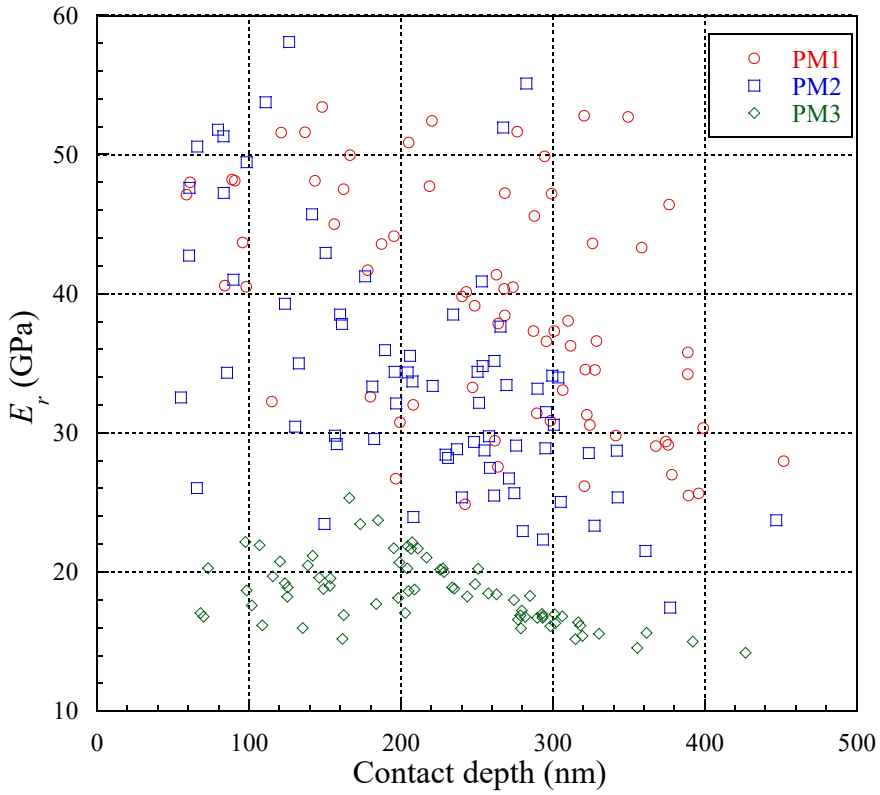

Figure 2.13 Plots of reduced Modulus and contact depth of 0.35 w/c sample by three polishing methods.

2.4 Conclusions and Recommendations

The effect of penetration depth, grid size and grid spacing on four cement paste samples was outlined in this chapter. The results and analysis obtained in the study proves that there exists a "critical indentation depth" for each sample and it increases with increase in w/c. Individual indentations shallower than the critical depth shows greater variability for all measured properties. Hence, load corresponding to the critical indentation depth should be considered as the peak load for nanoindentation test, which should be enough to homogenize the material under investigation. Further, the author recommends a grid size and grid spacing of 10 × 10 μm and 3 μm respectively for bulk characterization of cement paste. Increasing the spacing

and size leads to higher variability in measured properties, due to the intrinsic material heterogeneity and is expected. Other researchers may benefit from different grid sizes and spacing depending on the particular purpose of their inquiry. Accordingly, it should be known in advance what microstructural details of the material will be studied, as some phenomena and features are evident only at certain loads and imprint size.

The present study recommends the PM2 as the effective polishing method to obtain smooth representative sample for nanoindentation test. Scanning size, scanning rate, resolution and the tip used should be taken into account while addressing the RMS roughness. The study also indicates that surface roughness depends on the porosity and the age of the sample and thus the measured roughness should be considered in the context of the material being studied. Using same indenter tip (NI) for imaging and for estimating roughness enables locally relevant characterization of surface roughness for the eventual indentation event. The author believes that this approach is preferable to AFM based roughness measurements that are unlikely to be precisely located at the point of indentation.

The author believes that this study can serve as a quick guide for experimentalists to intelligently design their own nanoindentation experiments for cementitious materials. This study is focused on aleatory uncertainties associated with the material variability (bulk) and measurement technique and has intentionally avoided epistemic uncertainties [7, 53]. Therefore, the readers are cautioned to avoid overgeneralizing the conclusions if the individual hydration phases of the sample are under study.

Chapter 3 - Stress Relaxation and Creep Nanoindentation for Cement Paste

3.1 Introduction

Cement-based composite materials exhibit time dependent behavior. The viscoelastic behavior of concrete is primarily attributable to the complex microstructure of cement paste, which exist at the nano, micro, and macro scales [54, 55]. To better understand the long-term behavior of concrete structures, it is critical to examine the time dependent creep and relaxation properties. Creep is the time dependent increase in strain of a structural element under controlled or constant stress, whereas time dependent decrease in stress under a constant strain is defined as stress relaxation [56]. It is also vital to develop an effective and reliable theoretical model for their analysis and safety assessment [57]. The creep response of concrete has been studied extensively [58-62], but less is known about the relaxation response of concrete, despite the fact that creep and relaxation are intrinsically related. Relaxation is particularly of interest in prestressed concrete structures because the length of tendons may change due to varying load applied and the concrete creep and shrinkage. This change in length of tendons can lead to complicated stress redistributions. Consequently, the condition is more reminiscent of a relaxation test than a creep test [63, 64]. Thus, it is evident that stress relaxations account for prestress losses and should be considered in the design and analysis. Due to the fact that strain must be applied to the specimen at once and held constant during the relaxation test, at macroscale, testing this offer a considerable deal of difficulty to instrument selection, test design, and operation. Also, most of the commercially available instruments to test time dependent properties are load controlled. Thus, in contrast to creep data, the literature has limited information on cementitious materials' relaxation [65-67]. In the present study the nanoindentation technique is adopted to perform creep and relaxation tests on cement paste samples. Nanoindentation has evolved as an ideal mechanical testing technique for characterizing the microstructure of heterogeneous materials such as cementitious composites. Many researchers are increasingly using nanoindentation to measure the creep response of concrete [9, 10, 12, 68, 69]. Because the pointed and sharp tip allows for high spatial resolution and high levels of stress to be applied, nanoindentation can measure the hardness, elasticity, and

long-term time dependent behavior of cement paste in just minutes long experiments, reducing the length of transient creep-relaxation by orders of magnitude [64]. Standard macroscopic techniques would need years of testing, whereas statistical nanoindentation yields a large amount of data that can be analyzed in few seconds [68]. On the other hand, research on nanoindentation based relaxation in cementitious materials is scarce [64, 70]. Many studies focus on deriving the relaxation response from the creep behavior [54, 71-75]. Several numerical and analytical models have been widely employed to extract the relaxation parameters from the creep data of cementitious composite in the open literature [65-67, 71, 76, 77]. Numerical models are time consuming and less efficient in the case of inverse analysis and also computational accuracy of relaxation modulus derived from creep test data is poor [78]. With respect to the integrals expressed in the Prony series, a poorly conditioned matrix equation increases the complexity of the calculation [79].

There are, to the best of the author's knowledge, limited data on nanoindentation-based relaxation tests, and it appears that there is a need to construct a closed form analytical method to extract the time-dependent constitutive features of cementitious materials. Thus, in the present study, the relaxation behavior of cement paste is measured at the nanoscale. A time-dependent solution for the relaxation indentation experiment is developed using the elastic–viscoelastic correspondence principle and is used to fit the experimental data and in turn compared to analogous creep behavior. The analytical solution is also validated for a standard polycarbonate sample. Which is believed to be more homogeneous than cement paste. Other viscoelastic studies use creep or relaxation solutions to predict the relaxation or creep response of a material [54, 72, 78]. This study seeks to take that concept further and cross validate the analytical closed loop solution by feeding the relaxation fit parameters back into creep solution and vice versa.

3.2 Theory

This section reviews the contact mechanics theory used in the analysis of nanoindentation creep and stress relaxation data. The closed form solution derived using correspondence principle to analyze the data obtained from load controlled and depth controlled nanoindentation test is described in detail with flow charts.

3.2.1 Background Theory

Information on the mechanical properties, microscopic processes, and mechanisms of surface deformation and failure may be gleaned from the relationship between indentation load (P) and depth (h) during loading/unloading segments (Figure 3.1) of an indentation test [80, 81]. For spherical indenters with diameter *D*, the empirical equation $P/d^2 = f(d/D)$, where $f(d/D)$ is a characteristic material function, was derived by taking advantage of the relationship between load P and the size d (chordal diameter) of a residual impression, and it was then concluded that P/d^2 and d/D must be constant in accordance with the principle of geometrical similarity for impressions and indenter [82]. Furthermore, the indenter's geometric similarity leads to a relationship between the indenter's surface diameter d and the contact depth h_c left by a conical indentation. Extrapolating the above connection and applying the principle of geometrical similitude to diamond pyramidal indenters (Vickers, Berkovich, Knoop), leads to the quadratic P-h relation, i.e., $P \propto h^2$, where $P = (p)(g/2)h^2$, (p) is the true mean pressure and g is the geometrical factor of indenter [82, 83].

It is difficult to analyze time-dependent indentation using the constitutive relations. Load controlled indentation test were performed to study viscous and elastoplastic materials using a spherical indenter and a flat punch [84-86]. Correspondence principle is commonly employed to derive the analytical solution to indentation problem involving viscoelastic materials, wherein Laplace inversion of the elastic Hertz solution for spherical indentation yielded the desired viscoelastic solution. This was accomplished by taking use of the fact that the Laplace transform of a linear viscoelastic constitutive equation removes time dependence. But the solution was only valid provided the contact area is not decreasing with time [87, 88]. Later it is demonstrated that the aforementioned viscoelastic solution is valid for constant contact area and also for initial unloading phase (decreasing contact area) and successfully applied correspondence principle to construct the closed form analytical solution for conical indentation of cement paste [89].

3.2.1.1 Closed Form Analytical Solution

Sneddon's well-known load to depth relation for conical indentation on a fully elastic body [90] invites the application of the quadratic P–h relationship to materials that range from perfectly elastic to perfectly plastic and has been utilized to analyze the nanoindentation creep

data. Sneddon's elastic solution [90] in time regime for a conical indenter with the inclined face angle $\beta = 24.7^o$ (Figure 3.1) is given by:

$$h^2(t) = \frac{2\gamma^2}{gc}\frac{P(t)}{E'} \quad \text{Equation 3.1}$$

where $h(t)$ and $P(t)$ are time dependent indentation depth and load respectively, γ is contact impression profile parameter which is $\frac{\pi}{2}$ for pyramidal indentation, g is the area function = $3\sqrt{3}\tan\beta$, c is frontal factor which is $\tan\beta$ for a Berkovich tip, and E' is the elastic modulus defined by $E/(1-\nu^2)$ using viscoelastic Young's modulus E and Poisson's ratio ν of the material under study. For diamond indenter E is approximately 1TPa and is ignored.

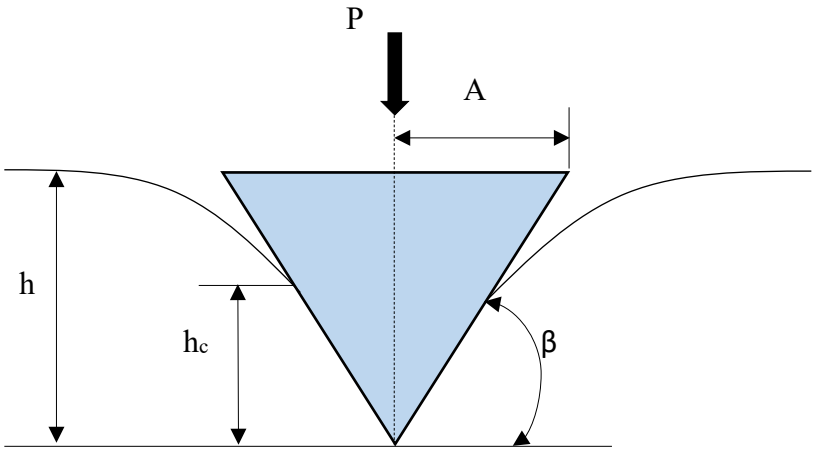

Figure 3.1 Schematic of Berkovich nanoindentation at load P.

The nanoindentation-based creep was modeled using the correspondence principle assuming linear viscoelasticity. The solution to a linear viscoelastic indentation problem in the Laplace domain is obtained by substituting the elastic constants (E') in the elastic solution (Equation 3.1) with the Laplace transform of the time-dependent expressions of the elastic moduli multiplied by the Laplace Carson Transform parameter (s) in the linear elastic solution. Then, using the inverse Laplace transform, the solution in the space domain is inverted to the time domain. In the transform domain, the relationship between the creep compliance function $J(t)$ and $E(t)$ is as (Equation 3.2).

$$\overline{E(s)} = \frac{1}{s^2\overline{J(s)}} \quad \text{Equation 3.2}$$

The Laplace transform of (Equation 3.1) yields

$$\overline{h^2(s)} = \frac{2\gamma^2}{gc}\ \frac{\overline{P(s)}}{s\overline{E'(s)}} \quad \text{Equation 3.3}$$

Since, a Heaviside step indentation load $P(t) = P_{max}\, H(t)$, the Laplace transform of the same is

$$\overline{P(s)} = \frac{P_{max}}{s} \qquad \text{Equation 3.4}$$

The Laplace transform of elastic modulus *(E')* is

$$\overline{E'(s)} = \frac{s\,\overline{E(s)}}{1-(\nu(s)^2)} \qquad \text{Equation 3.5}$$

assuming the time invariance of the Poisson's ratio of the indented material, inverse Laplace transform of Equation 3.3 gives

$$h(t) = 0.66\sqrt{P_{max}\, J(t)\,(1-\nu^2)} \qquad \text{Equation 3.6}$$

Equation 3.6 is similar to the creep solution derived in the literature [10], The difference is, in the present work inclined face angle for Berkovich is considered and the solution also incorporates γ and g parameters, which are neglected in the aforementioned solution. The experimentally obtained data was fitted using Equation 3.6 in Mathematica (Figure 3.2).

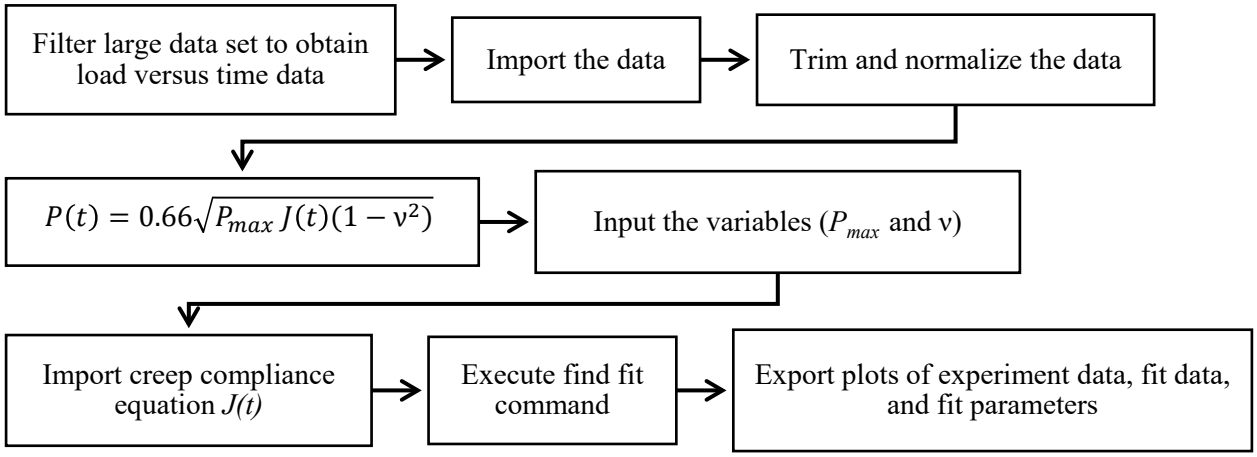

Figure 3.2 Flowchart for Mathematica code to fit the creep data.

For the current problem of relaxation, a constant indentation depth is applied, and the load will be monitored, thus 3.1 is algebraically rearranged as,

$$P(t) = \frac{gc}{2\gamma^2}\, h^2(t)\, E' \qquad \text{Equation 3.7}$$

To obtain the solution for relaxation indentation, the correspondence principle will be used, where in the time dependent parameters will be transformed to transform domain to eliminate time dependency and hence obtained solution in transform domain will be inverted back to time domain to fit the experimental data using inverse Laplace transform.

The Laplace transform of Equation 3.7 yields

$$P(s) = \frac{gc}{2\gamma^2}\, h^2(s)\ \overline{sE'(s)} \qquad \text{Equation 3.8}$$

Since a Heaviside step indentation depth $h(t) = h_{max}\, H(t)$, and

$$h^2(t) = [h_{max}\, H(t)]^2 \qquad \text{Equation 3.9}$$

the Laplace transform of Equation 3.9 is

$$\overline{h^2(s)} = \frac{(h_{max})^2}{s} \qquad \text{Equation 3.10}$$

The application of a Laplace transform to *E'(t)* facilitate the computation of the stress relaxation function *R(t)* as given by the equation below

$$\overline{E(s)} = \frac{1}{s^2 R(S)} \qquad \text{Equation 3.11}$$

assuming the time invariance of the Poisson's ratio of the indented material, substituting Equation 3.11 in Equation 3.8, and inverting it back into time domain gives

$$P(t) = \frac{2.28\, h_{max}^2\, R[t]}{(1-\nu^2)} \qquad \text{Equation 3.12}$$

The creep compliance function *J(t)* in the form of 3-unit kelvin chain is

$$J(t) = \frac{1}{E_0} + \frac{1}{E_1}\ \frac{\left(1-e^{-t/t_h}\right)}{(1-e^{-1})} + \frac{1}{E_2}\ \frac{\left(1-e^{-t/t_h}\right)}{(1-e^{-1})} + \frac{1}{E_3}\ \frac{\left(1-e^{-t/t_h}\right)}{(1-e^{-1})} \qquad \text{Equation 3.13}$$

Where, E_0, E_1, E_2, E_3 are fit parameters, t_h is the length of load holding segment

The relaxation modulus *R(t)* is derived from the creep compliance *J(t)* employing aforementioned correspondence principle Applying Laplace transform to Equation 3.13 and considering the relation between creep compliance and relaxation modulus function in transform domain (Equation 3.14), the Equation for Relaxation modulus *R(t)* (Equation 3.15) was derived by performing inverse Laplace transform in Wolfram Mathematica (Figure 3.3)

$$\overline{R(s)} = \frac{1}{s^2\, \overline{J(s)}} \qquad \text{Equation 3.14}$$

$$R[t] = \frac{R_0\left(R_s(e-1)+R_0\left(R_2R_3+R_1(R_2+R_3)\right)e^{-\frac{eR_0t(R_2R_3+R_1(R_2+R_3))+eR_s(t-t_h)+R_s(t_h-t)}{(1-e)R_st_h}}\right)}{R_s(e-1)+eR_0\left(R_2R_3+R_1(R_2+R_3)\right)} \qquad \text{Equation 3.15}$$

Where, R_0, R_1, R_2, R_3 are fit parameters and $R_s = R_1\, R_2\, R_3$

The derived solution is cross validated by feeding the relaxation fit parameters of relaxation modulus (Eq.15) into the creep solution to obtain creep compliance curve (Figure 3.4)

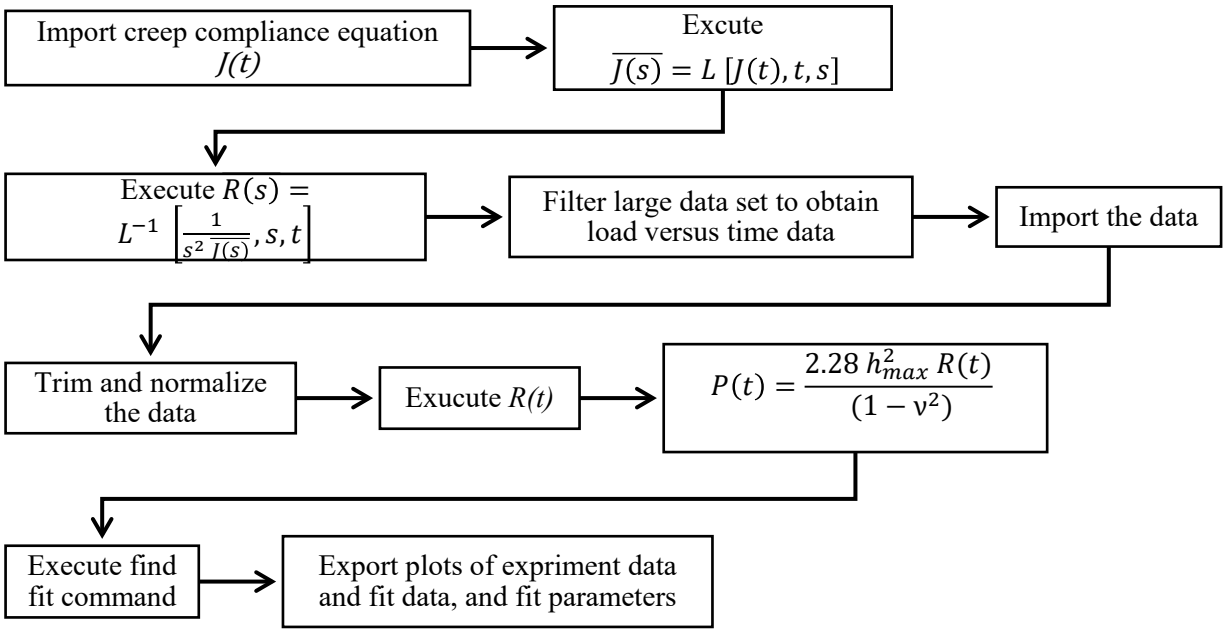

Figure 3.3 Flowchart for Mathematica code to fit the relaxation data.

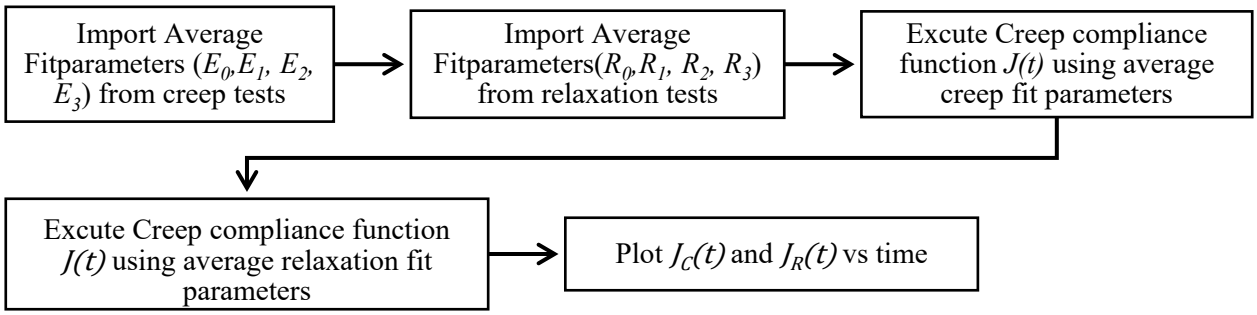

Figure 3.4 Flowchart for Mathematica code to obtain $J_C(t)$ and $J_R(t)$ vs time plot.

3.3 Experimental

The closed form analytical solutions derived in Section 3.2 is successfully verified for the indentation problem and applied to nanoindentation based creep and stress relaxation tests of cement paste and standard polycarbonate sample. The section presents in detail the preparation of cement paste and standard polycarbonate sample. The process of performing the statistical nanoindentation load and depth-controlled tests is also detailed in the following section.

3.3.1 Sample Preparation

For the purpose of this research, a sample of TYPE I/II cement with a water to cement ratio (w/c) of 0.35 was cast. Cylindrical plastic mold of 45 mm length and 17 mm diameter were filled with the paste. The sample was cured for 28 days in a 100% relative humidity condition devoid of extrusion before being placed in the moisture room. The Isomet diamond saw was used to cut the cured specimen into small discs of size approximately 17 mm diameter and 3 mm thickness with water as lubricant at a medium speed. The discs were allowed to air dry at ambient temperature till the time of testing. Considering the importance of polishing process for nanoindentation, the sample was impregnated with epoxy resin and after the epoxy is hardened, the exposed surface of specimen discs was polished using FEMTO 1100S polishing machine. Silicon-carbide abrasive discs with grit size ranging from 180 to 1000 was used for grinding and coarse polishing. The fine polishing of specimen was done using diamond lapping discs of size 3 μm, 1 μm, and 0.5 μm. The polishing machine wheel was maintained at a speed of 200 RPM, down-force of 18N to 22N and the sample and machine was allowed to rotate in the clockwise direction. To minimize dissolution of water-soluble hydration products, alcohol was used as lubricator during polishing. The time spent on each polishing disc is documented in (Table 3.1) below [91].

Table 3.1: Description of polishing process adopted.

Time (min)	0.5	0.5	1	1	30	30	120	45	45	45
Abrasive Grit / Size	180	240	320	400	600	800	1200	3 μm	1 μm	0.5 μm

3.3.2 Nanoindentation Based Creep and Relaxation Test

To perform statistical nanoindentation based creep and relaxation tests, a Hysitron Triboindenter model TI Premier was used. The nanoindenter is fitted with Berkovich tip, which is a three sided, diamond pyramidal probe with a half-angle of 65.35^{o}. Creep tests were carried out using a trapezoidal load function with three segments in load-controlled feedback mode. Load was increased from 0 μN to 1695 μN in five seconds, then held steady for 30s before being reduced to 0 μN in another five seconds. During relaxation tests, displacement-controlled feedback mode was used and a critical depth of 180 nm corresponding to the critical load [91]

was maintained constant for 30 s. To compare the test results of cement paste sample and validate the analytical solution derived for nanoindentation based relaxation test from creep using correspondence principle, similar tests with the same load function were performed on the standard polished polycarbonate sample. Table 3.2 summarizes the design parameters selected to perform the statistical nanoindentation based creep and relaxation tests.

Table 3.2 Summary of nanoindentation based creep and relaxation test.

Test	Sample	Load / Depth	Grid (μm)	
			Spacing	Size
Load Controlled	Cement paste	1695 μN	3	10 × 10
	Polycarbonate	164 μN	3	5 × 5
Displacement Controlled	Cement paste	180 nm	3	10 × 10
	Polycarbonate	180 nm	3	5 × 5

3.4 Results and Discussion

The time dependent stress relaxation and creep of cement paste is considered to be the dominant mechanism leading to concrete creep and relaxation [92]. Thus, in the present study, a statistical nanoindentation based load and depth-controlled tests were performed on cement paste and polycarbonate sample. Figure 3.5 and 3.6 displays the plot of experimental and fit creep data of an individual indent of cement paste and polycarbonate sample respectively and confirms that Equation 3.6 yields a good fit. In both the cases the r^2 value for curve fitting was more than 0.98.

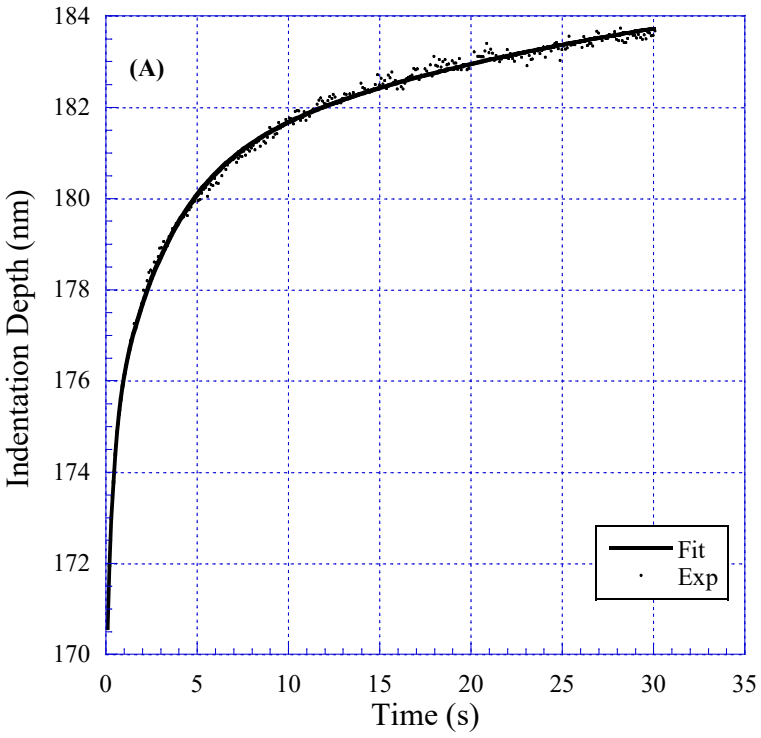

Figure 3.5 Plot of nanoindentation depth vs time for a typical 30 s experiment of cement paste, with the fit function included for comparison.

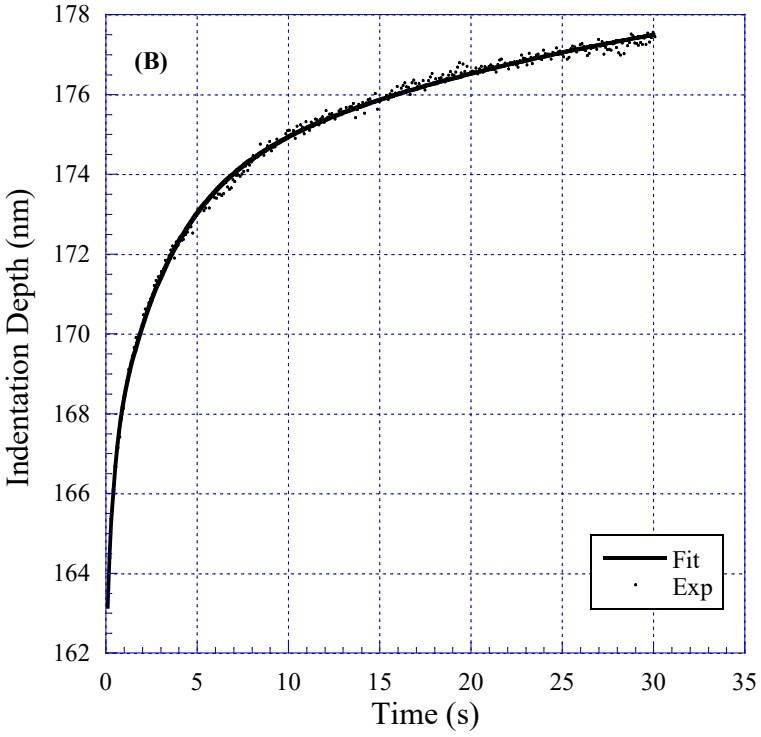

Figure 3.6 Plot of nanoindentation depth vs time for a typical 30 s experiment of polycarbonate, with the fit function included for comparison.

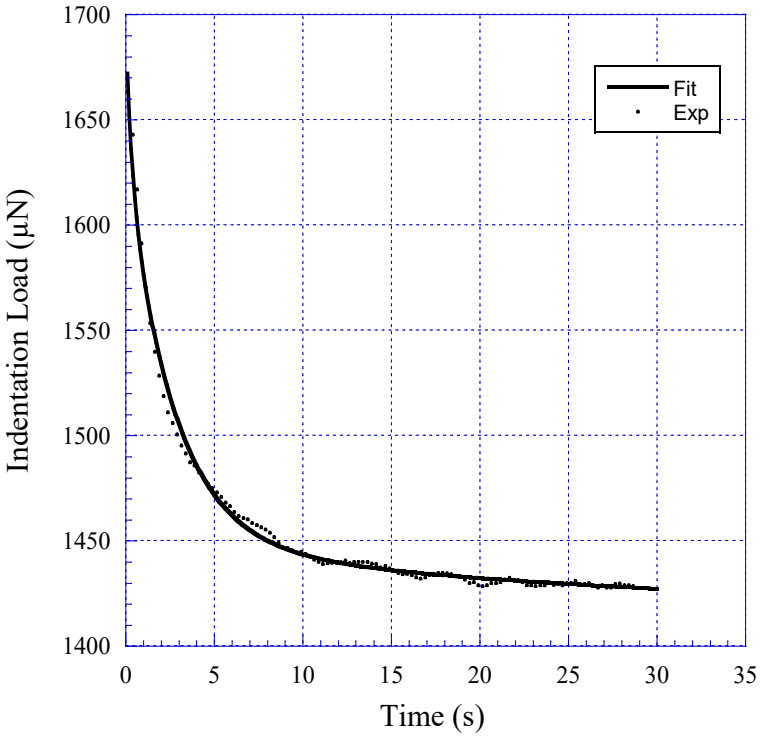

Figure 3.7 Plot of nanoindentation load vs time for a typical 30 s experiment of cement paste, with the fit function included for comparison.

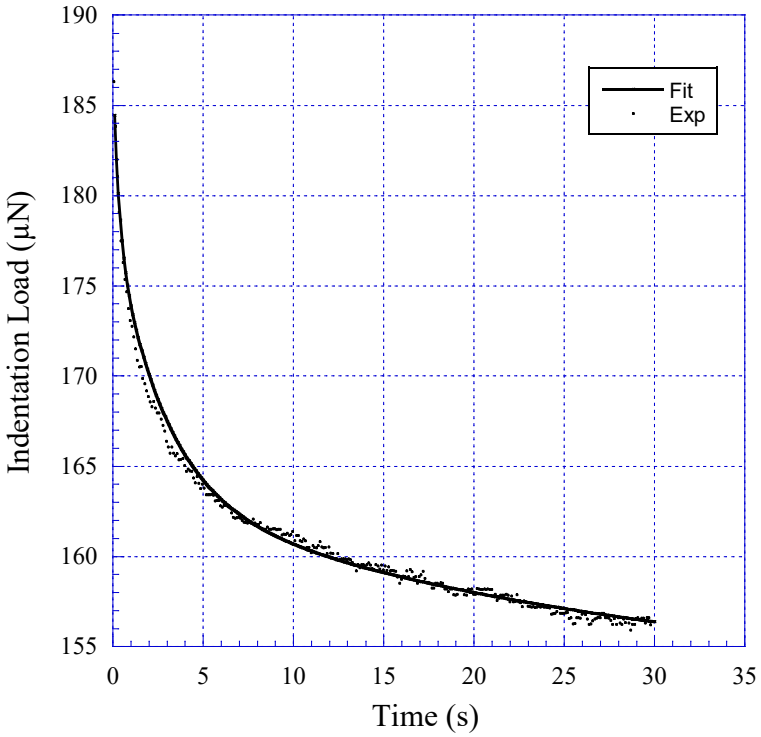

Figure 3.8 Plot of nanoindentation load vs time for a typical 30 s experiment of polycarbonate, with the fit function included for comparison.

As Figure 3.7 and 3.8 shows, it appears that the solution (Equation 3.12) derived using correspondence principle is applicable for relaxation data and indicates general agreement between the experimental and the fit relaxation data with a r^2 value greater than 0.98.

Thus, on a statistical basis it is evident that the fitted data and experimental data from creep and relaxation tests exhibit strong convergence. The relaxation modulus of standard polycarbonate at 30 s for all the 25 depth-controlled indentations is approximately $R(t=30s)$ = 1.995 GPa and the value is comparable to the $R(t)$ of 2.224 GPa obtained by three-point bending relaxation test at 30^0C [93]. Figure 3.5, 3.6, 3.7, and 3.8 demonstrate that the analytical constitutive solution, which was developed using the Laplace transform and inverse transform in conjunction with the assumption of linear viscoelasticity and time independent Poisson's ratio, effectively captures the creep and relaxation behavior and establishes its applicability to both homogeneous (polycarbonate) and relatively less homogeneous materials (cement paste). Signal to noise ratio is better in relaxation test compared to the creep tests for same testing time, load is less noisy compared to the depth (Figure 3.5 to 3.8). This might be because in nanoindentation creep testing, the load, rather than the stress, is maintained constant.

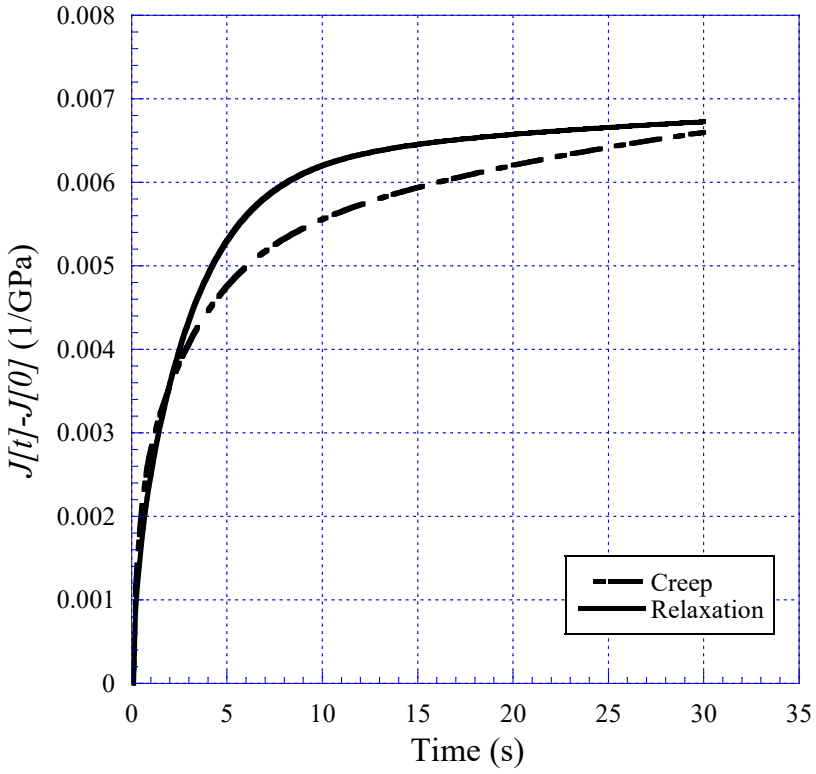

Figure 3.9 Experimentally obtained $J(t)$-$J(0)$ versus approximation as the inverse of an experimentally obtained relaxation function for cement paste.

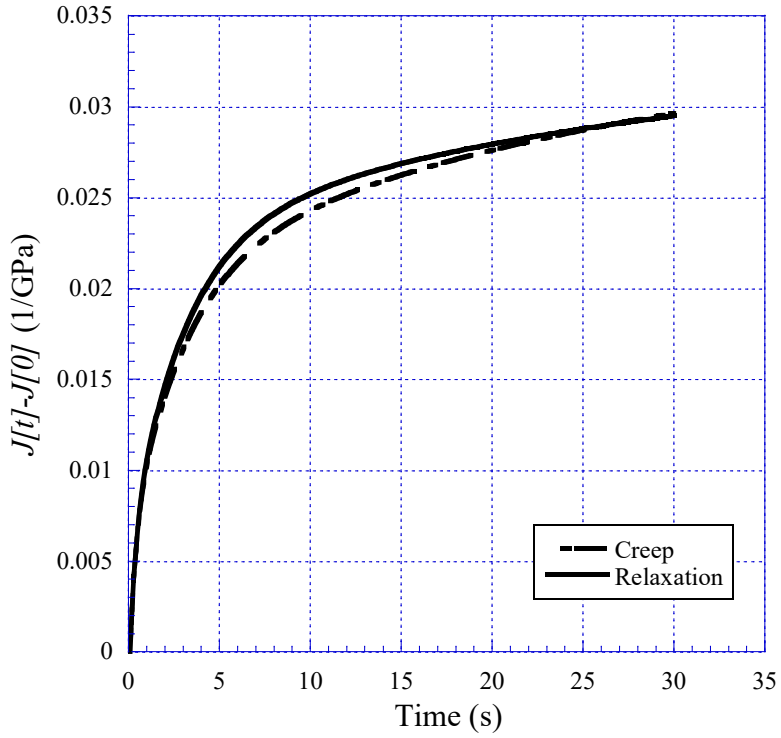

Figure 3.10 Experimentally obtained $J(t)$-$J(0)$ versus approximation as the inverse of an experimentally obtained relaxation function for polycarbonate.

To address the creep behavior of the cement paste, the most commonly used creep compliance $J(t)$ parameter is calculated. The experimentally obtained creep compliance calculated using Equation 3.13 and the inverse of relaxation function through inverse Laplace Transform, which was measured during the relaxation test show a reasonable correlation and indicates that the nanoindentation based relaxation test data could be used to obtain the creep compliance. The normalized creep compliance data from 30 s creep and stress relaxation test was statistically tested using F test. The p-value was greater than α (0.05), suggesting no difference between the data in both the samples.

It can be seen that after approximately 3 seconds the relaxation solution starts to deviate (higher) from the creep compliance of polycarbonate and cement paste sample (Figure 3.9 and 3.10). The deviation is significant in cement paste sample compared to polycarbonate. Even though the inverse of the compliance function initially deviates from the creep function, it eventually tends to converge to the true creep compliance value $J(t)$. Thus, the author believes that nanoindentation studies with a longer holding segment are required to verify this trend.

To explain the difference in creep and relaxation solution, the average stress decay was plotted against holding time with one standard deviation error bars (Figure 3.11 and 3.12). Plot

shows that a difference in the stress decay exists between the creep and relaxation tests. The difference is observed approximately after 3 seconds similar to the creep compliance curve (Figure 3.9 and 3.10) and is more prominent in cement paste sample compared to polycarbonate. The rate of stress decay is more in relaxation test and possibly explains the deviation of creep compliance curve from relaxation solution observed in Figure 3.9. The tip shape geometry of Berkovich probe and its sensitivity to different microstructural mechanisms of cement paste and polycarbonate is a possible contributor to stress decay observed in relaxation test.

Also, creep in cementitious materials is known to be sensitive to rate of loading, below a threshold stress level, the cement paste continues to creep and above the threshold the curve appears to remain constant [94]. The complex and heterogeneous microstructure of cementitious materials contribute to more pronounced stress decay difference creep and relaxation data in paste compared to the homogeneous polycarbonate sample.

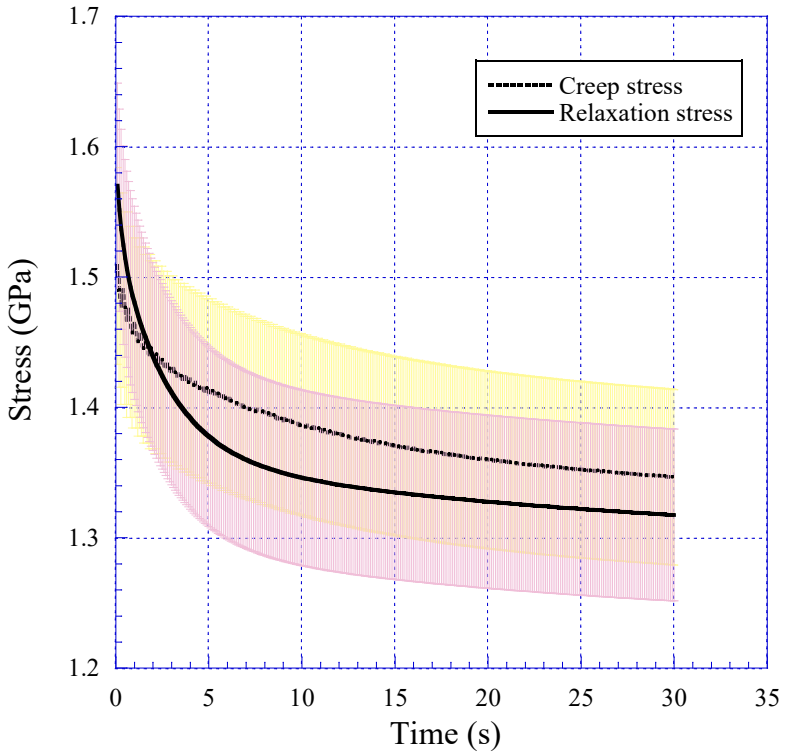

Figure 3.11 Rate of stress decay in creep and relaxation test of cement paste.

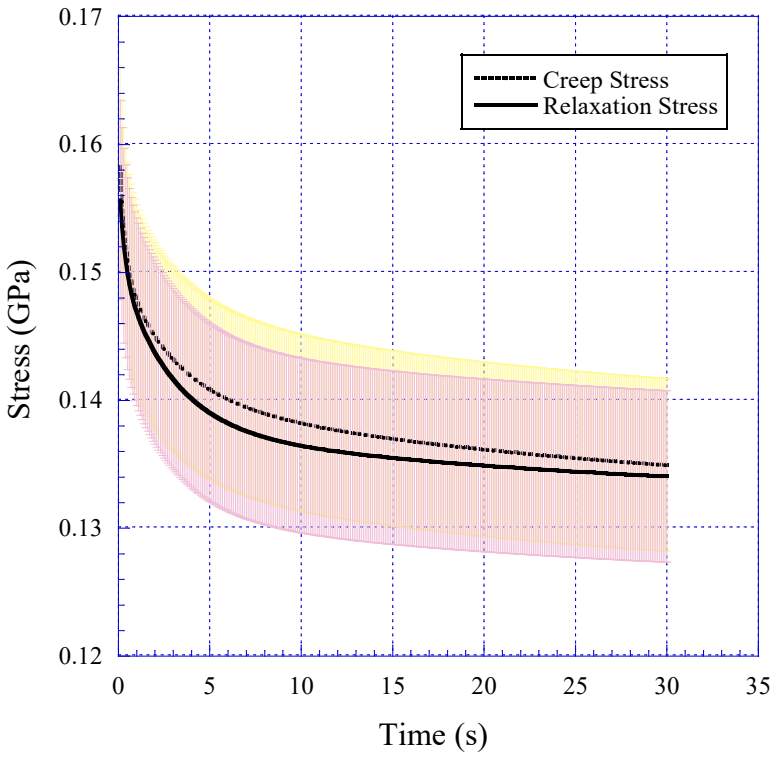

Figure 3.12 Rate of stress decay in creep and relaxation test of polycarbonate.

Table 3.3 Average fit parameters and reduced modulus.

Sample	**Test**	**Average Fit Parameters (GPa)**				**Reduced Modulus (GPa)**
		E_0	E_1	E_2	E_3	E_r
Cement Paste	Creep	27.684	806.854	537.522	589.073	43.096
	Relaxation	24.315	1456.89	315.527	1592.671	43.494
Polycarbonate	Creep	2.286	72.924	36.681	60.023	3.152
	Relaxation	2.334	71.065	41.935	45.712	3.182

The average fit parameters for creep and relaxation tests are listed in Table 3.3. The mean reduced modulus from creep and relaxation nanoindentation test for cement sample is 43 GPa (Table 3.3) which is in good agreement with the actual value of 30 – 45 GPa [50, 91]. Polishing the samples using isopropyl alcohol rather than water as lubricator resulted in slightly increased values of E_r for the cement paste than was shown in some earlier studies [46]. The reduced modulus for standard polycarbonate sample is 3.6 (Table 3.3) and is in accordance with the typical range of 2.7 – 3.2 GPa [48]. The solutions appear to be interconvertible and successful in

capturing the viscoelastic behavior, suggesting that nanoindentation is an effective tool for performing relaxation tests.

3.5 Conclusions

Closed loop feedback control was used to conduct statistical nanoindentation-based creep and stress relaxation tests on cement paste sample. The study is also coupled with load and depth-controlled tests on polycarbonate to enhance understanding and comparison of the model to analyze viscoelastic behavior. An elastic-viscoelastic correspondence principle is utilized to develop constitutive analytical solution for time dependent creep and stress relaxation properties. The work demonstrates that the Laplace transform, and inverse transform may be performed analytically, yielding compact equations for creep compliance and relaxation modulus. Recognizing that the relaxation function of the materials under study can actually be obtained or approximated as the inverse of the compliance function in the Laplace transform domain, the relaxation function which accurately characterize the stress relaxation in cement paste is developed. A good agreement between the analytical solution with that observed experimentally validates the theoretical/experimental framework for viscoelastic nanoindentation with r^2 value greater than 0.98 in all the cases for both samples. In addition, the study closes the loop by getting creep compliance curve from relaxation solution, thus cross validate the solution.

The results demonstrate that nanoindentation tool can be effectively used to characterize the viscoelastic behavior of both homogeneous and inhomogeneous materials in which properties vary spatially. With the assumption of linear viscoelasticity and time-invariant Poisson's ratio, the constitutive analytical solution obtained is restricted in its application. Relaxation tests show a higher stress decay rate than creep testing, which is likely due to the Berkovich tip shape geometry and stress level sensitivity exhibited by the materials. This approach minimizes the high level of equipment and operating requirements. Direct relaxation measurement with corresponding closed form analytical solution offers better approach for extracting relaxation data and can be employed for future investigation of viscoelastic behavior of cementitious materials. Further the author advocates that the future research should involve other tip geometries to robustly validate the solution derived.

Chapter 4 - Investigation of Viscoelastic Properties of Irradiated Cement Paste Using Statistical Nanoindentation

4.1 Introduction

Due to its structural performance, radiation shielding capacity and irradiation resistance, concrete is widely used in nuclear power plants [95]. Due to the long-term exposure of such concrete components to radiation and temperature, it is vital to study the degradation of irradiated concrete. Neutron radiation and gamma-ray radiation are the two principal sources of radiation that degrade concrete. It is considered that neutrons interact with subatomic particles, the lattice spacing inside the material may alter as a result of the impact, mostly affecting the aggregates, whereas gamma radiation considerably affects the cement paste through radiolysis [96]. Long-term operation of nuclear power plants has prompted research in long-term aging effects in concrete and metallic structures. Radiation effects on concrete structures is one of the numerous concrete aging degrading mechanisms relevant to long term plant operations [97]. Reviewing the literature, it can be seen that the influences of these radiations are studied individually to assess the mechanical properties of concrete [70, 98]. Many studies documented reduction in the strength, and modulus of elasticity of irradiated concrete [99, 100], but fail to address the question whether this deterioration is due to temperature or radiation.

It is very well known that concrete is a viscoelastic material that exhibits creep and stress relaxation characteristics with aging [101, 102]. Creep influences long-term crack growth by relaxing stresses in the cement paste [103] altering the damage pattern in the structural component along with substantial deformations and deviations from the projected position of the structure [104]. Radiation-induced volumetric expansion (RIVE) occurs when fast neutrons amorphize the minerals in aggregates. RIVE causes stresses to build up in the hardened cement paste, which are then relieved by cracking or relaxation [105, 106]. On the other hand, radiolysis due to gamma radiations is the significant factor impacting the water in the cement paste. This dehydration due to exposure to gamma rays may also alter the creep and stress relaxation behavior of concrete/cement paste [70].

Recent studies have focused on understanding the creep and stress relaxation behavior of irradiated concrete [69, 70, 107-109]. However, the existing data is still limited, and part of it is

on bulk concrete, some on cement mortar, and some on synthetic calcium silicate hydrate (C-S-H), making it difficult to generalize the phenomena. Some studies showed that the creep of irradiated concrete at macroscopic and microscopic scale is reduced [69, 110] and other studies showed increase of creep in irradiated sample [104, 111], and some no significant change [109]. Previous research has devoted limited consideration to the direct impact of neutron and gamma irradiation on concrete creep and stress relaxation. Given the difficulty of controlling specimens and hygrothermal conditions in macroscale creep and stress relaxation experiments, the current study employs nanoindentation to perform creep and stress relaxation testing on irradiated samples.

The advantage of using nanoindentation to test the irradiated samples is twofold. Firstly, the ability to perform indentation tests at shallow depth (< 3μm), which assures the uniform radiation dosage. Secondly, the ability to obtain sufficient number of statistically significant data fairly quickly. Studying deformation at the nanoscale provides insight into macroscale long-term viscoelastic response [68]. Owing to the handful of studies and data available to address the effect of combined neutron and gamma radiation on concrete creep and stress relaxation, the present work seeks to measure and understand effects of ionizing and nonionizing radiation on concrete mechanical properties, in particular the instantaneous elastic modulus and short-term creep and relaxation modulus. Knowing that creep and stress relaxation originates from calcium silicate hydrate (C-S-H) in cement paste, statistical nanoindentation was performed on three samples with 0.3, 0.4 and 0.5 water to cement ratio (w/c) irradiated with combined neutron and gamma radiations. The reduced modulus (Er) which represents elastic deformation both in the sample and the indenter tip, creep compliance and relaxation modulus were compared with control samples.

4.2 Materials and Sample Preparation

Three samples were cast from TYPE I/II cement with w/c [91] of 0.35, 0.40, and 0.50 for the current investigation. The paste was poured into 45 mm length and 17 mm diameter cylindrical plastic molds. All of the samples were cured for 28 days in a 100 percent relative humidity condition, and none of the samples were extruded before being placed in the wet room. The specimens were removed from the cured cement paste samples by using a Isomet diamond blade saw at medium speed and water as a lubricant to cut coin size discs. The discs were let to

dry in room temperature. The exposed flat surface of the samples size 3mm thick and 17 mm diameter was polished with FEMTO 1100S automated polishing machine using silicon-carbide abrasive discs. Diamond lapping discs were used for further polishing. During this polishing process isopropyl alcohol was used as lubricant to prevent any dissolution of water-soluble hydration products, primarily calcium hydroxide. The polishing machine wheel and the specimen rotated in the same direction at a speed of 200 RPM, at a downforce of 18 to 22 N. The time of polishing on each abrasive size was varied in this (Table 3.1).

4.3 Neutron and Gamma Irradiation

Each of the three cement samples and iron wires were placed in 4 mil thick LDPE bagging and heat sealed. A second barrier of heat-sealed LDPE surrounded all samples. The LDPE provided containment of the activated materials and a water barrier. The final arrangement was placed in a HDPE sample holder as shown in Figure 4.1 Arrangement of cement samples and iron wires within sample holder. Assembly placed in central thimble of reactor for irradiation.. Samples were separated to minimize flux depression and non-uniformity. Iron wires were placed between samples to estimate flux variation across the three samples. The reactor was ramped to approximately 500kW thermal power over approximately 1.15 minutes and maintained for 1 hour. Due to cooling system and high-power operation, the reactor pool temperature varied from a low of 22.0˚C to a maximum of 32.2˚C while the samples were in the central thimble. Following a manual SCRAM, the reactor power was reduced to less than 50 kW (10% of steady state) within 0.08 minutes. Samples were removed from the reactor core region within 17 minutes. Thus, the samples were irradiated for approximately 60 +/- 2 minutes. The irradiation dose was estimated from iron co-witness wires. An estimate of the neutron flux during irradiation was determined by analyzing the activation of each iron wire. Thermal neutron flux was calculated based on the activation of Fe-58 to Fe-59. The average thermal neutron flux across the three wires was 2.34×10^{12} +/- 1.06×10^{11} cm^{-2} sec^{-1}. Using the threshold reaction for Fe-54 to Mn-54 ($E_{threshold}$ = 0.8 MeV, $E_{average}$ =2.8 MeV), the average fast flux for the three wires was 2.77×10^{12} +/- 1.93×10^{11} cm^{-2} sec^{-1}. For the one-hour irradiation, the thermal fluence was 8.43×10^{15} +/- 3.82×10^{14} n cm^{-2} and the fast fluence was 9.97×10^{15} +/- 6.93×10^{14} n cm^{-2}. From the KSU TRIGA Mark II Research Reactor training manual, the gamma dose rate at 500 kW power is 5.0×10^{4} rad sec^{-1} resulting in a total dose of 180 Mrad for a one-hour irradiation.

Prior to irradiation the cement samples elemental mass was estimated based on the cement mill certificate. The resulting quantities of each element were individually assessed for activation using the NIST Database/Tool and a decay period of 60 days was determined. To allow for safe removal of the activated materials, samples were moved to a position in the central thimble outside of the core region (negligible neutron flux) for initial radioactive decay. After decaying in the central thimble for nine days, the samples were stored in a lead box in an administratively controlled cabinet in the K-State Reactor facility. After 60 days the samples were removed and surveyed, and the resulting gamma readings were within the expected levels. The samples were then transferred to the K-State nanoindentation facility. Samples were stored a controlled laboratory environment of approximately 23˚C and 40% RH for the duration of the post-irradiation decay and subsequent nanoindentation testing.

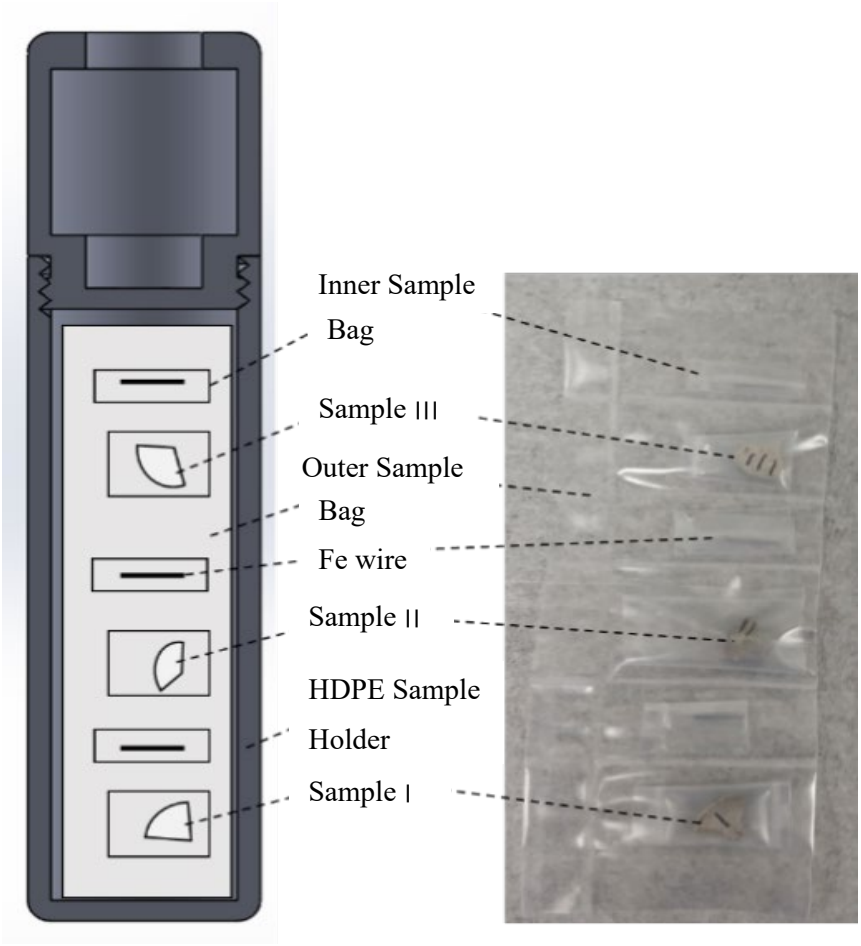

Figure 4.1 Arrangement of cement samples and iron wires within sample holder. Assembly placed in central thimble of reactor for irradiation.

4.4 Nanoindentation Testing

The Hysitron Triboindenter model TI Premier was used to perform the nanoindentation testing. A typical Berkovich probe was used to make basic elastic indents with trapezoidal load function of 5s loading, 2s holding and 5s unloading to determine the critical depth and corresponding critical load, the load was varied from 500 μN to 5000 μN [91]. Table 4.1 below details the maximum critical load used to perform reference creep test on control and irradiated samples with varying w/c ratio. the second (longer) reference frequency segment of the step load function is analyzed as the creep. This technique is insensitive to changes in drift rates and allows tests to run over long durations of time. During relaxation tests, displacement-controlled feedback mode was used, and the maximum critical depth used are tabulated (Table 4.1).

Creep and relaxation tests with minimum were performed on irradiated samples using a load and depth control feedback gain with achieving maximum load/depth in 5s, maintaining it steady for 30s, and unloading for 5s. Statistical creep nanoindentation with 10 x 10 grid size and 3 μm spacing was employed, and the corresponding data of depth versus time and the E_r [16] was recorded. The time dependent creep compliance and relaxation modulus curves are plotted to compare the test results of controlled and irradiated cement paste sample using the closed form analytical solution (Equation 3.13 and Equation 3.15).

Table 4.1 Summary of nanoindentation based creep and relaxation test.

Sample	**Creep Test Max. Load (μN)**		**Relaxation test Max. Depth (nm)**	
	Controlled	Irradiated	Controlled	Irradiated
0.35	1695	1900	180	250
0.40	1800	2500	275	350
0.50	2695	3225	300	400

4.5 Results and Discussions

The strength, stiffness, and viscoelastic behavior of the cement paste are determined by the hydrogen bonding of the water inside the layers with C-S-H hydration product. Thus, the E_r, the short-term creep compliance, and the relaxation modulus obtained from creep and relaxation based statistical nanoindentation of irradiated with combined neutron and gamma radiations and

control cement paste samples are compared. It can be clearly seen that the E_r value obtained from both creep and relaxation test is significantly reduced for all three irradiated cement paste sample compared to the control (Table 4.2).

Table 4.2 Reduced Modulus (E_r) of irradiated and control cement paste sample.

		Mean Reduced Modulus, E_r (GPa)		
Sample (w/c)		**0.35**	**0.40**	**0.50**
Control		48.87	47.83	32.39
Irradiated	Relaxation test	18.31	16.63	9.28
	Creep test	19.06	16.50	8.22

Figure 4.2 to 4.7 presents the box and whisker plot for the E_r of irradiated and control cement paste samples. In contrast to prior research [69, 70], the results demonstrate a 61 % drop in E_r value in 0.35 w/c, 65 % in 0.40 w/c, and 75 % in 0.50 w/c in irradiated samples as compared to control samples.

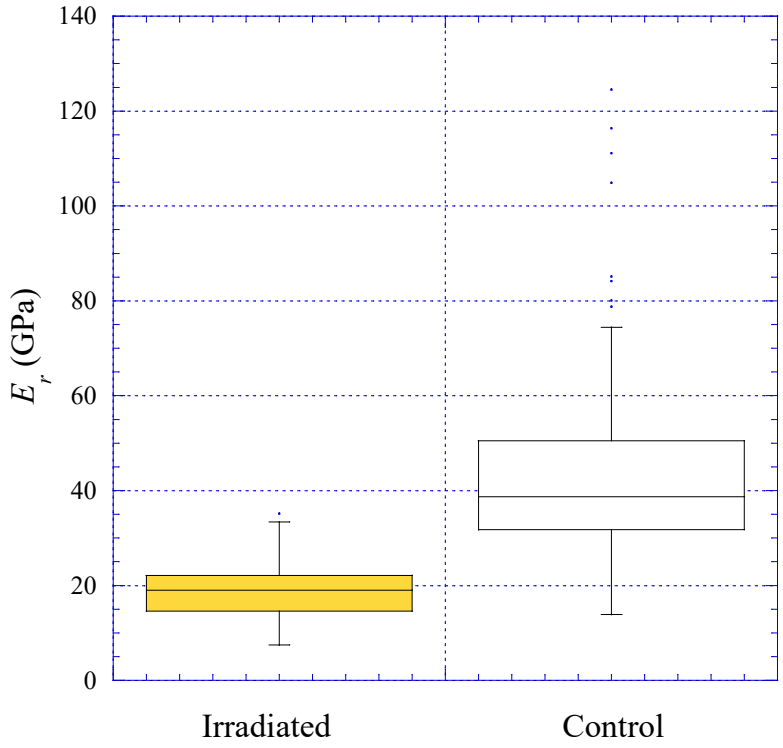

Figure 4.2 The box and whisker plot for mean E_r of 0.35 w/c irradiated and control cement paste sample obtained from creep nanoindentation test.

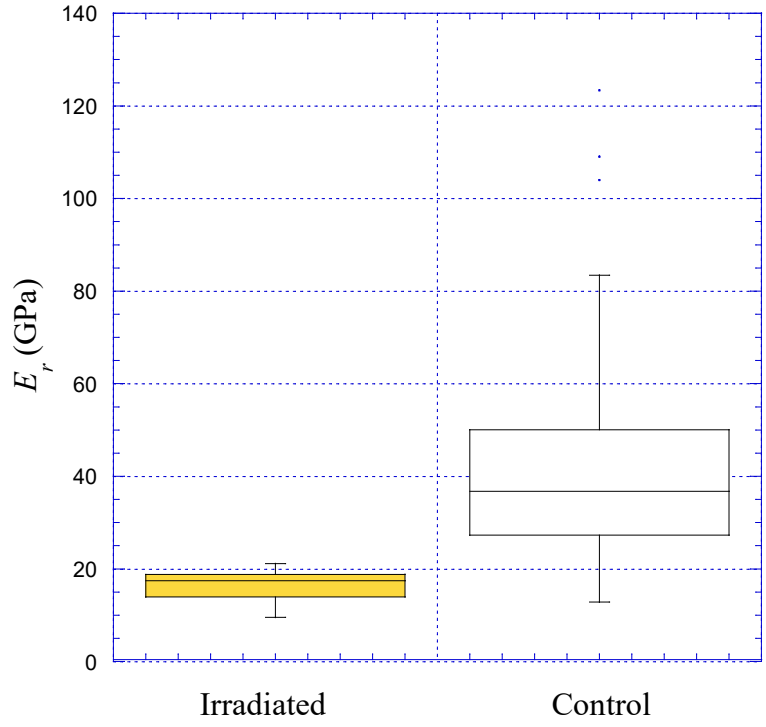

Figure 4.3 The box and whisker plot for mean E_r of 0.40 w/c irradiated and control cement paste sample obtained from creep nanoindentation test.

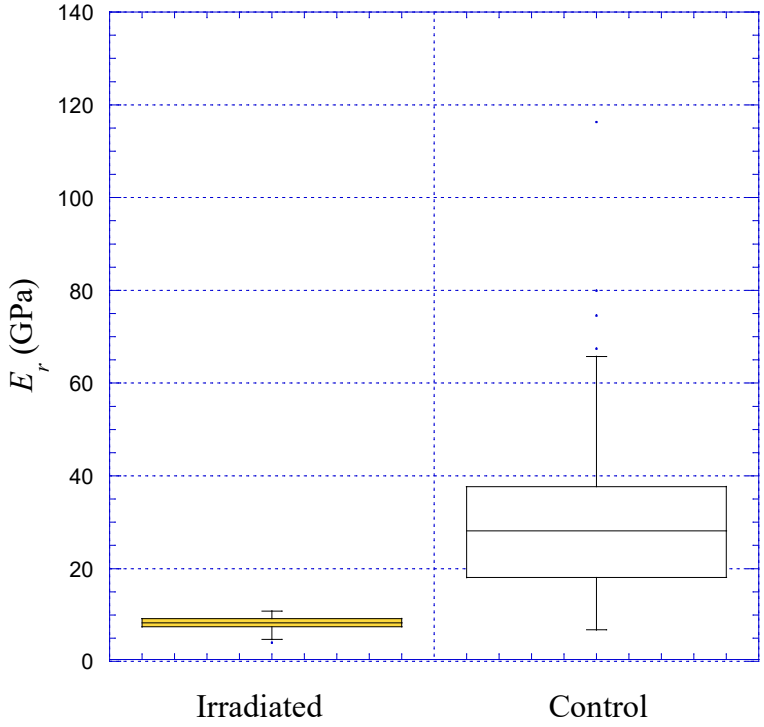

Figure 4.4 The box and whisker plot for mean E_r of 0.50 w/c irradiated and control cement paste sample obtained from creep nanoindentation test.

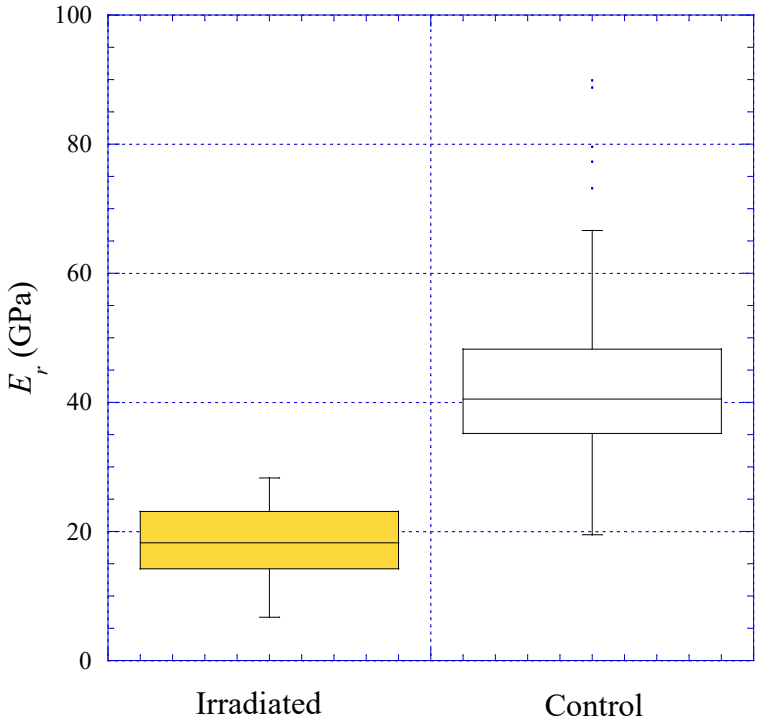

Figure 4.5 The box and whisker plot for mean E_r of 0.35 w/c irradiated and control cement paste sample obtained from relaxation nanoindentation test.

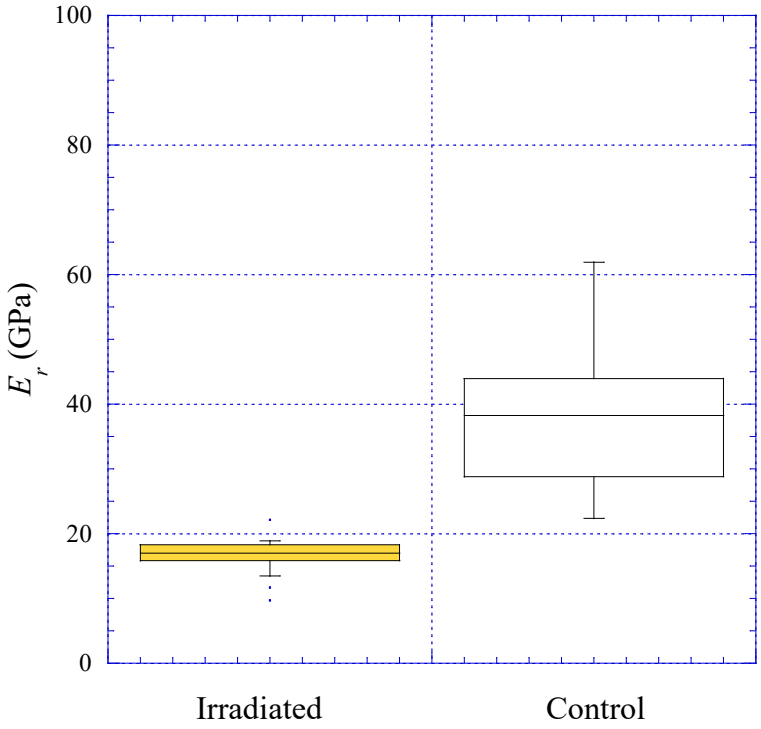

Figure 4.6 The box and whisker plot for mean E_r of 0.40 w/c irradiated and control cement paste sample obtained from relaxation nanoindentation test.

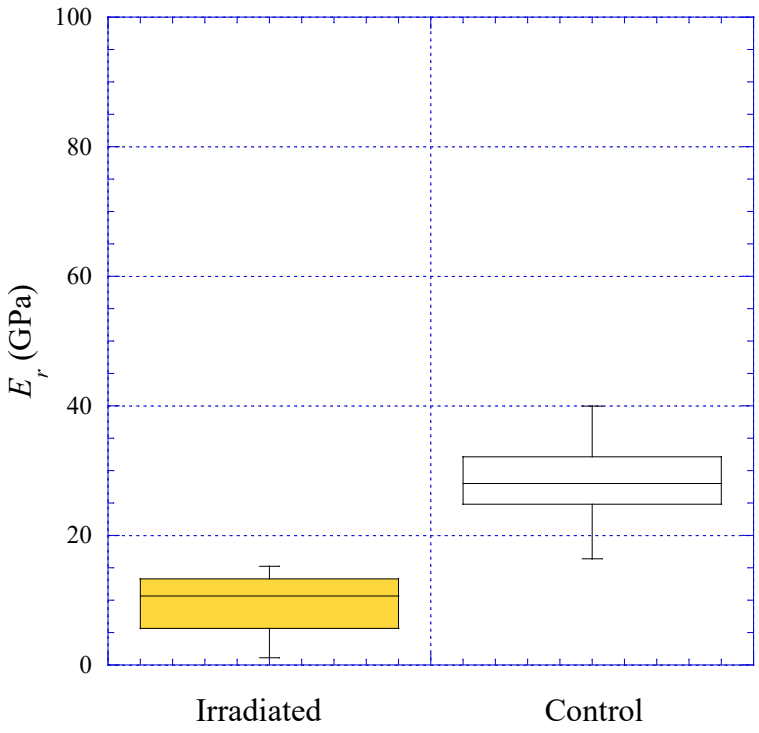

Figure 4.7 The box and whisker plot for mean E_r of 0.50 w/c irradiated and control cement paste sample obtained from relaxation nanoindentation test.

The data was tested for normality using the Kolmogorov-Smirnov test [112]), and it was discovered that the data was not normally distributed. Mann Whitney U test [113], which is used when the data are not normally distributed was employed with a confidence level of 95% to test the significance of the data obtained. The nonparametric test showed that the difference between the E_r data of irradiated and control sample is statistically significant with p-value vanishingly small ($p<0.05$) for all the samples.

The decrease in the stiffness of irradiated samples can be related to the somewhat influence of neutrons on the water phase of cement paste even [114]. Despite the fact that the neutron fluence (1.95×10^{16} n cm^{-2}) was less than the reference level of 1×10^{19} n cm^{-2} [99], the considerable loss in E_r reported may be attributed to the sample's uniquely elevated sensitivity to damage as a result of pre-polishing prior to irradiation and small specimen size. It should be noted that neutron penetration depth is shallow in bulk concrete as the concrete acts as an effective shield. Thus, nanoindentation appears to be an efficient tool to study the neutron effect on the elastic modulus as it is noted that the first layer of concrete (10–50 cm) is where thermal neutrons generate heat [115] and NI is capable of indenting shallow depth (<3μm).

A number of studies attributed reduction in concrete stiffness to the neutron irradiation [99, 114, 116]. When a neutron collides with a nucleus, the neutron loses energy while the nucleus emits dispersed gamma rays and ejects a neutron [96]. Since in the present study the samples are irradiated with both neutron and gamma radiation, the decrease in E_r can be explained majorly by the radiolysis caused by gamma radiations. Also, cement hydrates undergo amorphization because of gamma radiation absorption, which causes them to disintegrate leading to decreased modulus. It is noted in the literature [97] that nuclear heating occurs due to attenuation of radiation by sample and this increased temperature changes the pore structure of the sample producing microcracks which adversely affect the mechanical properties. Unhydrated cement may be further hydrated by gamma heating, accelerating the production of C-S-H. However, in the current investigation, the maximum temperature observed during irradiation was 32.2˚C, implying that the combined neutron and gamma radiation is the primary contributor to the deteriorating impact on the modulus of the cement paste sample.

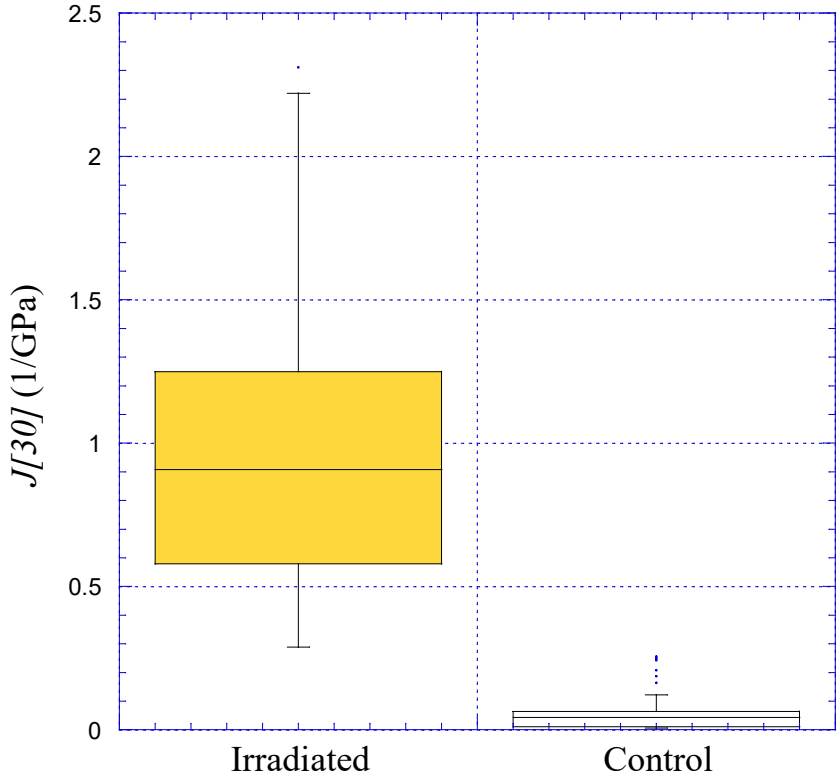

Figure 4.8 Box and whisker plot of creep compliance 0.35 w/c for irradiated and control cement paste samples at 30 seconds.

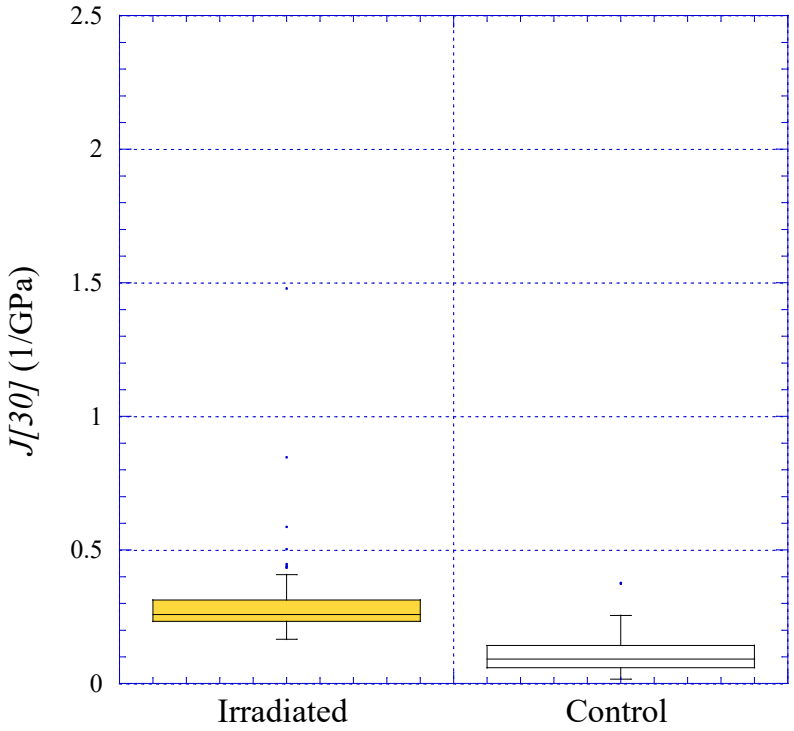

Figure 4.9 Box and whisker plot of creep compliance for 0.40 w/c irradiated and control cement paste samples at 30 seconds.

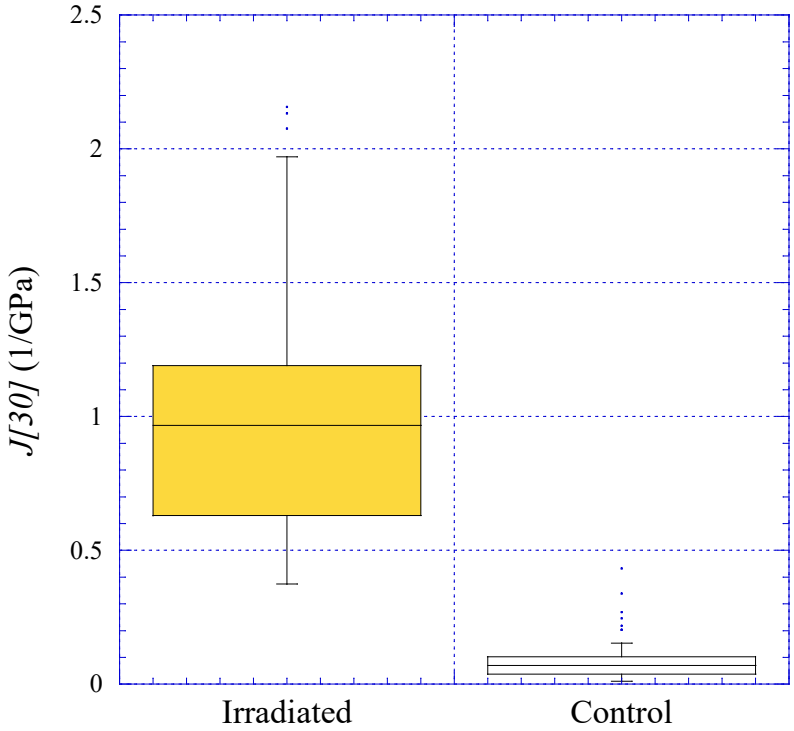

Figure 4.10 Box and whisker plot of creep compliance for 0.50 w/c irradiated and control cement paste samples at 30 seconds.

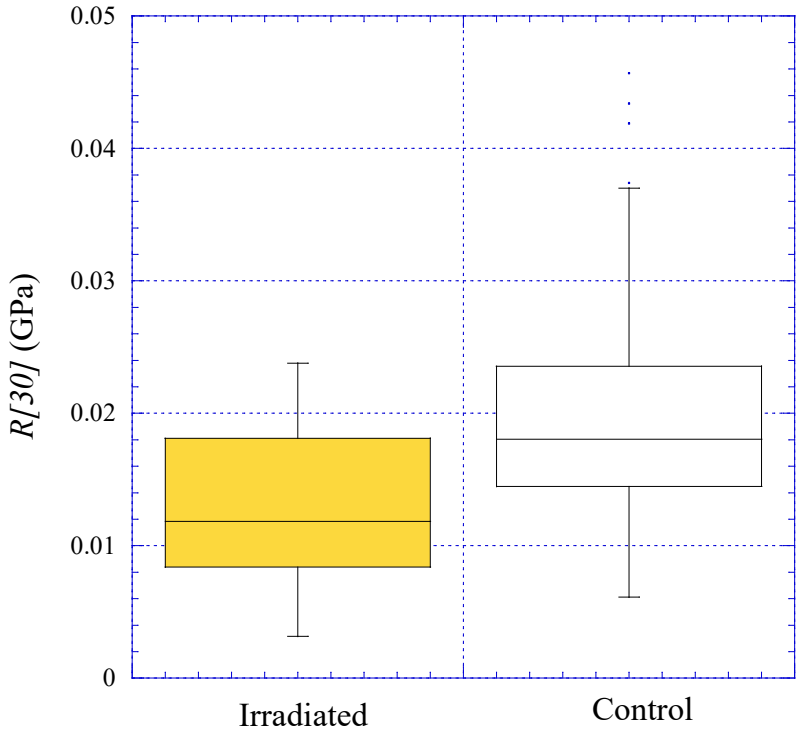

Figure 4.11 Box and whisker plot of relaxation modulus for 0.35 w/c irradiated and control cement paste samples at 30 seconds.

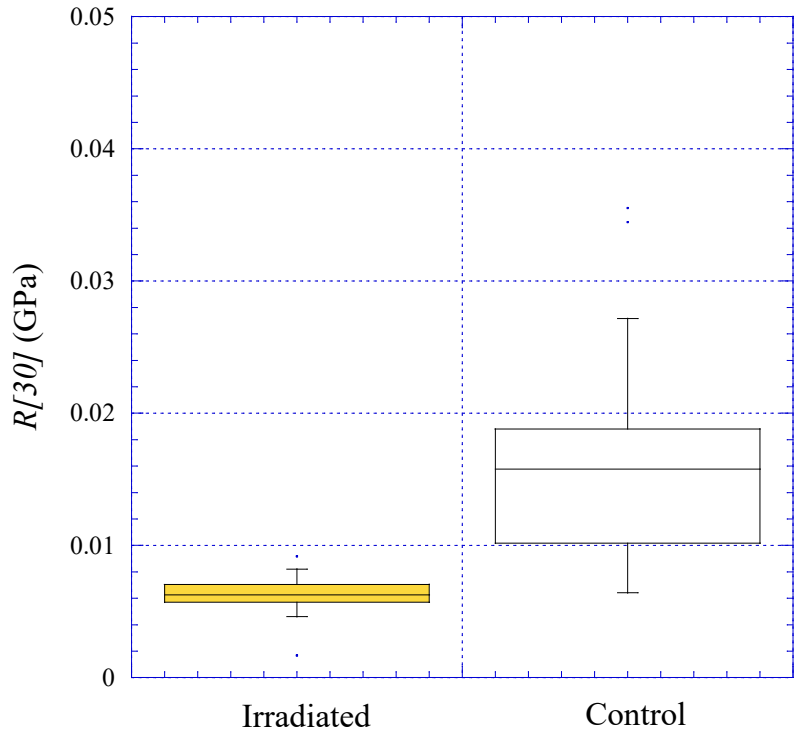

Figure 4.12 Box and whisker plot of relaxation modulus for 0.40 w/c irradiated and control cement paste samples at 30 seconds.

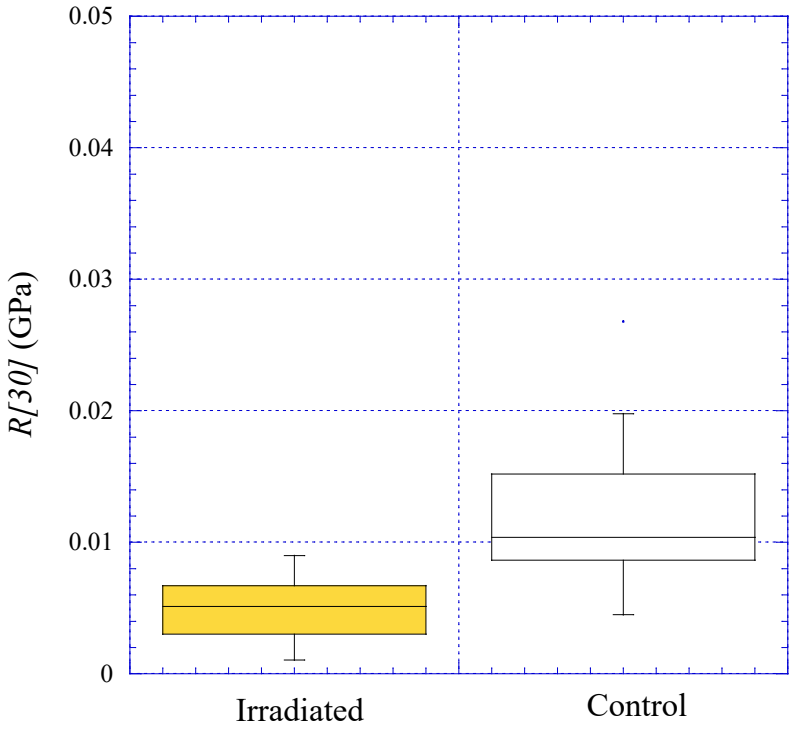

Figure 4.13 Box and whisker plot of relaxation modulus for 0.50 w/c irradiated and control cement paste samples at 30 seconds.

The radiolysis of water in cement paste due to gamma radiation influences the microstructure of C-S-H and the change is majorly observed at nanoscale [117]. Thus, the data obtained from statistical reference creep and relaxation nanoindentation tests on the irradiated and control cement paste samples are analyzed and presented in the study. The creep compliance *J[t]* and relaxation modulus *R[t]*of irradiated and control sample at 30 second holding time obtained from 100 indents is presented in the form box whisker plot as shown in Figure 4.8 to 4.13.

The results indicated that the creep compliance of irradiated samples is higher than the control samples and is true for all the samples (Figure 4.8 to 4.10). Similarly, it is shown in Figure 4.11 to 4.13 that the relaxation modulus of irradiated samples is decreased compared to control samples and the percentage of decrease is increased with w/c ratio. The statistical significance of the non-normal creep data at 30 second holding time was tested using Mann Whitney U [113] test with confidence level of 95% and it was evident from the test that data from irradiated and control samples are significantly different.

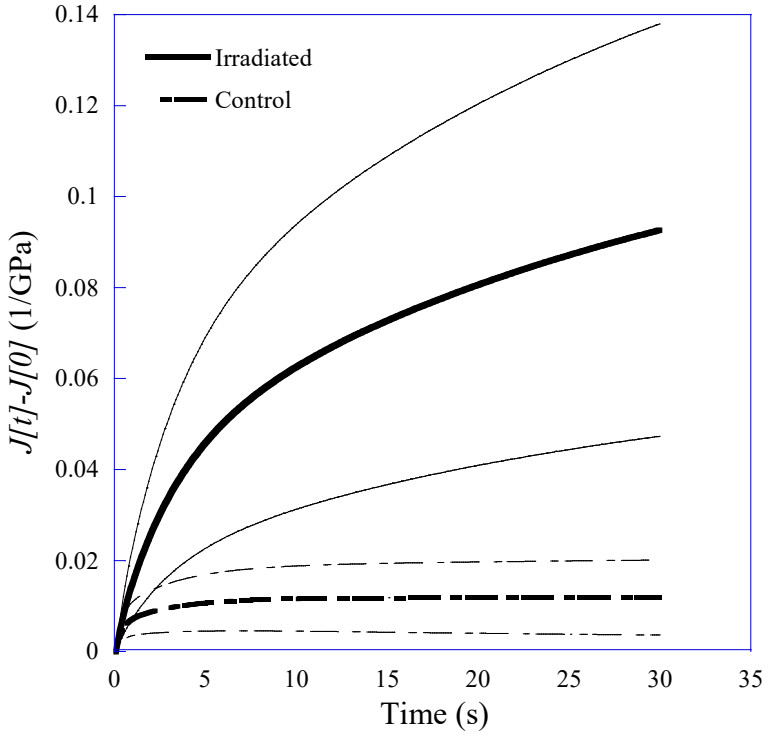

Figure 4.14 Normalized creep compliance of 0.35 w/c irradiated and control cement paste.

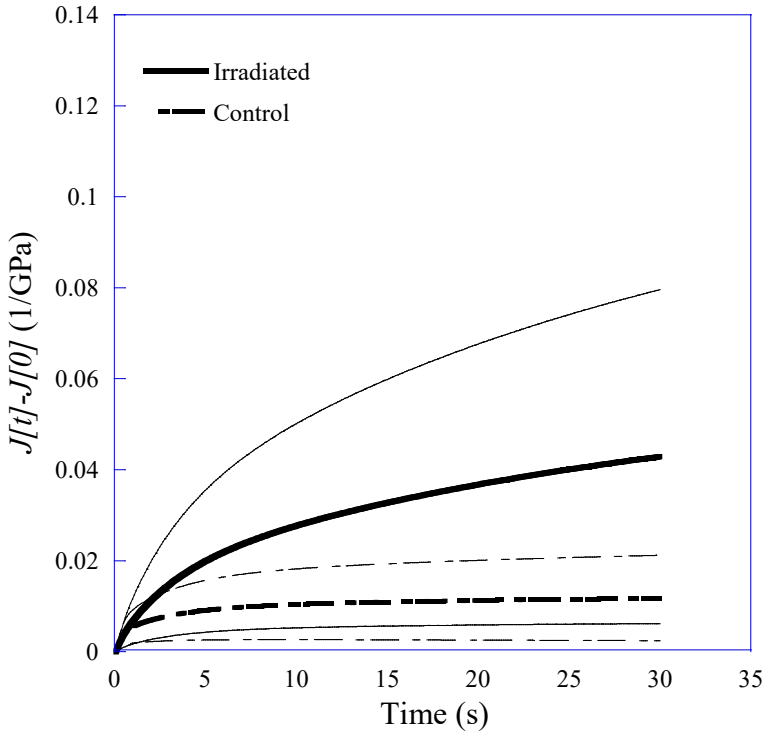

Figure 4.15 Normalized creep compliance of 0.40 w/c irradiated and control cement paste.

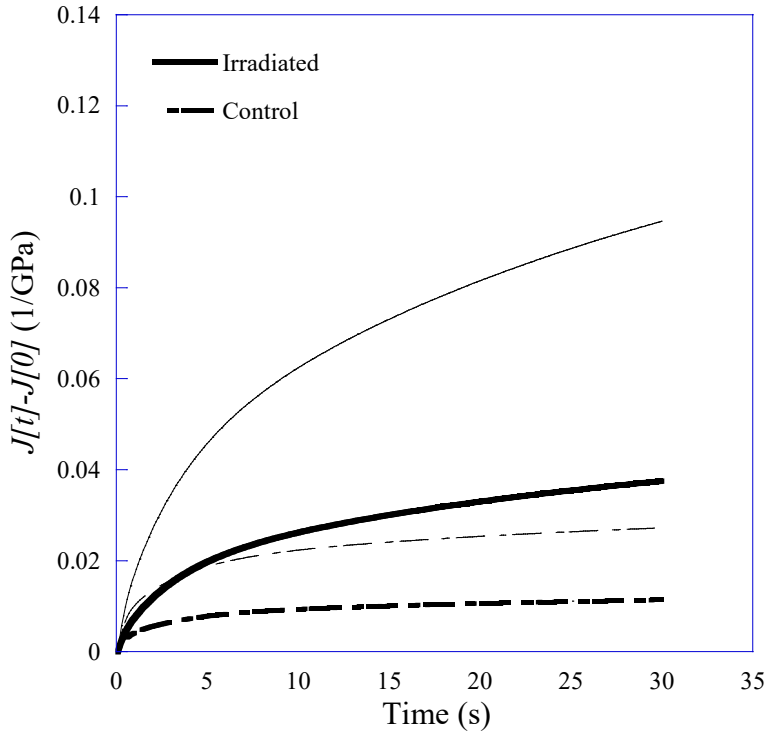

Figure 4.16 Normalized creep compliance of 0.50 w/c irradiated and control cement paste.

The fitted creep compliance (*J [t]- J [0])* and relaxation modulus *(R[t]-R [0])* curves and the corresponding one standard deviation (upper and lower bound) curves for irradiated and control cement paste samples is shown in Figure 4.14 to 4.16.

The one standard deviation curve was calculated as a function of holding time *(t)* from the large dataset of 100 load and depth-controlled indents. For 0.35 w/c sample, the normalized creep compliance is significantly higher than the control sample, and it can also be observed that upper and lower bound of standard deviation (Figure 4.14) for the two samples do not fall within each other indicating the considerable increase of creep in irradiated sample. Similar pattern of increased creep compliance is noted in 0.40 w/c irradiated sample (Figure 4.15)The sample with 0.5 w/c displays higher creep than the control sample (Figure 4.16), here, the lower bound of the standard deviation curve is not presented since the values were less than zero and therefore invalid. Parallelly, it is clearly observed that the relaxation modulus curves of irradiated samples are lower than the control samples.

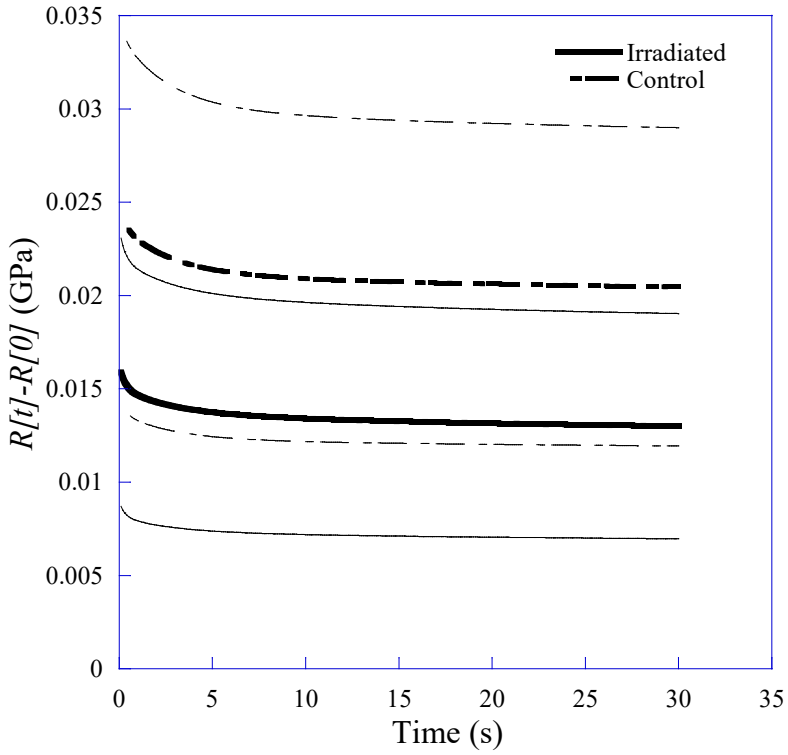

Figure 4.17 Normalized relaxation modulus of 0.35 w/c irradiated and control cement paste.

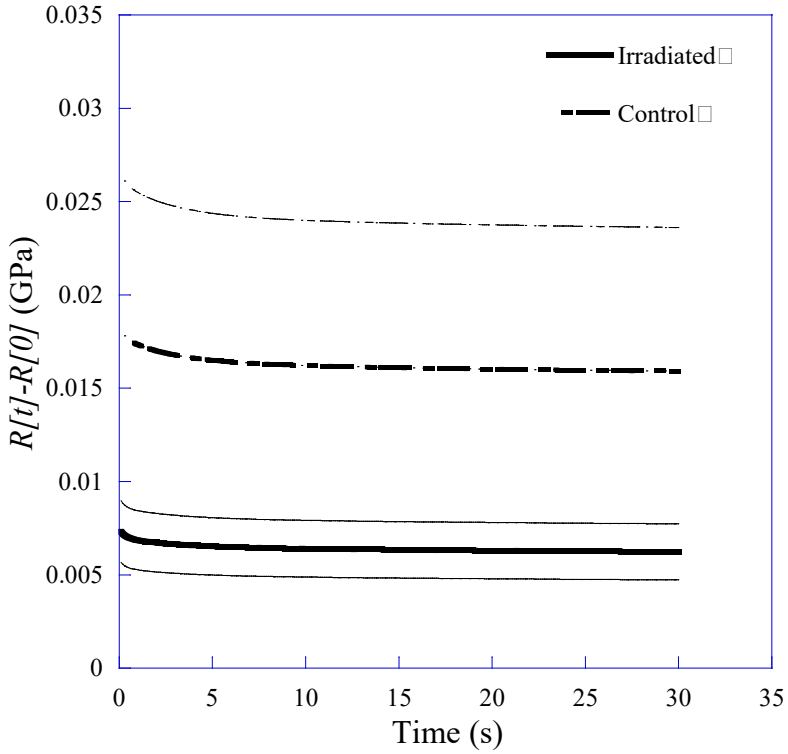

Figure 4.18 Normalized relaxation modulus of 0.40 w/c irradiated and control cement paste.

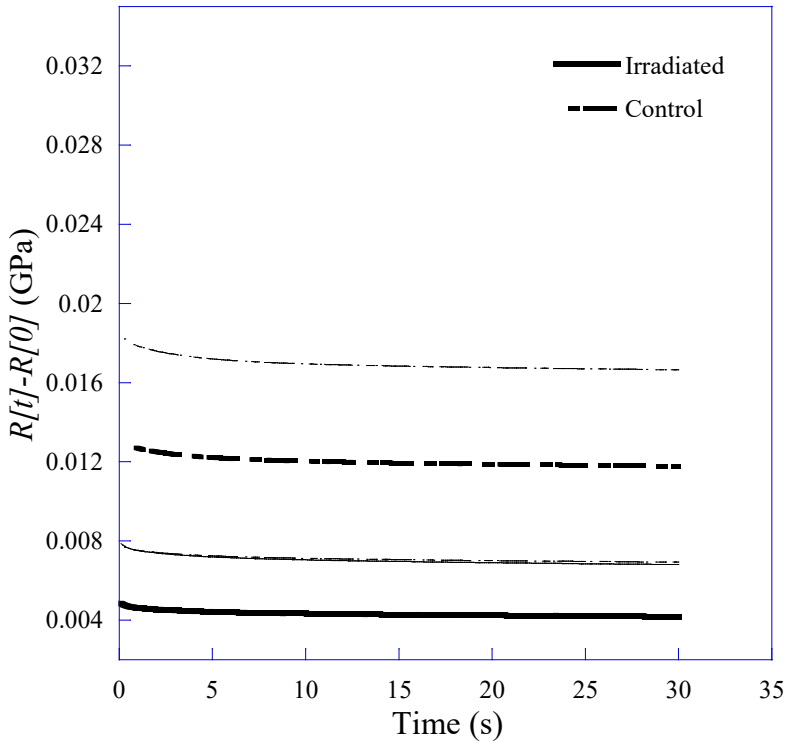

Figure 4.19 Normalized relaxation modulus of 0.50 w/c irradiated and control cement paste.

In 0.35 w/c sample (Figure 4.17) it can be seen that the lower bound of standard deviation curve for control sample interferes with the irradiated sample curves. This might be due to the grid indentation is performed on a slightly porous phase or unhydrated cement and may require increasing the grid size. Nonetheless, the statistical analysis proves that the relaxation data *(R[t])* are significantly different, comparable with the creep results. 0.4 w/c and 0.5 w/c samples (Figure 4.18 and 4.19) show similar pattern of decrease in relaxation modulus for irradiated samples and there are no overlapping standard deviation curves (negative values are omitted).

It should be noted that the creep compliance and relaxation modulus are reduced with increase in w/c (Figure 4.14 to 4.19). Study of influence of irradiation on creep [114] ascertain that creep is expected to increase with increasing levels of exposure. But many studies have reported contradictory results [70, 108, 110]). Neutron irradiation leads to reduction in the strength of concrete [99], since strength is dictated by the hydrated cement paste, the increase in the creep compliance and reduction in the relaxation modulus of the irradiated samples under study is explainable. Viscoelastic behavior of concrete is sensitive to temperature and is primarily regulated by the presence and movement of moisture and the porosity of the hydrated

cement paste. Another possible explanation for increase in creep compliance and decrease in relaxation modulus is increase in porosity due to irradiation with gamma radiation as documented in previously published result [98]. The release of hydrogen gas due to radiolysis can create pressure inside the layered porous microstructure of C-S-H leading to the formation of microcracks, altering the creep resistance. Nuclear radiations are inclusive of ionizing and non-ionizing radiations and the influence of these radiations on the water molecules in the C-S-H may boost the porosity and leads to increase in the creep and stress relaxation of irradiated samples.

Table 4.3 Mean depth/load observed for irradiated and control cement paste samples.

	Mean contact depth h_c, (nm)		
Sample (w/c)	**0.35**	**0.40**	**0.50**
Irradiated	1489	645	1193
Control	219	343	330
	Mean load P, (μN)		
Irradiated	1880	2945	3512
Control	1625	2517	2742

The observed mean load and depth during nanoindentation creep and relaxation tests for irradiated samples was considerably higher compared to the control sample (Table 4.3). This increase in contact load/depth in irradiated samples may be due to increase in porosity and microstructure. The provided justification for increased creep in irradiated samples is based on the previously published research and further investigation is necessary for the samples under study to confirm the aforementioned explanation. A consistent trend was not observed between the cement samples with different w/c.

4.6 Conclusions

The present work was focused on studying the combined effect of neutron and gamma radiation on E_r and viscoelastic behavior of cement paste. All samples were polished prior to irradiation, which increased the sensitivity of the sample surface to damage. Nanoindentation based creep and relaxation tests were performed on irradiated and control cement paste samples with 0.35 w/c, 0.40 w/c and 0.50 w/c. The results are summarized as follows:

1. Compared to the control samples, all irradiated samples showed a drop in E_r, and the degree of the percentage loss increased with increasing porosity of the sample. The data is statistically significant.
2. Reduction in reduced E_r confirms the possible mechanism of neutron-induced damage on the solid phase of cement hydrates at nanoscale. Further investigation is recommended to strengthen the result by performing chemical structural analyses.
3. Present study documented significant increase in the creep and stress relaxation of irradiated cement paste samples irrespective of the w/c, unlike limited studies in the literature. A consistent trend was not observed with respect to the creep behavior between the different irradiated cement paste samples as opposed to stress relaxation.
4. Because the sample were irradiated with combined neutron and gamma radiations, the study was unable to separate the effects from neutron and gamma or the possible synergy between them. Possible mechanisms contributing to the increase in creep and stress relaxation may be due to internal gas pressures caused by water hydrolysis under gamma irradiation and damage to the porous structure of the C-S-H microstructure.
5. For Portland cement paste, it was found that the deleterious effect of irradiation on creep and lowered modulus might occur at neutron and gamma doses that are much less than the threshold level of about 10^{19} n cm^{-2} and 200MGy cited by previous researchers.

It is important to study the porosity of irradiated cement paste microstructure using scanning electron microscope and XRF to understand its possible effect of combined neutron and gamma irradiation on the creep of cement paste.

Chapter 5 - A Study of Aging Viscoelasticity of Cement Paste Using Nanoindentation

5.1 Introduction

The materials which exhibit both viscous and elastic responses are known as viscoelastic; the strength and deformation under stress of viscoelastic materials are dependent on load duration. Hence, to envisage the performance and to anticipate the useful life of a material, modeling and testing the material properties, including time as a dependence is must. The test for creep is to predict deformation. The strength and the related stress relaxation tests are to measure the loss of stress at constant strain. Viscoelasticity has a unique role in terms of effective mechanical characteristics of heterogeneous materials determined by scale transition and remains an underdeveloped research topic.

Concrete structures are known to suffer aging related deformation, which can eventually eliminate their functionality. It is very well known that concrete is a viscoelastic material that exhibits creep and stress relaxation characteristics with aging [101, 102]. To understand the long-term behavior of prestressed and conventional concrete members subjected to changing load histories, it is necessary to study the aging properties of concrete. As aging can be defined with different variables it becomes difficult to model these properties and in turn results in ambiguous predictions of long-term performance. These phenomena may lead to serviceability issues and structural failures at the later stage of the service life of the concrete. Continuous hydration of cement, combined with the accumulation of cracking and dissolution of hydration products, results in the development of properties that are dependent on mix design, time, stress, temperature and humidity [118].

Since the rate of change in mechanical properties of cement paste is very significant at an early age (less than 28 days), a study of this period of the evolution of the paste should give the greatest insight into the mechanisms responsible for behavior [118]. Thus, studying cement paste with respect to different geometry and properties such as creep and aging effects will more precisely explain the long-term behavior of concrete, as aggregate inclusions are typically non-aging and elastic. Creep is typically modeled by viscoelastic constitutive equations and in order to have a reliable prediction of possible early age cracking due to shrinkage and thermal stress or

long-term performance comes with a proper understanding of ageing viscoelastic behavior. Aging in cement paste is directly related to changes in its microstructure and can be attributed to hydration process in addition to relaxation of hygro-chemically induced self-equilibrated prestress of the microstructure [59]. Degradations processes (e.g., leaching), which can be coupled with the viscoelastic behavior of the material itself, can be also a source of the aging behavior [119].

Aging creep is challenging to envisage as the microstructure evolves after the initial load application and creeps unevenly [101]. Despite its practical importance, experimental information on the creep characteristics of cement paste at ages less than 72 hours is scarce in the literature. There are currently several hypotheses that attempt to characterize the viscoelastic behavior of cementitious composites [17, 59, 118-121], however the majority of them fail to completely capture the viscoelastic behavior. One possible explanation for this is that cement-based materials are composite materials with stochastic matrix arrangements that are complex to model; further the internal chemical components of cement-based materials alter during the hydration process, including the dissolution of existing components and the formation of new component materials, a process known as aging [101].

5.2 Constitutive Theories for Aging Viscoelastic Materials

A considerable amount of research has been conducted to develop reliable mathematical models for the viscoelastic behavior of viscoelastic materials, and many simple constitutive models have been effectively exploited, such as the Maxwell model, the Kelvin-Voigt model, and the Standard Linear Solid Model [122]. All these models prove to generate effective simulations for a linear viscoelastic material under different forms of stresses but fail to consider the effect of hydration reaction on creep of concrete [120, 121]. The two popular theories employed to model the aging creep are discussed in detail in the following sections.

5.2.1 Solidification Theory

The solidification theory was initially derived by Bazant (1977) to explain the aging effect on concrete creep. The main concept of the model is that “hydration products are non-aging viscoelastic materials and that aging effects are present on the bulk scale as a result of the gradual solidification of new hydration products” [102]. According to the model, individual

layers of the hydration products must solidify independent of stress which shows that the layers which are formed at the age t' are only stressed by loads which are applied after t'. The solidification theory is demonstrated in below figure [123].

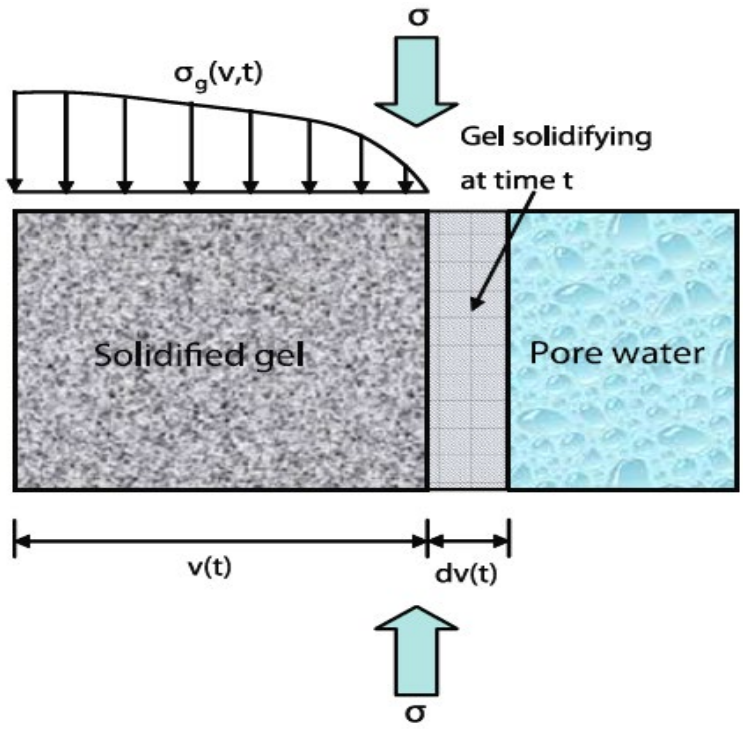

Figure 5.1 Conceptual diagram of solidifying material subjected to applied stress, σ. Carol and Bazant (1993).

The ultimate form of the constitutive equation for uniaxial loading and deformation is as shown in the below equation.

$$\frac{\partial \varepsilon(t)}{\partial t} = \frac{J_0}{\gamma(t)}\frac{\partial \sigma(t)}{\partial t} + \frac{1}{\gamma(t)}\int_0^t \frac{\partial J_t(t-t')}{\partial t'}\frac{\partial \sigma(t')}{\partial t'}dt' + \frac{\partial \varepsilon^f(t)}{\partial t} \qquad \text{Equation 5.1}$$

J_0 denotes instantaneous elastic uniaxial compliance, $\gamma(t)$ denotes aging function for the material (representing the volume fraction of solidified material), $J_g(t - t')$ denotes non-aging viscoelastic uniaxial compliance of the cement gel which is dependent on a single variable $(t - t')$, and $\varepsilon^f(t)$ denotes free strain. Since J_g is dependent on a single variable, it can be expressed by models such as a Kelvin chain. Another form of the constitutive equation for a solidifying, linear viscoelastic material is expressed as:

$$\sigma(t) = \int_0^t \gamma(t')\frac{\partial \varepsilon(t')}{\partial t'}E_g(t-t')dt' \qquad \text{Equation 5.2}$$

Where (t) is the aging function, $E\ (t - t'\ )$ *i*s the non-aging viscoelastic uniaxial moduli of the solidifying phases [124].

From Equation 3.1 the elastic component may be written as:

$$\frac{\partial \varepsilon(t)}{\partial t} = \frac{J_0}{\gamma(t)} \frac{\partial \sigma(t)}{\partial t} \qquad \text{Equation 5.3}$$

The above equation explains that the instant strain in the material is reliant on the age when the load was initially applied. The main advantage of the solidification theory is that it can be effectively used to model the aging viscoelastic properties of both concrete and cement paste. Solidification theory cannot be physically represented by a simple change in the rate of viscoelastic response.

5.2.2 Time–Shift Approach

A characteristic of thermorheologically simple materials is that the shape of the functions on the log time scale does not change with loading age. By measuring the viscoelastic compliance or modulus at multiple ages and selecting one age to be the 'master', the retardation or relaxation times for the other ages are simply shifted by a constant factor until they fall in line with the master curve on a log–log plot [102].

The time–shift approach used for modeling aging viscoelasticity corresponds with the time–temperature superposition principle. The principle states that the change in the temperature leads to increase or decrease in the relaxation times[122]. The outcome is basically a shift in the constitutive functions along the log time axis without changing the shape of the curves. The aging of viscoelastic materials may be explained using temperature superposition principle.

The shift coefficients for each age can be determined and fit to a function A_t using the following equation [102].

$$A_t = \left(\frac{t_{ref}}{t}\right)^{\mu} \qquad \text{Equation 5.4}$$

Here t_{ref} is the reference master age, t is the current age, and μ is a fitting/shift parameter [125]. The constitutive equation for an aging material is given as [126]

$$\varepsilon_{ij}(t) = \int_0^t S_{ijkl}\left(\xi(t) - \xi(t')\right) \frac{\partial \sigma_{kl}(t')}{\partial t'} dt' + \varepsilon^f(t)\delta_{ij} \qquad \text{Equation 5.5}$$

where ξ is a pseudo-time and $\xi(t) - \xi(t')$ is expressed as [102]

$$\xi(t) - \xi(t') = \int_{t'}^{t} \frac{dt''}{A_t(t'')} \qquad \text{Equation 5.6}$$

It has been proved that the shape of the relaxation function was conserved during aging, and this technique could be utilized to cement paste to explain aging effect on short-term early age stress relaxation [127].

The time–shift approach is phenomenological and is not linked to any specific proposed aging mechanism, per se [102]. The ability of the time–shift approach to accurately model the aging of a viscoelastic material simply implies that the aging manifests itself as nothing more than a change in the retardation or relaxation rate with age, with no change in ultimate magnitudes of viscoelastic behavior. For example, for a material characterized by a Kelvin chain, aging according to the time–shift approach would simply be represented by age-dependent viscosities or age dependent retardation times in a Dirichlet or Prony series expansion [102].

In the present study the author proposes to model the aging creep behavior of cement paste at nanoscale using microstructure dependent solidification and time-shift approaches.

5.3 Methodology

The neat cement paste sample with 0.35 water to cement ratio was prepared as described in Section 3.3.1 and was polished using method PM1 (Table 3.1). Characterizing the aging creep behavior of cement paste at nanoscale requires hydration reaction to be arrested. Previous studies have documented various methods of arresting hydration and subsequent drying techniques. Some of the most common techniques are microwave drying, oven drying, dry ice drying, freeze drying and solvent exchange [128-131]. According to the literature review, solvent exchange and freeze drying methods preserve the microstructure of the cement paste and cause the least damage to the sample[132]. Thus, in the present study the ongoing hydration of the cement paste sample was arrested using solvent exchange and the freeze-drying method. The following sections discuss the procedures adopted for each method.

5.3.1 Solvent Exchange Method

The hydration of the sample is arrested using solvent exchange method with isopropyl alcohol. This method is considered to be effective compared to other hydration freeze methods as it best protects the microstructure[128]. In an effort to arrest the hydration of 0.35 w/c sample at different ages, slices of sample of size approximately 3 mm thick and 16 mm diameter (Figure 5.2) were submerged in isopropyl alcohol after desired time of casting (0.25D, 0.5D, 1D, 2D, 3D, 7D, and 28D) with a solvent to sample ratio of 100:1. The sliced sample discs are soaked in the solvent for 7 days in a glass beaker and is sealed using aluminum foil. The solvent is renewed every hour for the first 8 hour and then for every 24 hr. After 7 days of soaking the samples are dried in oven for 24 hr. at 100^{o}C to desorb alcohol from the hydrated cement paste pore surface [133]. Thereafter samples were stored in vacuum desiccator until further testing. Solvent exchange can arrest hydration in the depth of interest within a short period of time. Thus, enables study of a given "age".

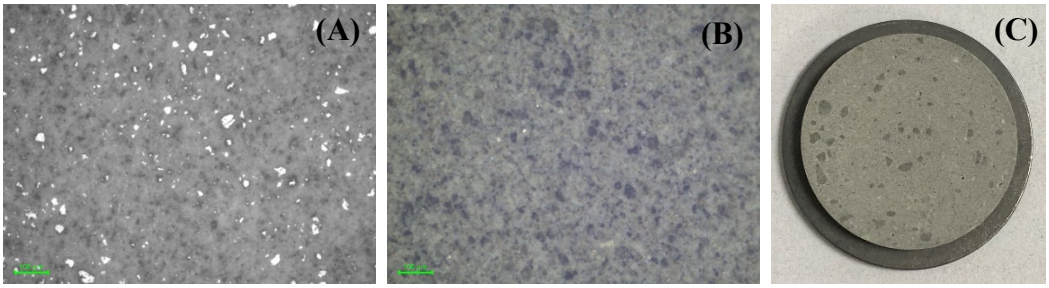

Figure 5.2 Images of 0.35 w/c whose hydration was arrested using solvent exchange method at (A) 0.25D (B) 28D (C) Polished 0.35 w/c sample disc of approximately 16 mm dia.

5.3.2 Freeze Drying Method

Freeze-drying is a typical method used in many different industries, including the agricultural and food sectors as well as the biological sciences[134]. Freeze drying is also considered to causes less damage to the microstructure of the cement paste than oven drying. Approximately 2g of the cement paste after a particular time of interest (0.25D, 0.5D, 1D, 2D, 3D, 7D, and 28D) was placed in a steel container. The container was fully immersed in the 3L Dewar containing liquid nitrogen (-196 °C) for 5 minutes. The ice microcrystals may be formed due to this rapid cooling process at a very low temperature. This mechanism restricts the formation of large ice crystals that would otherwise form in larger pores and creates compressive

stress in smaller porosity zones that have not yet completely frozen [128, 132, 134]. Then, the sample was carefully removed from liquid nitrogen and was immediately placed in the plastic vials and was covered with a cloth. The vials were then placed in the Labconco FreeZone Benchtop freeze dryer for at least 2 days, where in the temperature was maintained below -50 °C and vacuum at 0.1 Torr. The samples then removed from freeze dryer were stored in vacuum desiccator until further testing.

5.3.3 Nanoindentation Based Creep Tests

A Hysitron Triboindenter model TI Preimer fitted with Berkovich indenter tip is used to perform reference creep tests on the specimen with a step load function in which the second (longer) reference frequency segment will be analyzed as the creep. A cohort of statistical nanoindentation based creep experiments at a maximum critical load of 1695μN with grid size and grid spacing of 10 x 10 and 3 μm were performed on cement paste samples at various ages. The maximum critical load was of on different cementitious materials was performed.

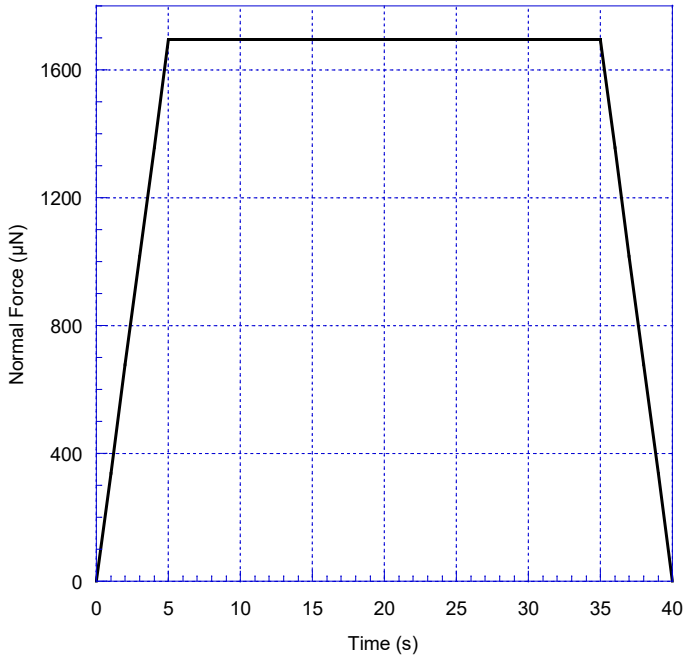

Figure 5.3 Step load function with a constant maximum load P_{max} = 1695 μN.

The nanoindentation test consisting of a trapezoidal shape load history with 5s loading segment, 30s holding segment and 5s unloading segment is shown in Figure 5.3. The short

loading and unloading segments are selected to minimize any creep during this time. The data of reference indent displacement (nm) and E_r (Gpa) are extracted to perform analysis. The use of nanoindentation to perform creep/relaxation tests has the benefit of greatly minimizing the time of transitory creep-relaxation owing to the high degree of stress caused by the indenter tip sharpness [64].

5.3.4 Constitutive Modeling of Aging Creep Using Solidification Theory

The well-known solidification theory which was discussed in Section 5.2.1 is also considered and applied to model the aging creep behavior of early age cement paste in the present study. The theory does not consider any non-solidified elements of the cement paste such as water, cement grains, and pore solution. This approach solely based on the formation of hydration (solidifying) products with time in a stress-free state. In other words, already formed hydration products are subjected to stress and is a function of degree of hydration at the time of load application (Figure 5.1). The aging function [102] as a function of time *t* for solidification approach is given as

$$\frac{1}{\gamma(t)} = \beta_1 e^{-\omega_1 t} + \beta_2 e^{-\omega_2 t} \qquad \text{Equation 5.7}$$

where β and ω are constants, using elastic-viscoelastic correspondence principle the creep compliance equation can be written as

$$J(t) = \frac{1}{\gamma(t)}\left(\frac{1}{E_0} + \sum_{i=1}^{3} \frac{1}{E_i} \frac{\left(1-e^{-t/t_h}\right)}{(1-e^{-1})}\right) \qquad \text{Equation 5.8}$$

The reduced modulus of each age is normalized to pseudo reference age (28D) and the aging function Equation 5.7 is fit the aging reduced moduli data. Unique age factor is obtained for each age and the measured creep data of 28D (pseudo reference age) is fit to Equation 5.8. Thereafter based on the average fit parameters (Equation 5.8) of reference age and the particular aging function $\gamma(t)$, the creep compliance of all other early age samples is predicted.

5.3.5 Constitutive Modeling of Aging Creep Using Time-Shift Approach

As discussed in the Section 5.2.2, the time-shift method was used to model the aging creep of cement paste. It is crucial to ensure that no aging of the sample occurs at any time

throughout the creep testing for this method to be useful for cement paste. This was accomplished by successfully stopping the ongoing hydration using solvent exchange and freeze dry method. The master age for the sample was 28 days, and all the other age samples are shifted to fall in line with the master age by adjusting the age factor μ and then the measured creep compliance was plotted against the pseudo time $\xi(t) - \xi(t')$ on a log scale and is given by

$$\xi(t) - \xi(t') = \frac{t^{1+\mu} - t'^{1+\mu}}{1+\mu} \quad \text{Equation 5.9}$$

The creep compliance equation to obtain the predicted (shift) creep behavior is expressed as

$$J(t,t') = \frac{1}{E_0} + \sum_{i=1}^{3} \frac{1}{E_i} \frac{\left(1 - e^{-\left(\xi(t) - \xi(t')\right)/t_h}\right)}{(1 - e^{-1})} \quad \text{Equation 5.10}$$

The measured creep compliance curves and the respective fit parameters were obtained (Figure 3.2) using Equation 3.13. After obtaining the age factor μ and the measured average fit parameters for all age samples, the creep compliance curves of early ages are predicted using μ and the average fir parameters of the reference master age (28D). The creep compliance equation to obtain the predicted (shift) creep behavior is expressed as Equation 5.10. The flowchart of the process for obtaining μ, $\xi(t) - \xi(t')$ and applying the time-shift approach to model the aging creep behavior of early age samples is shown in Figure 5.4 and Figure 5.5.

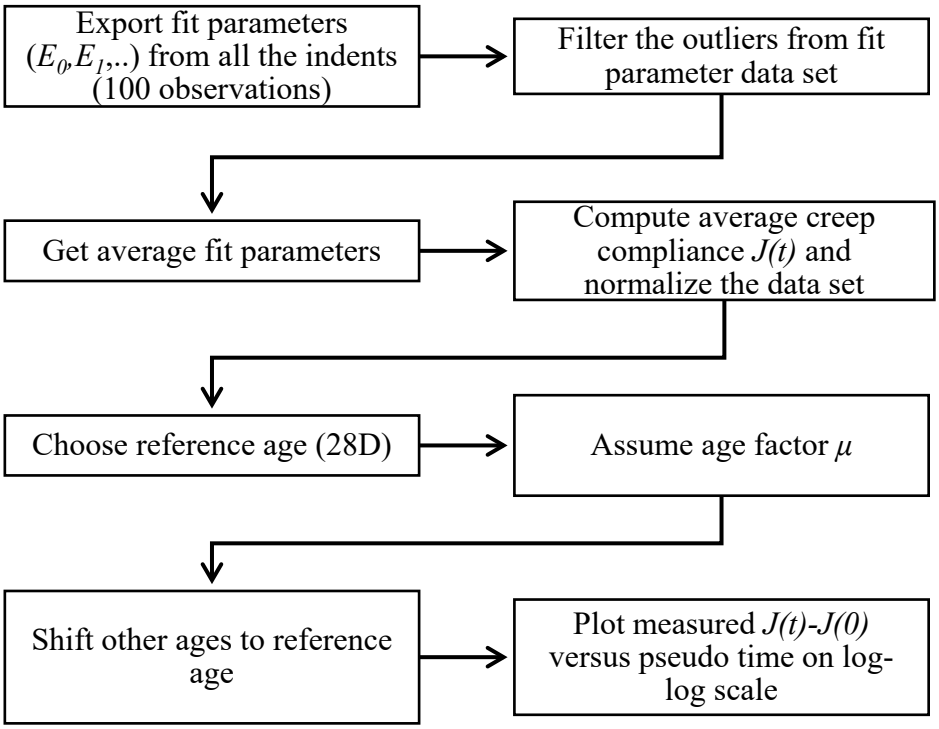

Figure 5.4 Flowchart of the process for obtaining age shift factor and pseudo time.

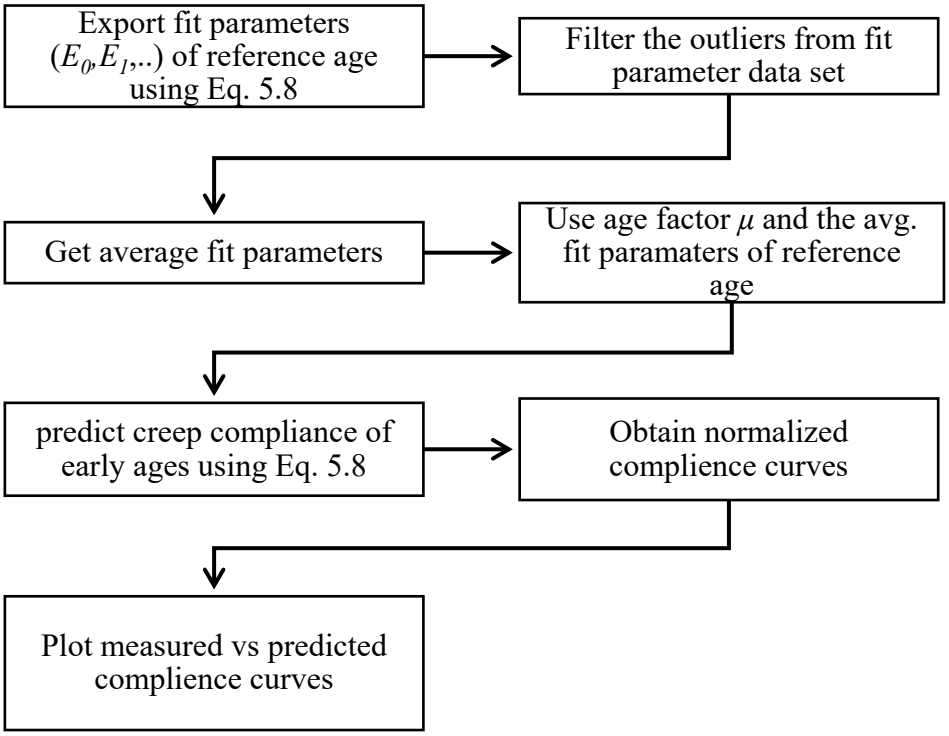

Figure 5.5 Flowchart of the process for applying the time-shift approach to model aging creep.

5.4 Results and Discussions

The following sections discusses the efficacy of using solidification and time shift methods to predict the aging creep behavior of early age cement paste at the nanoscale. In addition, the reduced modulus is explored in relation to the two methods used to arrest the hydration reaction of cement paste: solvent exchange and freeze drying.

5.4.1 Solidification Theory

The aging function $\gamma(t)$ was obtained using Equation 5.7 and was directly fit to the aging reduced modulus elastic compliance. This aging function depends on the volume fraction of already formed solidified hydration phases. Two fit parameters in the aging function (Equation 5.7) ensured good agreement between the fit and the experimental reduced modulus elastic compliance.

The fit between the elastic compliance data (normalized to 28 days) and the aging function of cement paste at different ages (prepared using solvent exchange and freeze-drying methods) is shown in Figure 5.6 and 5.7 below. The modified correspondence principle was employed to determine the aging function (Equation 5.7) to avoid the complicated computation of constitutive equation requiring numerical analysis [102]. The adopted form of aging function reasonably fits the elastic compliance data for required age of the cement sample. The cement paste samples are fully characterized with the knowledge of aging function and average fit parameters of the reference age (28 days).

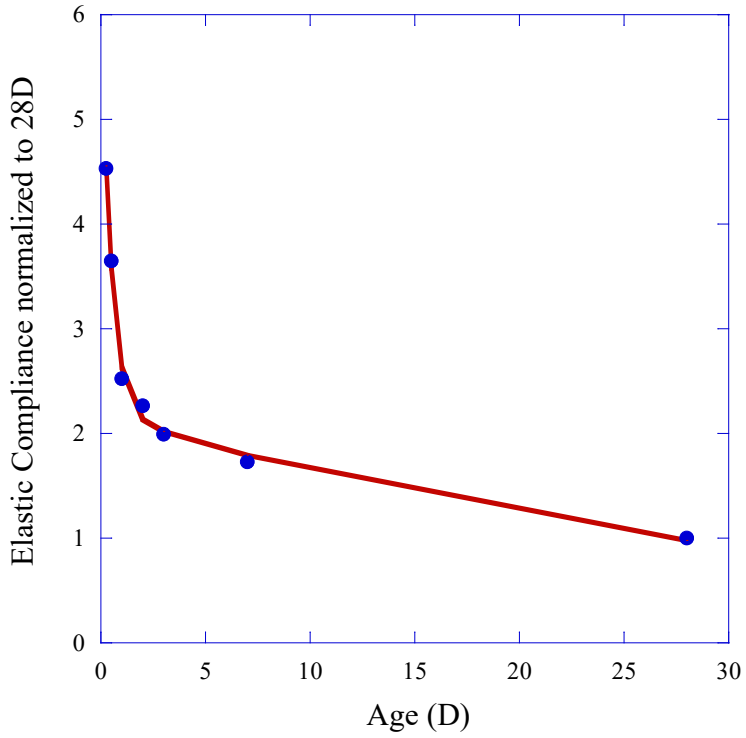

Figure 5.6 Normalized aging elastic compliance fit to the aging function of cement paste: hydration arrested using solvent exchange.

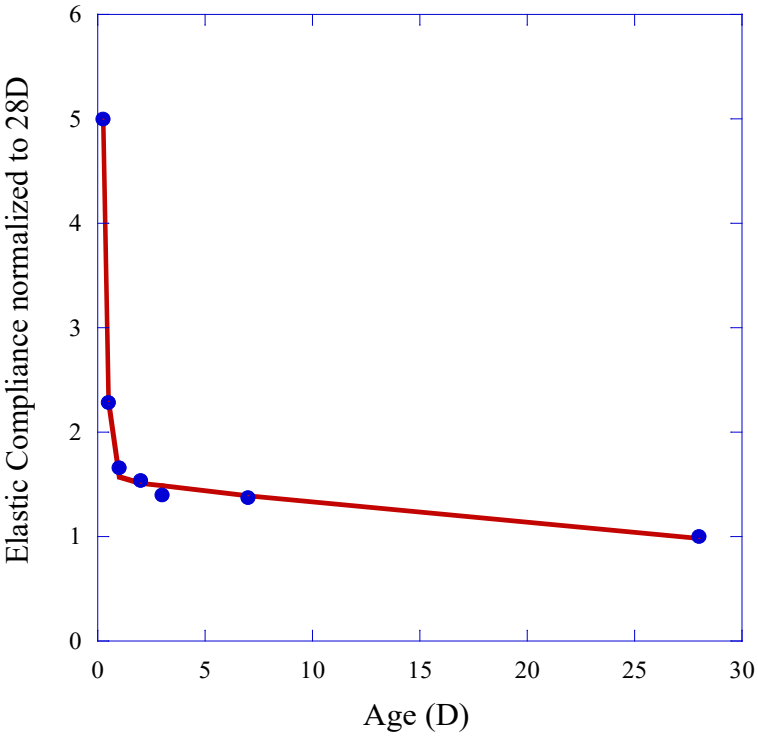

Figure 5.7 Normalized aging elastic compliance fit to the aging function of cement paste: hydration arrested using freeze-drying.

The creep response of early age samples (hydration arrested using solvent exchange method) is predicted and compared with the measured data as seen in Figure 5.8 to 5.14. It can be observed that the solidification theory is able to account and predict the aging creep behavior of cement paste of early ages using the fit parameters of 28 days. Specifically, the predicted compliance shows good agreement with the measured compliance of early age samples (Figure 5.8 and 5.9), asserting that rate of hydration reaction is the important factor contributing for the aging of the cement paste. As seen in the graph, the shape of the compliance function is not preserved, the possible reason for this might be that the solidification approach disregards the effect of dissolution of cement particles or any other unhydrated phases of the cement paste on the viscosity or stiffness and only takes into account the effect of newly formed hydration products. Since the rate of growth of new hydration phases is significant during the early ages, the method efficiently models the instantaneous elastic response, as can be seen in the plots.

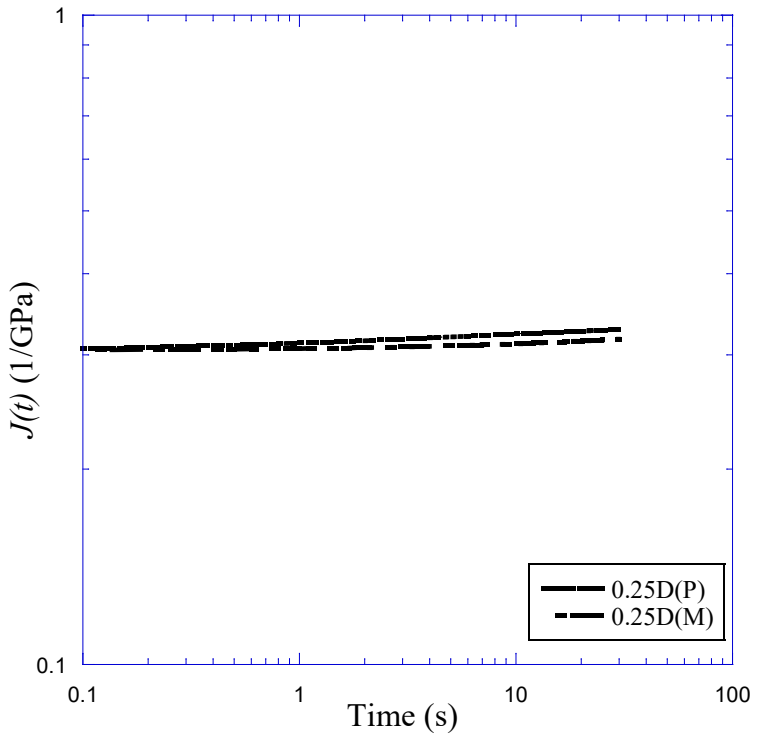

Figure 5.8 Measured and predicted normalized creep compliance of 0.25D cement paste using solidification theory: hydration arrested by solvent exchange method.

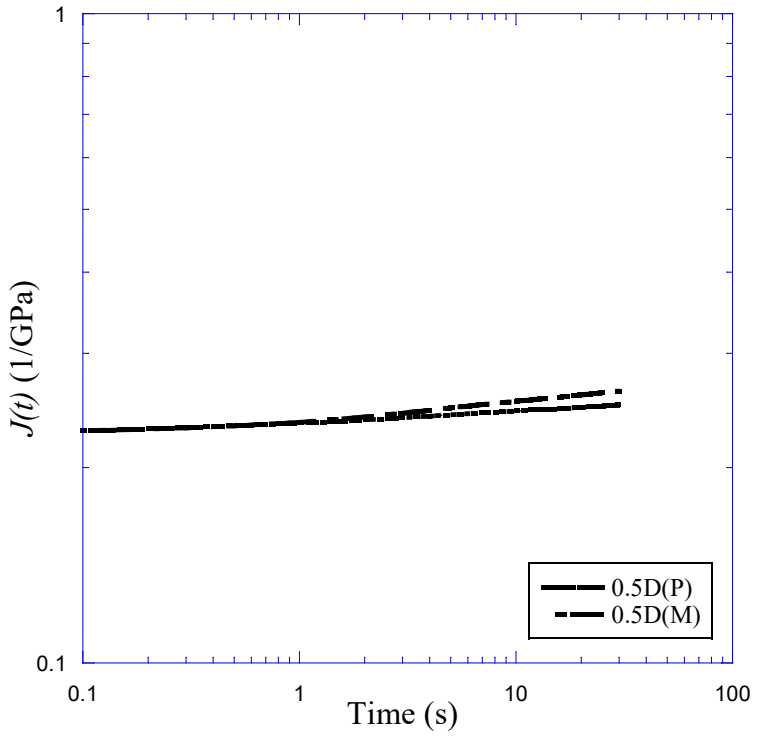

Figure 5.9 Measured and predicted normalized creep compliance of 0.5D cement paste using solidification theory: hydration arrested by solvent exchange method.

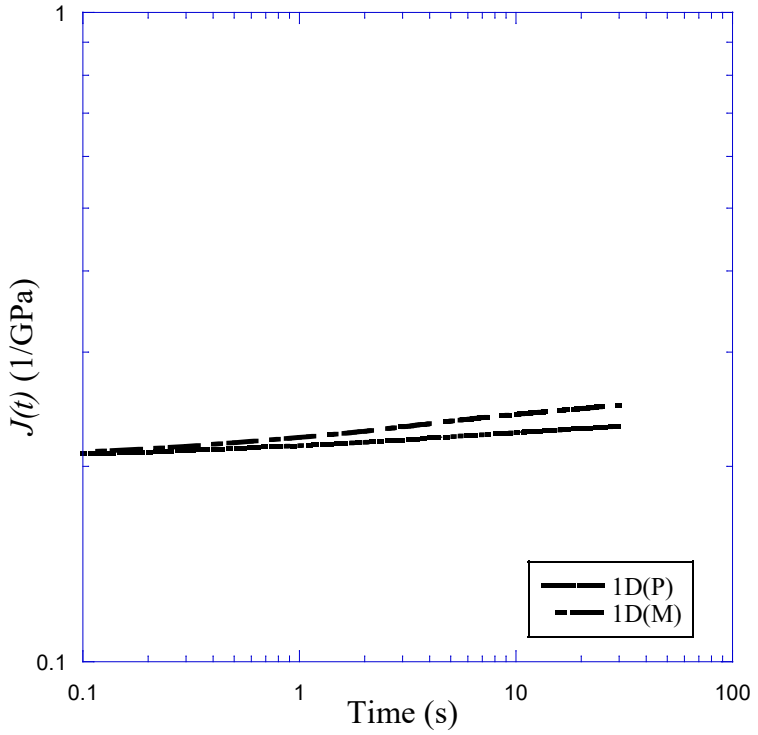

Figure 5.10 Measured and predicted normalized creep compliance of 1D cement paste using solidification theory: hydration arrested by solvent exchange method.

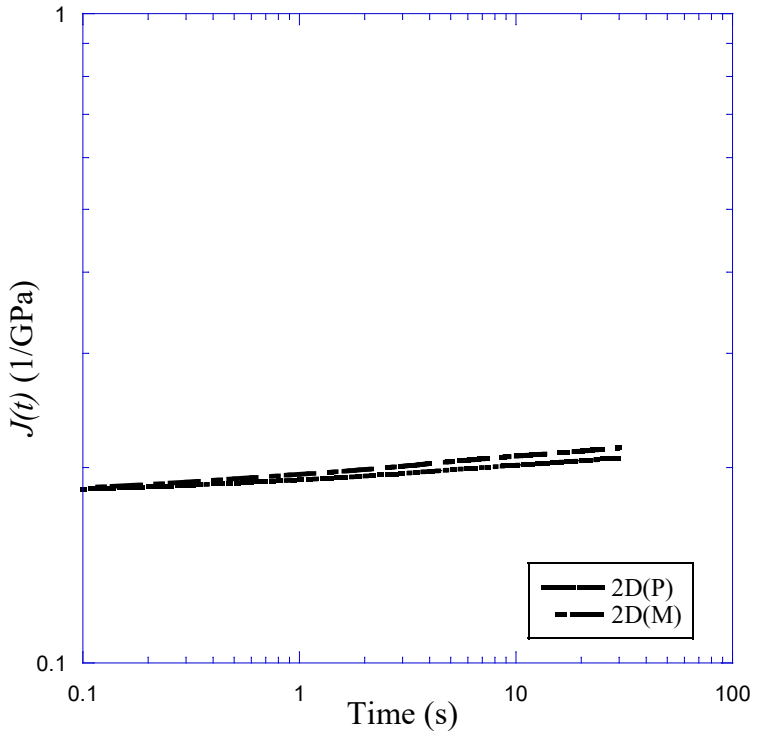

Figure 5.11 Measured and predicted normalized creep compliance of 2D cement paste using solidification theory: hydration arrested by solvent exchange method.

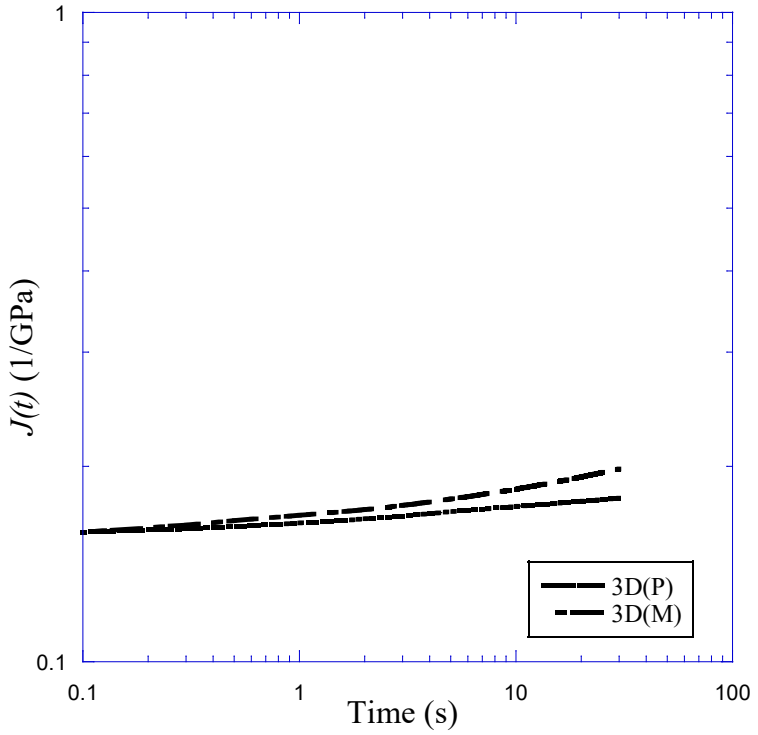

Figure 5.12 Measured and predicted normalized creep compliance of 3D cement paste using solidification theory: hydration arrested by solvent exchange method.

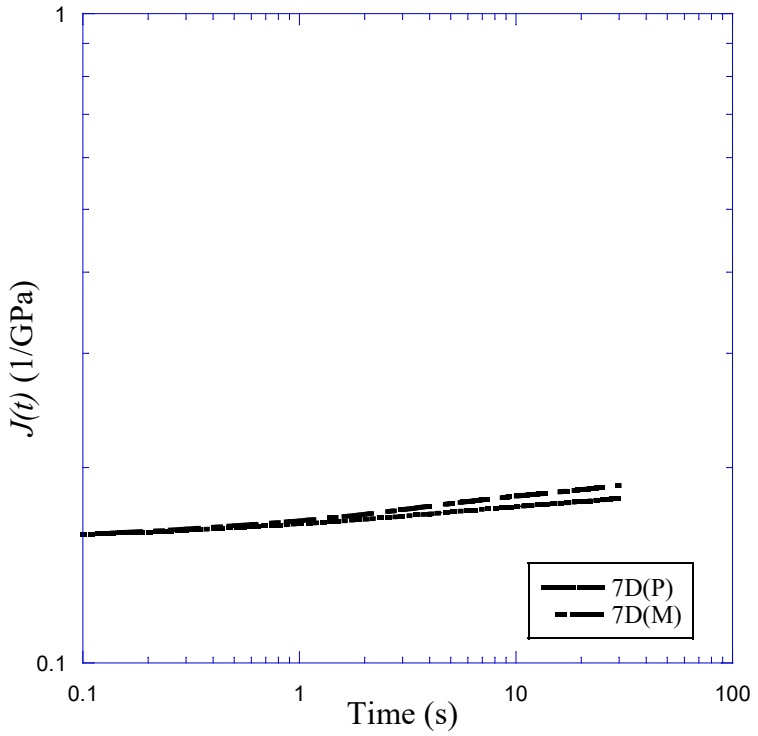

Figure 5.13 Measured and predicted normalized creep compliance of 7D cement paste using solidification theory: hydration arrested by solvent exchange method.

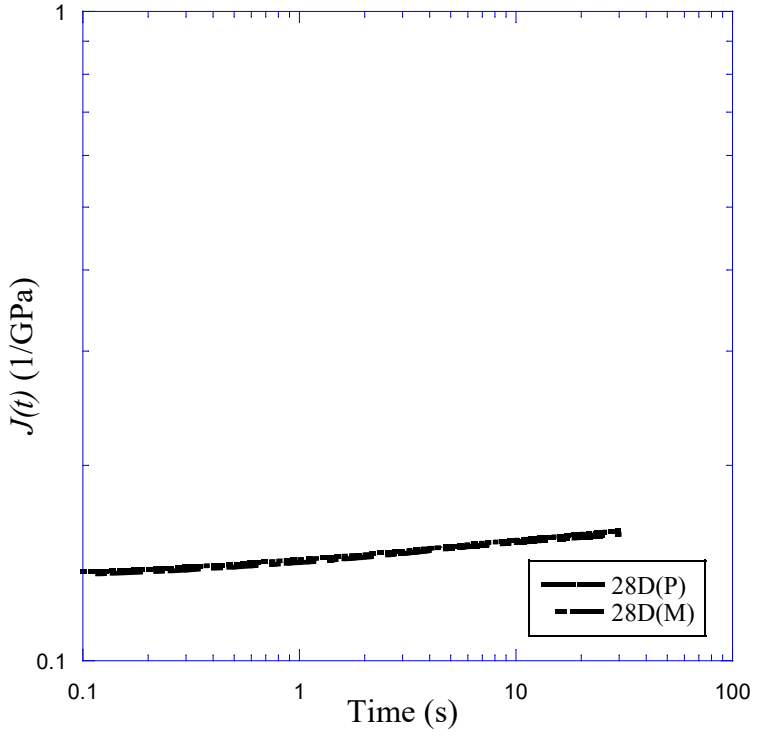

Figure 5.14 Measured and predicted normalized creep compliance of 28D cement paste using solidification theory: hydration arrested by solvent exchange method.

When the stress is applied at later ages, the creep rate and magnitude are visibly reduced for each material (Figure 5.8 to 5.14) due to aging, which is defined as filling the pores of hardened cement paste with the hydration products as indicated in the aging function. This demonstrates that freezing the hydration of cement paste using isopropanol exchange preserves the porous structure of the sample and causes little to no damage to the microstructure.

The creep compliance of cement paste samples whose hydration is arrested using freeze drying method at various ages is predicted and compared with the measured data as seen in Figure 5.15 to 5.21. The solidification theory is less effective in predicting the aging creep of 0.25D and 0.5D (Figure 5.15 and 5.16) samples compared to other age samples. As discussed previously, this might be due to the inability of freeze-drying method to preserve the microstructure of the cement paste sample. Further, the graphs show that no obvious pattern of the creep response decreasing with the age of the sample is seen. Along with modifying the microstructure of the cement paste, the high vacuum in the freeze dryer disintegrates ettringite and monosulphate [135] and critically damage the porous structure. The solidification works best to model the aging viscoelastic properties of cement given that the hydration of the sample is arrested. The theory only considers the intrinsic strain response to the stress applied on the already formed hydration phases and neglects aging due to the dissolution or polymerization of C-S-H with the degree of hydration. Thus, it is crucial to carefully eliminate aforementioned phenomena in the cement paste sample through hydration freeze to successfully employ the solidification theory to model aging creep.

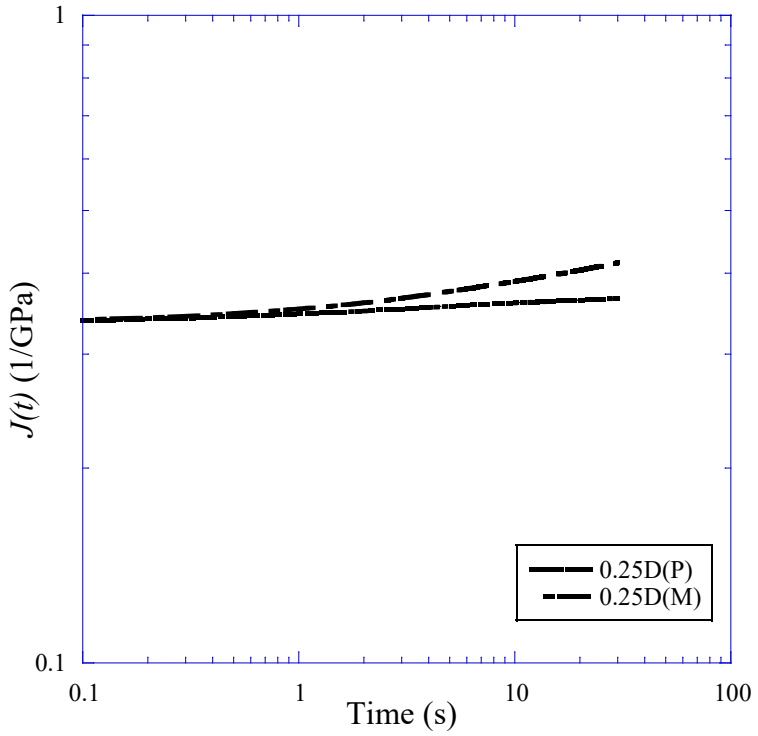

Figure 5.15 Measured and predicted normalized creep compliance of 0.25D cement paste using solidification theory: hydration arrested by freeze drying method.

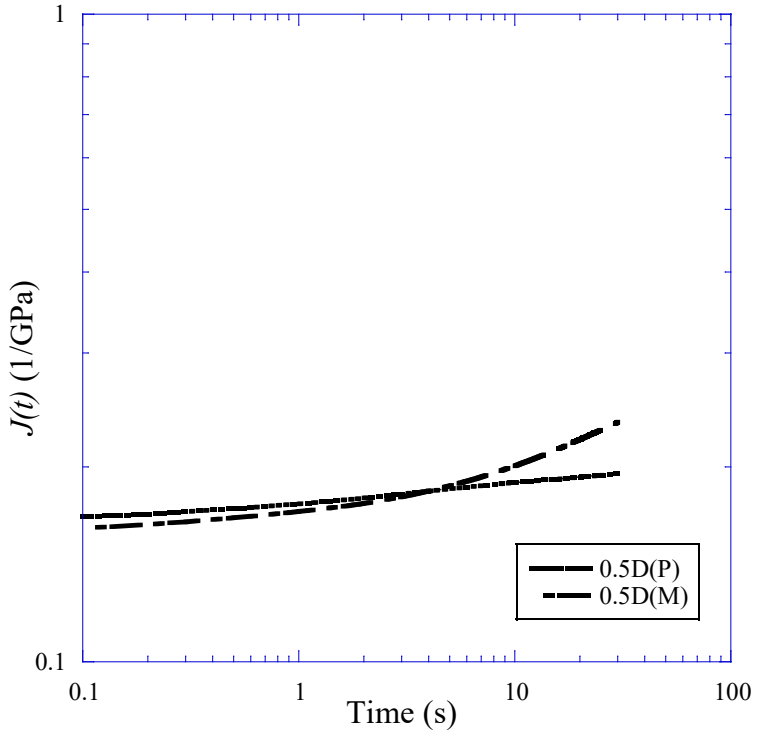

Figure 5.16 Measured and predicted normalized creep compliance of 0.5D cement paste using solidification theory: hydration arrested by freeze drying method.

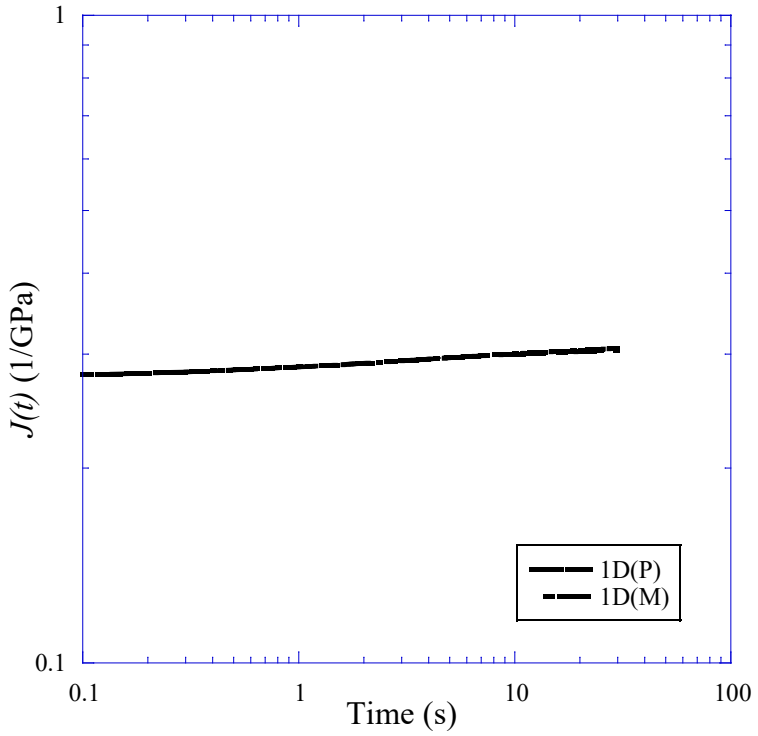

Figure 5.17 Measured and predicted normalized creep compliance of 1D cement paste using solidification theory: hydration arrested by freeze drying method.

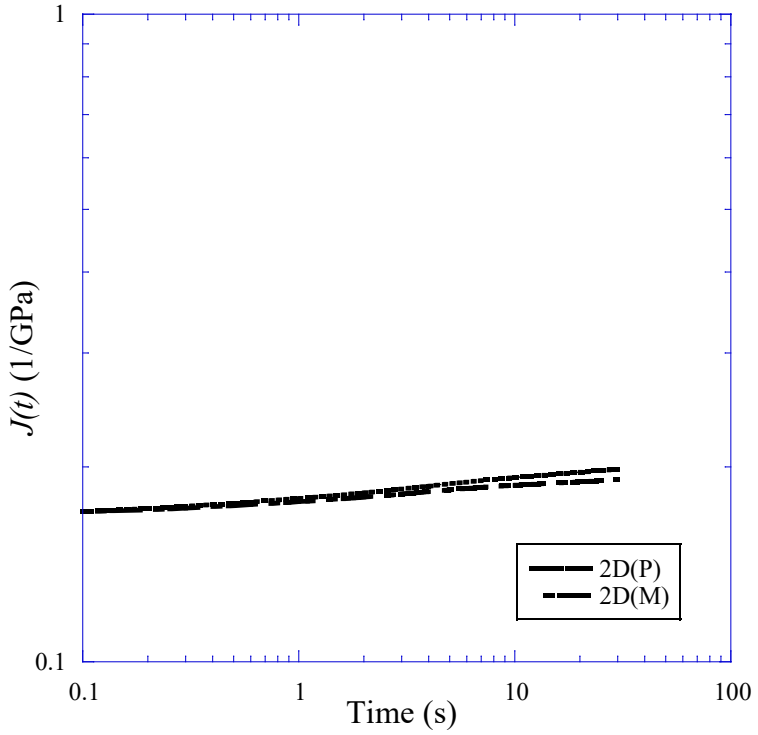

Figure 5.18 Measured and predicted normalized creep compliance of 2D cement paste using solidification theory: hydration arrested by freeze drying method.

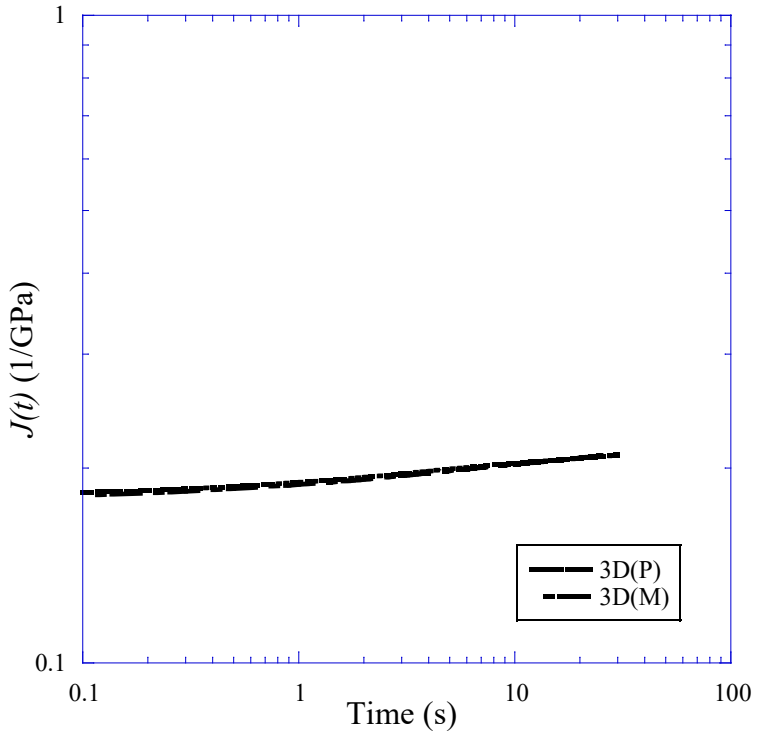

Figure 5.19 Measured and predicted normalized creep compliance of 3D cement paste using solidification theory: hydration arrested by freeze drying method.

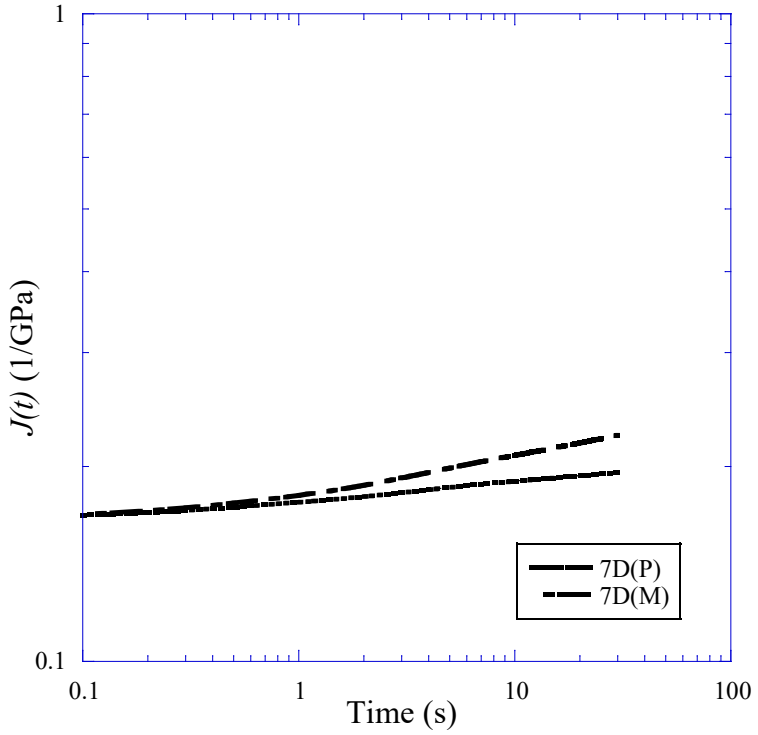

Figure 5.20 Measured and predicted normalized creep compliance of 7D cement paste using solidification theory: hydration arrested by freeze drying method.

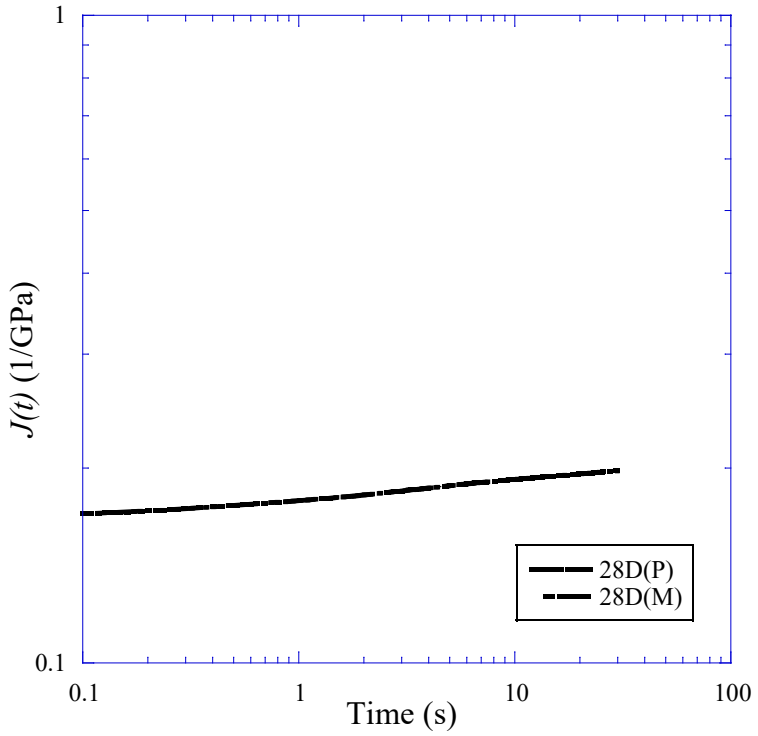

Figure 5.21 Measured and predicted normalized creep compliance of 28D cement paste using solidification theory: hydration arrested by freeze drying method.

5.4.2 Time Shift Approach

The load applied to model aging creep was a step function that stayed constant during the test. As a result, the measured creep compliance was directly plotted against pseudo time (Equation 5.9), and the age factor μ was modified until the measured creep compliance was consistent across all other ages (Figure 5.22 and 5.23). Because nanoindentation allow the sample to be unloaded after each indent, the aging that occurs during each test is accurately accounted for. Furthermore, freezing the hydration of cement paste samples using the solvent exchange and freeze-drying technique at the specified time (age) ensured that the snapshot principle was not violated. This is evident from the Figure 5.22 and 5.23. Using this fitting procedure, all ages were concurrently adjusted, allowing the precise estimation of μ.

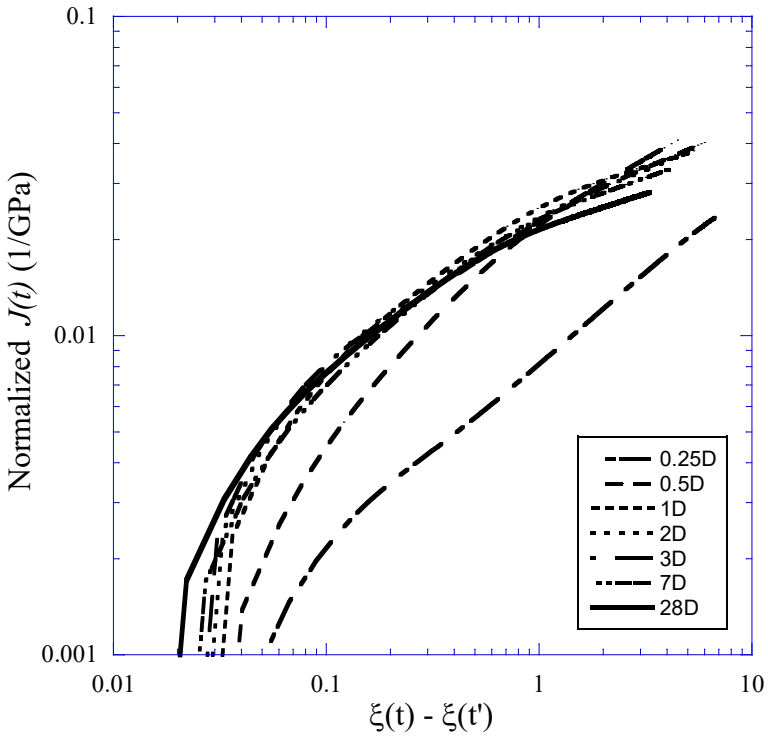

Figure 5.22 Shifted compliance of all age cement paste samples using age factor μ: hydration arrested using solvent exchange method.

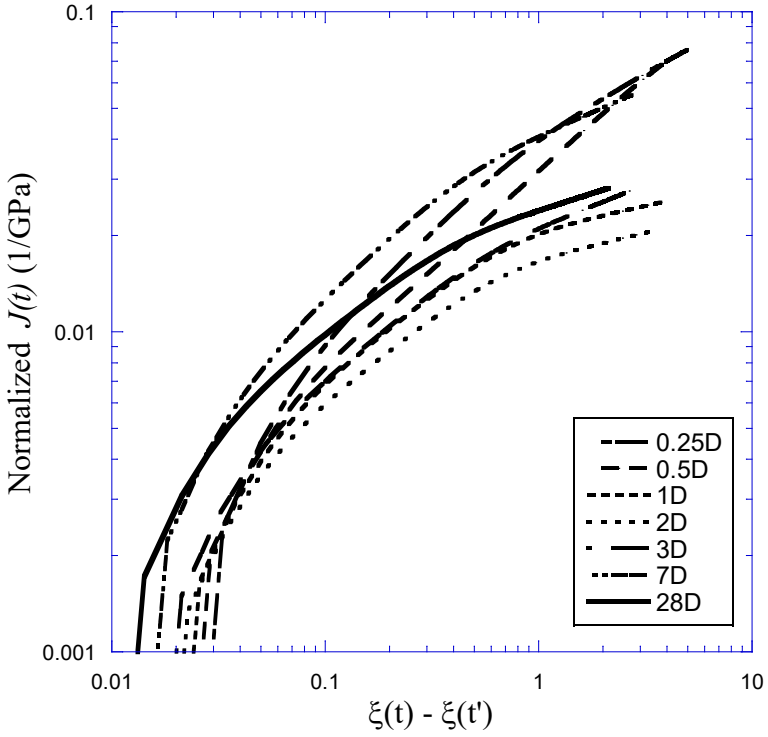

Figure 5.23 Shifted compliance of all age cement paste samples using age factor μ: hydration arrested using freeze-drying method.

Figure 5.22 and 5.23 shows the normalized shifted compliances (Equation 5.10) of cement paste sample whose hydration is stopped using solvent exchange and freeze-drying method. It can be clearly seen in Figure 5.22 that except for 0.25D and 0.5D age samples, all other age samples clearly align with each other. The result indicates that the aging creep behavior of early age samples cannot be completely modelled using time shift approach. This is because the rate of hydration is significant in the early ages as the aforementioned method fails to account for the change in strain response due to solidification. It is apparent from the Figure 5.23 that shifted compliance curves for 0.25D and 0.5D fail to maintain the shape of the compliance function in comparison to other age samples, this is because the freeze-drying approach fails to preserve the pores in the finest pore size region and crystallization of the pore water is expected and disturbs the microstructure of the cement paste [136].The plots of shifted compliances shows that the curves of all ages except for 0.25D and 0.5D reasonably fall in line with the reference age (28D). Particularly in case of solvent exchange method the overlap of compliance functions with reference age is prominent compared to the freeze-drying method.

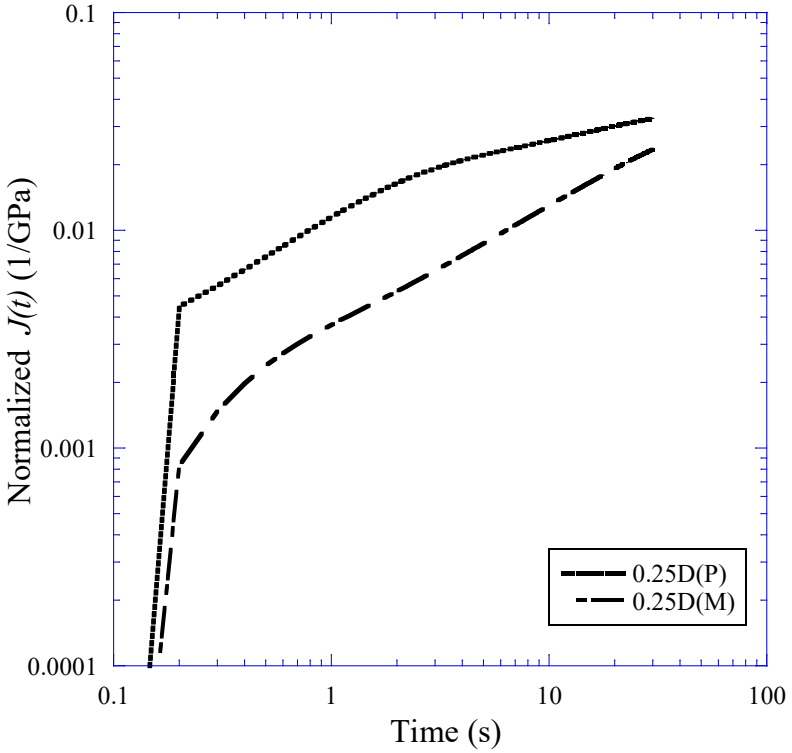

Figure 5.24 Measured and predicted normalized creep compliance of 0.25D cement paste using time shift approach: hydration arrested by solvent exchange method.

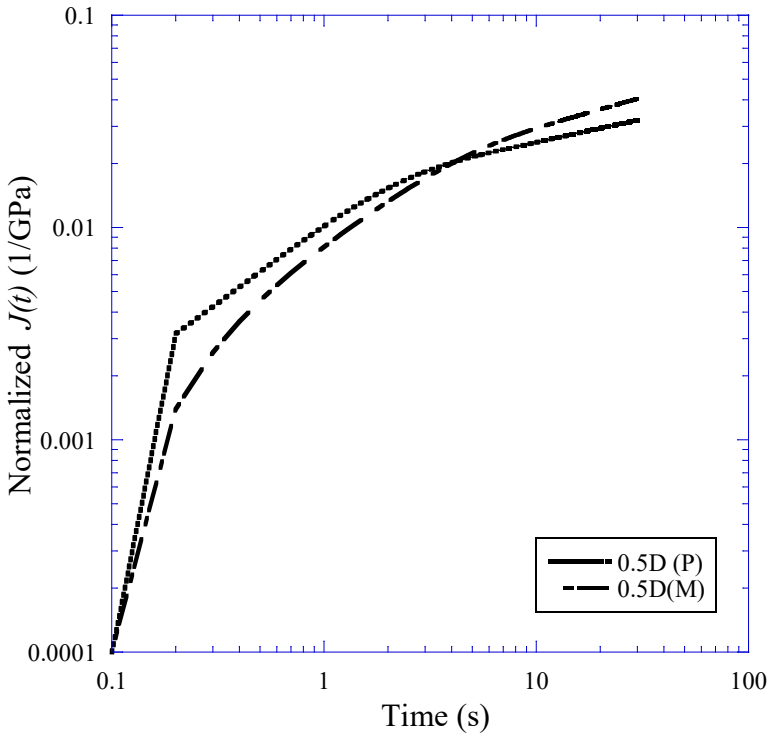

Figure 5.25 Measured and predicted normalized creep compliance of 0.25D cement paste using time shift approach: hydration arrested by solvent exchange method.

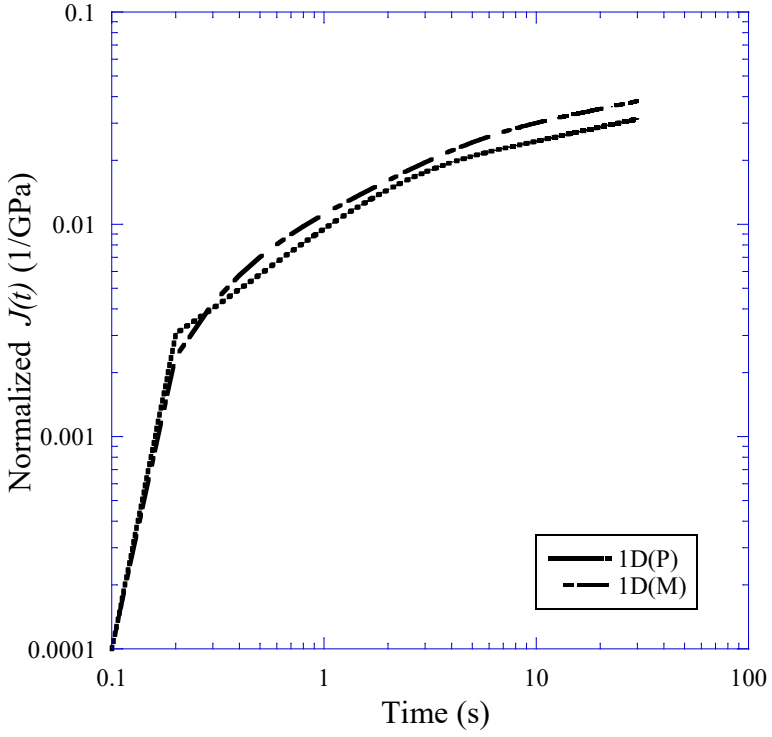

Figure 5.26 Measured and predicted normalized creep compliance of 1D cement paste using time shift approach: hydration arrested by solvent exchange method.

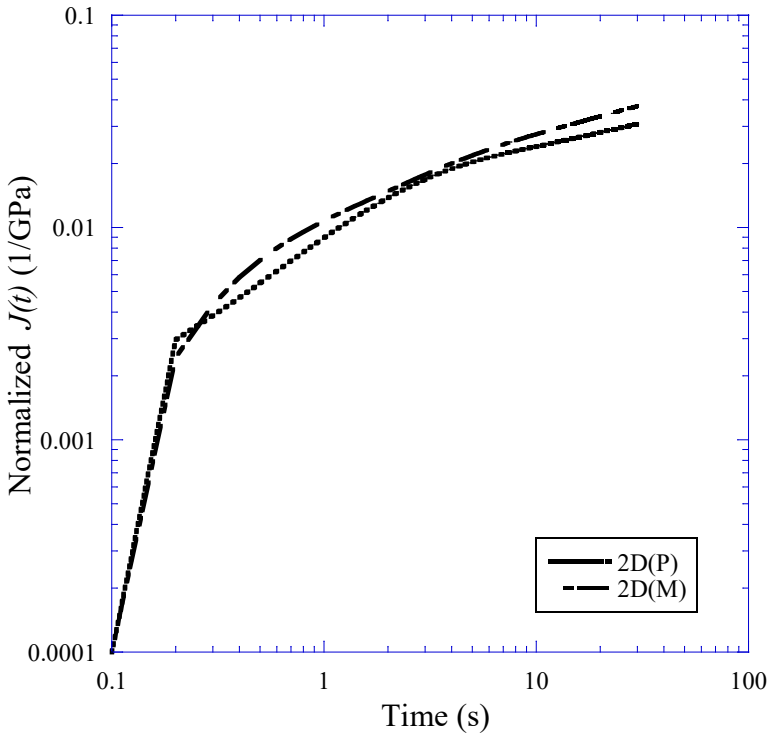

Figure 5.27 Measured and predicted normalized creep compliance of 2D cement paste using time shift approach: hydration arrested by solvent exchange method.

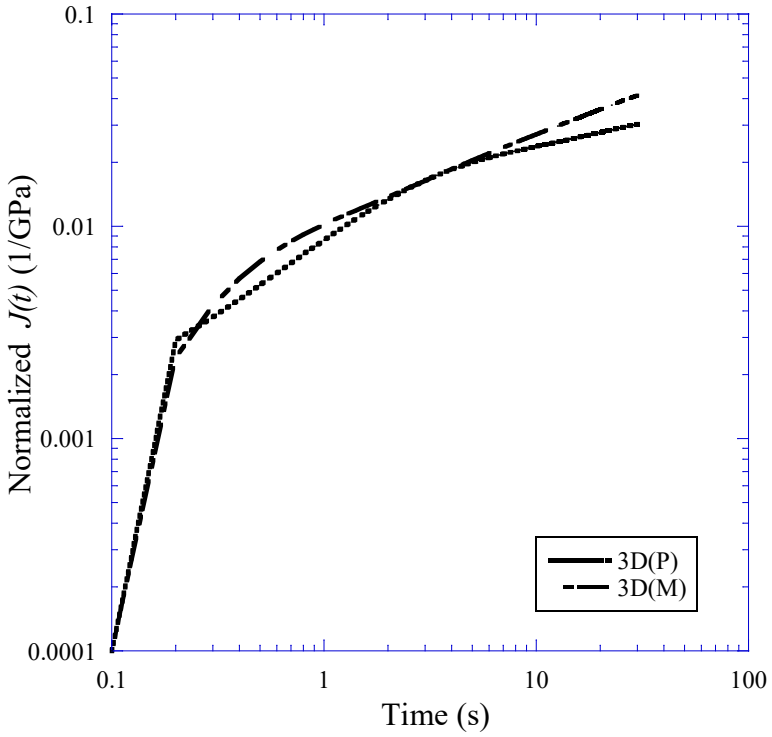

Figure 5.28 Measured and predicted normalized creep compliance of 3D cement paste using time shift approach: hydration arrested by solvent exchange method.

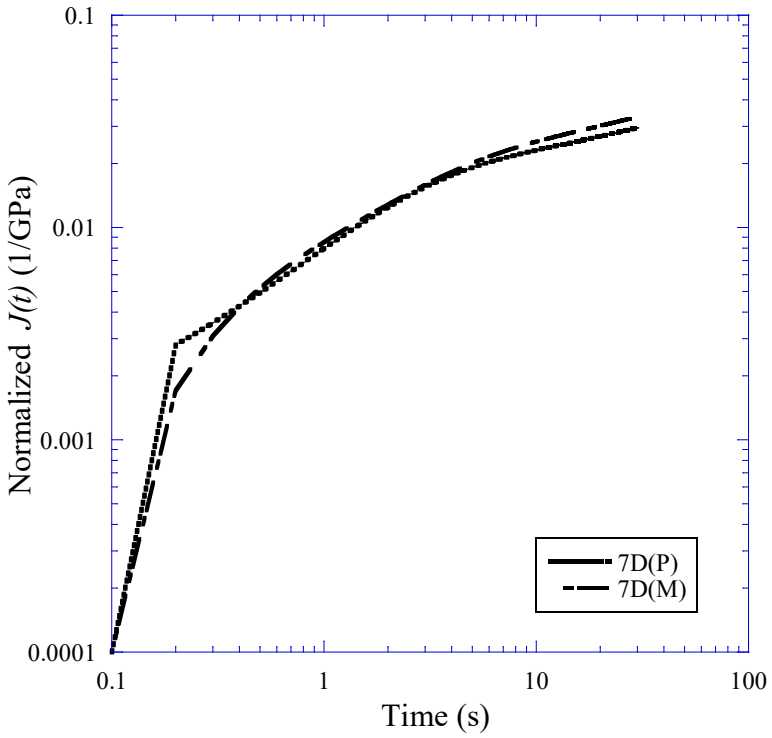

Figure 5.29 Measured and predicted normalized creep compliance of 7D cement paste using time shift approach: hydration arrested by solvent exchange method.

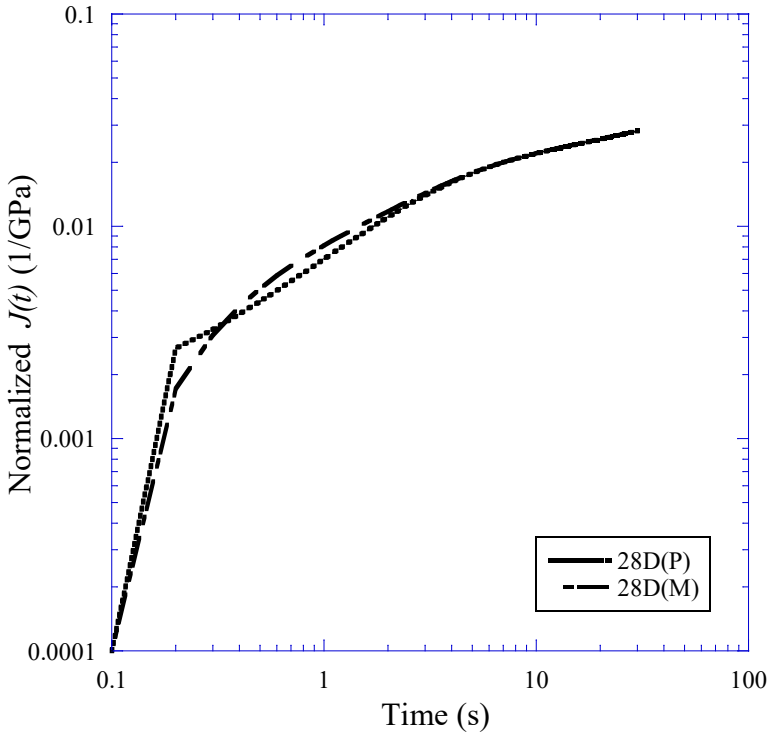

Figure 5.30 Measured and predicted normalized creep compliance of 28D cement paste using time shift approach: hydration arrested by solvent exchange method.

The measured and predicted compliance curves plotted using the fit parameters of reference age and aging shift parameter μ for all other age samples whose hydration reaction was arrested using solvent exchange method are shown below (Figure 5.24 to 5.30).

The predicted curves show decent fit with the measured data and the fit show excellent match particularly for later ages (Figure 5.26 to 5.30). The statistical analysis of the data through F test also indicates that the measured and the predicted creep data are not statistically different with p-value being considerably greater than the α (=0.05). The results highlights that the time shift approach is less sensitive to the change in intrinsic C-S-H aging rate specially at early age (Figure 5.24 and 5.25), confirming that the constitutive model is phenomenological and is unrelated to any particular suggested aging process (solidification or dissolution). The resulted predicted creep response of 1, 2, 3, 7, and 28 days (Figure 5.26 to 5.30) strengthens the argument that the time shift approach is capable of accounting for aging at later ages or long-term creep response that occurs in absence or low rate of hydration reaction.

The small size of the sample (17mm x 3mm) and testing at short length scale allows to freeze the hydration of the cement paste successfully at desired age. Stopping further hydration of the sample avoids under prediction of creep at later ages and minimizes error in determining the aging shift parameter μ. It is challenging to predict aging creep using test data obtained from a macroscale compliance test in which the cement paste sample is continually hydrating. In macroscale creep testing it is difficult to neglect the aging occurring in successive time frame. This incapability of time shift approach to account for the formation of new hydration products results in significant difference between the measured and predicted compliance, emphasizing the need of studying the viscoelasticity of cement paste/concrete at nanoscale versus the meso/macro scale. Time shift approach appears to yield agreeable prediction compliance curves for the cement paste sample whose hydration is stopped using solvent exchange method.

The measured and predicted creep compliance curves plotted using the fit parameters of reference age and aging shift parameter μ for all other age samples whose hydration reaction was arrested using freeze drying method are shown below (Figure 5.31 to 5.37).

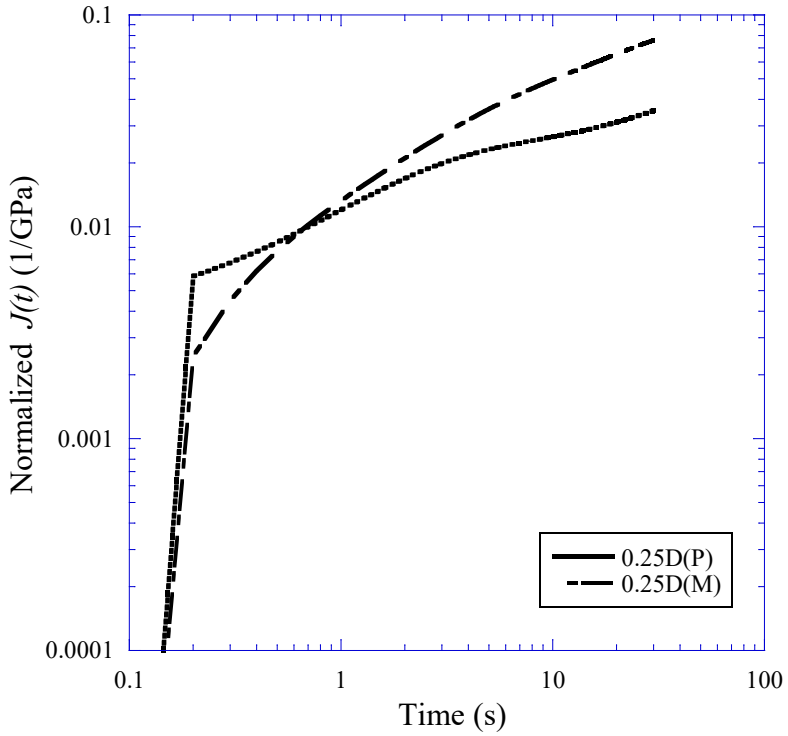

Figure 5.31 Measured and predicted normalized creep compliance of 0.25D cement paste using time shift approach: hydration arrested by freeze drying method.

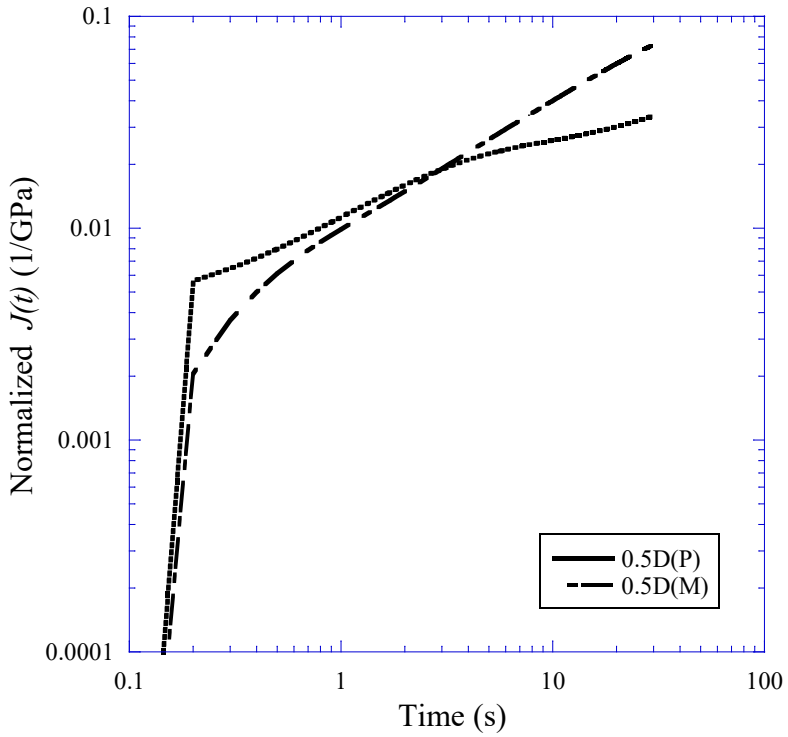

Figure 5.32 Measured and predicted normalized creep compliance of 0.5D cement paste using time shift approach: hydration arrested by freeze drying method.

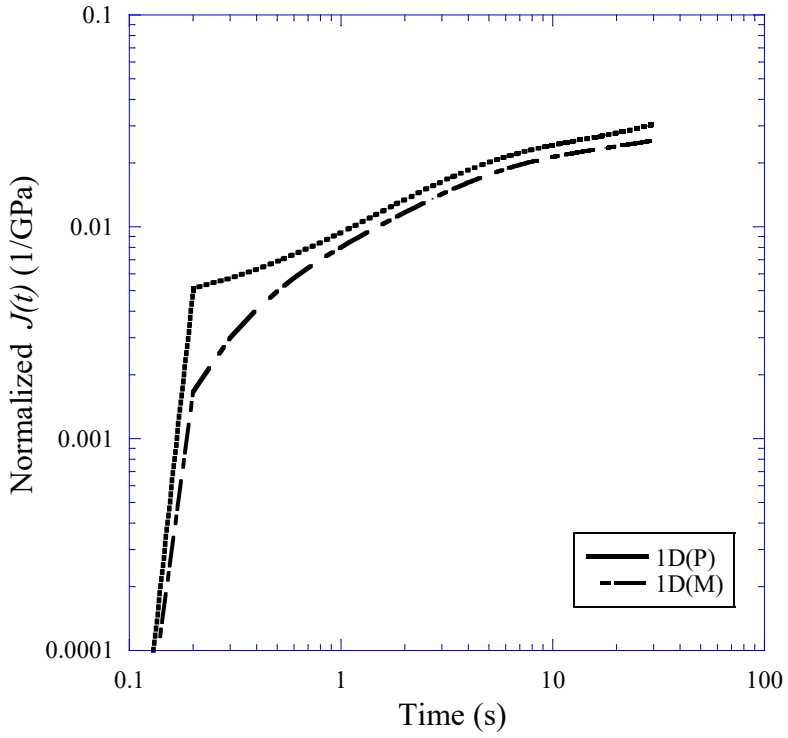

Figure 5.33 Measured and predicted normalized creep compliance of 1D cement paste using time shift approach: hydration arrested by freeze drying method.

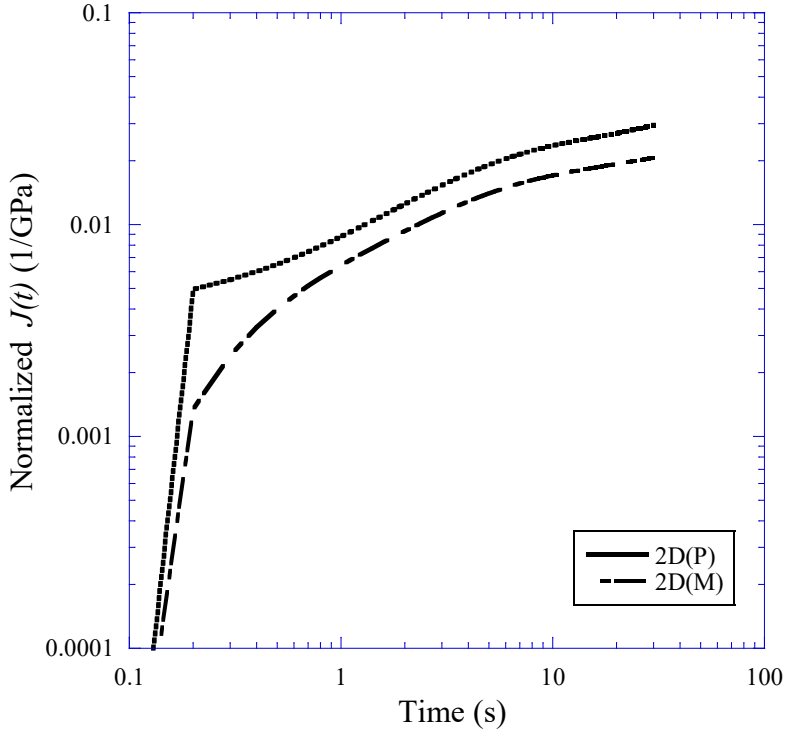

Figure 5.34 Measured and predicted normalized creep compliance of 2D cement paste using time shift approach: hydration arrested by freeze drying method.

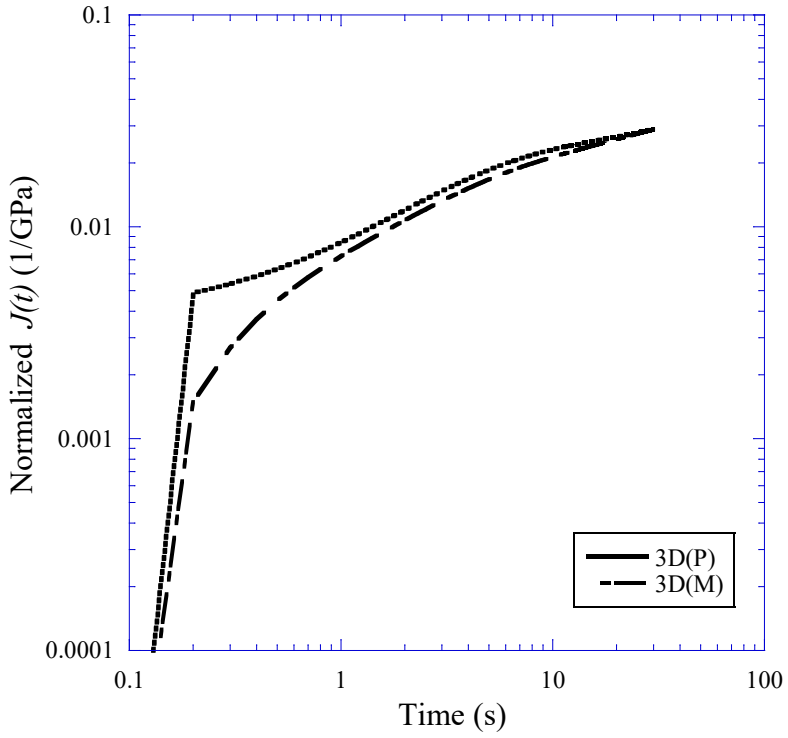

Figure 5.35 Measured and predicted normalized creep compliance of 3D cement paste using time shift approach: hydration arrested by freeze drying method.

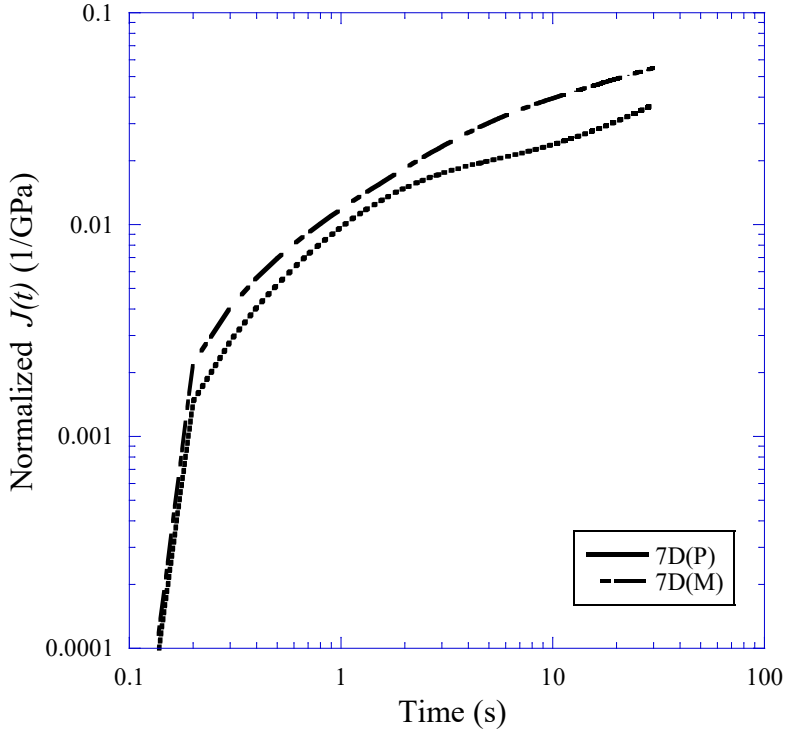

Figure 5.36 Measured and predicted normalized creep compliance of 7D cement paste using time shift approach: hydration arrested by freeze drying method.

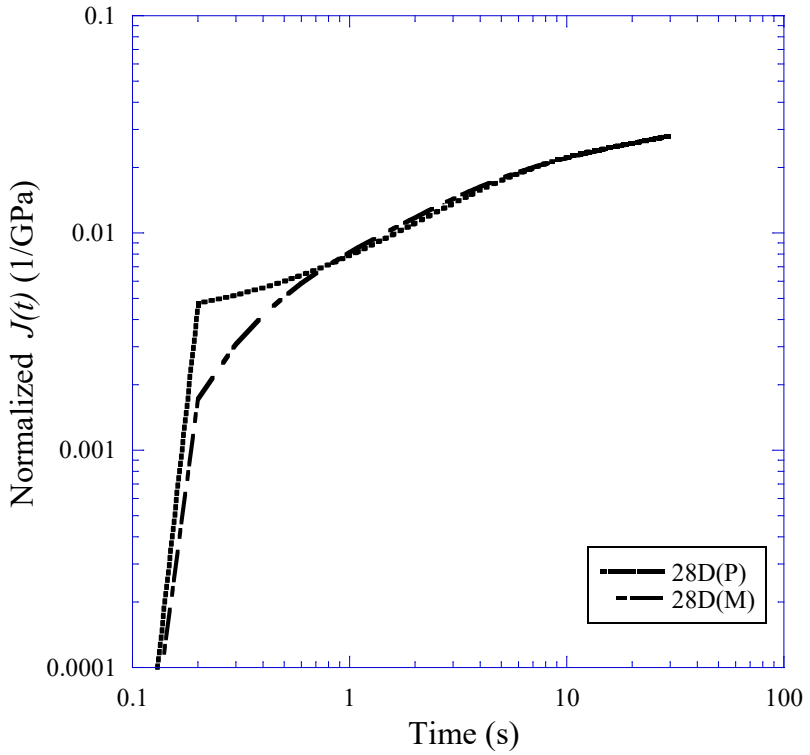

Figure 5.37 Measured and predicted normalized creep compliance of 28D cement paste using time shift approach: hydration arrested by freeze drying method.

The statistical F test confirms that the measured and predicted creep compliance data is statistically significant, asserting that time shift approach has the ability to model aging viscoelasticity of cement paste irrespective of hydration freeze method. Evidence that the time shift method is appropriate for modeling viscoelastic aging is provided by plots (Figure 5.31 to 5.37) showing the conservation of the form of the compliance curve. However, the time shift model is deficient in its ability to account for the instantaneous creep response caused by elastic aging at any age. The discrepancy in predicted and measured compliance function is more prominent in the samples whose hydration is arrested using freeze drying method compared to solvent exchange method. The reason is that the freeze-drying method alters the original microstructure of the cement paste mainly by rearranging the fine pores related to C-S-H, especially at the nanoporosity level [134]. Although the time-shift approach provides a more accurate estimate of aging creep at later ages, it does not account for the strain response of newly formed hydration products in the early-age sample.

Table 5.1 presents the reduced modulus values and average maximum displacement for the cement paste sample whose hydration is arrested using solvent exchange and freeze-drying

method. The table indicates that the microstructure of the sample is aging (due to formation new hydration phases and dissolution of unhydrated phases).

The increase in the modulus with the age of the sample confirms the efficacy of hydration freeze methods (solvent exchange and freeze drying) employed in the present study. The complex microstructure of the cement paste at nano scale answers the deviation between the modulus values of the two hydration methods. Good agreement of the mean modulus values at later age (7D and 28D) of the sample (Table 5.1) can be seen compared to the samples at early hydration stages. However, the reduced modulus values are still comparable and is of little concern at early ages. As discussed already, the freeze-drying method is known to damage the microstructure by critically altering the pore structure of the cement paste sample. Table 5.1 demonstrates that for 0.25D and 0.5D sample prepared from freeze drying method, the maximum displacement recorded during creep based nanoindentation test with a constant load of 1695μN is considerably higher than the samples obtained from solvent exchange.

Table 5.1 Comparision of solvent exchange and freeze drying method with respect to reduced modulus and maximum displacement.

Sample (days)	**Mean Reduced Modulus, E_r (GPa)**		**Max. Displacement (nm)**	
	Solvent Exchange	Freeze Drying	Solvent Exchange	Freeze Drying
0.25	8.0	7.2	396.5	1854.7
0.5	9.9	15.9	442.9	1764.2
1	14.4	21.9	467.9	403.3
2	16.0	23.6	409.4	376.8
3	18.2	25.9	403.6	377.7
7	21.0	26.5	400.9	414.0
28	36.3	38.5	253.9	266.9

The percentage increase in the displacement for 0.25D and 0.5D samples between the two hydration freeze methods is approximately 350% and 300% respectively. This indicates that the freeze-drying method fails to solidify the water in amorphous state and enhance the possibility of crystallization. When the samples are placed in freeze dryer at high vacuum

pressure (0.1 Torr), it was observed that the microstructure was damaged due to microcracks produced during the sublimation of the solid ice to gaseous state [137]. Furthermore, hydraulic pressure, crystallization pressure, and pressure from volume expansion, may be generated during the freezing process and might cause damage to the porous structure of the cement paste [138] (increase in the porosity). Thus, the higher displacement values for samples at early hydration stage agrees with the previous studies stating that soaking the cement paste sample in liquid nitrogen and successive drying at high vacuum is not recommended.

5.5 Conclusions

The framework of viscoelastic nanoindentation analysis presented in this chapter is based on the time dependent constitutive equations. Cement paste sample with w/c of 0.35 was prepared and the hydration of the sample was arrested using solvent exchange and freeze-drying methods. The aging viscoelasticity of cement paste samples is modeled using time shift and solidification approaches. The results are summarized as follows:

1. Recognizing the presence of C-S-H at the nanoscale, the primary contributor to concrete's viscoelasticity, the nanoindentation technique is shown to be an essential tool to characterize the aging viscoelastic characteristics of cement paste.
2. Adopting the approach of freezing the hydration of cement paste at age of interest allowed to investigate the samples successfully using nanoindentation and model the aging creep using two constitutive models. The hydration freeze methods have established that the hydration is instantly arrested in the first few layers of the cement paste sample. The ability of hydration freeze methods combined with capability of nanoindentation to perform indentation at shallow depths (<3 μm) proved the reliability of the creep test data of samples at desired age.
3. The study clearly demonstrated that solvent exchange is the preferred method to prepare the cement paste samples to study the aging properties at short length scale. The study demonstrates that the freeze-drying method substantially affects the pore structure of the cement paste causing an increase in the porosity as depicted by the considerable increase in the maximum indent depth of the samples, particularly in early hydration stages.

4. In the context of pyramidal indentation, the time shift technique and solidification theory were successfully modified and developed and were productively used to model the aging creep of cement paste at the nanoscale.
5. Time shift method and solidification theory are significantly sensitive to the various aging process of cement paste such as solidification, dissolution, and polymerization of hydration products. The significant errors due to violation of snapshot principle was totally avoided by restricting any further hydration or aging of the cement paste sample.
6. The time shift approach appears to be promising fit to model the aging viscoelasticity of cement paste at later ages. The method accounts for the inherent viscoelastic aging by simply shifting the relaxation time but is restricted in accounting for the hydration related effects. Additional shortcoming of the time shift technique in predicting the aging creep of cement paste is that it is dependent on the form of the aging factor used.
7. The solidification theory is better able to characterize the viscoelastic aging behavior of the cement paste in comparison with the time shift model. The major drawback of solidification theory is that it disregards other aging process such as dissolution or polymerization of hydration products and assumes the stresses carried by unhydrated phases is zero. But this assumption was validated by arresting the hydration of cement paste.
8. The proposed study demonstrates that solidification theory can be effectively employed to predict the aging viscoelasticity of cement paste. Unlike at macroscale, the model at nanoscale convincingly characterizes the aging creep by taking into consideration the aging associated with formation of new hydration phases and rate type aging.

The present study advocates to freeze the hydration of the cement paste using solvent exchange method to model the viscoelastic aging behavior of the cement paste at nanoscale using solidification theory.

Chapter 6 - Conclusions

The overall motivation of the thesis is to study the aging viscoelastic properties of cement paste at nanoscale. Because of their slenderness and considerable flexibility, prestressed concrete structures are especially vulnerable to creep effects, and are highly crucial in the safety study of nuclear reactor containments and vessels. The stress relaxation generated by creep is beneficial in alleviating the consequences of cooling, differential creep, shrinkage, and differential settlements, but it is unfavorable in the event of a stress loss in prestressing tendons. With the goal of better understanding long term performance of concrete and cementitious composites, nanoindentation based creep and stress relaxation experiments were performed on cement paste samples with varying porosity and at different ages. To achieve the aforementioned goal the study was structured into four objectives: i) address and reduce the uncertainties of using nanoindentation to study cementitious materials, ii) derive closed form analytical solutions to model the nanoscale viscoelastic properties of cementitious composites, iii) study effect of creep and stress relaxation on the long-term performance of irradiated cement paste iv) nanoscale modeling to characterize the aging viscoelastic behavior of cement paste.

The study towards identifying and reducing the uncertainties associated with nanoindentation concluded that it is important to achieve the porosity dependent critical indentation depth. To homogenize the cementitious material and to obtain reliable data, choosing load corresponding to the critical indentation depth is critical. The result of the study also indicates that to design statistical/grid nanoindentation (grid size and grid spacing) depends on what microstructural details or the hydration phases of the cement paste the researcher wants to study. To satisfy the assumption (ideally smooth sample surface) involved with the nanoindentation technique was investigated and it was concluded that the surface roughness depends on the water to cement ratio and the curing age of the sample and thus to acknowledge the heterogeneity of the microstructure, the measured roughness should be considered in the context of the material being studied. The study clearly recommends PM2 discussed in Section 2.2.2 and 2.3.3, as an efficient polishing technique to obtain smooth representative sample for nanoindentation test. The intention of the study was to present a quick guide for experimentalists to intelligently design their own nanoindentation experiments for cementitious materials. Further in an attempt to publish a standard for preparing samples and designing the statistical

nanoindentation experiments for cementitious materials, the study may need to investigate the individual hydration phases using the approach of deconvolution technique.

The viscoelastic properties of cement paste are characterized by performing nanoindentation based creep and relaxation tests and is discussed in detail in Chapter 3. The aim of the study is to develop an effective and reliable theoretical model to analyze the creep and stress relaxation data. The findings suggest that, given the challenges (instrument selection, test design, test time, and operation) involved in applying consistent strain at a macro scale, nanoindentation is an efficient method for studying stress relaxation. In the study, closed form simple analytical solutions were derived to obtain, creep compliance function and relaxation modulus of the indented viscoelastic material (cement paste and polycarbonate). The constitutive solution to model the creep of the cement paste is derived using elastic-viscoelastic based correspondence principle. The inverse relationship between the creep and stress relaxation parameter in the frequency domain was successfully utilized to interrelate the creep and stress relaxation of cement paste. The results indicate descent agreement between the analytical solution and experimentally obtained data. Additionally, results show that the analytical closed loop solution is cross validated by feeding the relaxation fit parameters back into creep solution and vice versa. The reliability of the solutions derived was verified on the standard, more homogeneous polycarbonate sample. Finally, the study believes that direct relaxation measurement with corresponding closed form analytical solution offers better approach for extracting relaxation data and can be employed for future investigation of viscoelastic behavior of cementitious materials.

Cementitious materials have proved to have excellent shielding capacity, energy absorption, durability, and high temperature resistance and hence used widely in nuclear power plants. Although the impact of radiations on the mechanical properties of concrete and cementitious materials has received substantial study, little is known about the creep and stress relaxation behavior of these materials after they have been exposed to radiation. Understanding cement paste's viscoelastic behavior allows for a detailed assessment of the long-term performance of irradiated concrete structures. Recent interest in extending the operating license of nuclear power plants has called for in detail study of time dependent properties of cementitious composites. Thus, the present work intends to add to the scant experimental data available through performing nanoindentation based creep and stress relaxation experiments on

irradiated and controlled cement paste sample with water to cement ratio of 0.35, 0.40, and 0.50. The specimens were exposed to combined neutron and gamma radiations for a time period of approximately 60 minutes. The total gamma dose received by the sample was calculated to be 180 Mrad and the total neutron flux (fast and thermal) was 5.11×10^{12} cm^{-2} sec^{-1}. The framework of viscoelastic nanoindentation analysis presented and discussed in Chapter 3 was used to characterize the stress relaxation and creep properties of cement paste. The time dependent creep compliance and relaxation modulus curves showed agreeable match between analytical solution and experimental data. The results demonstrated significant increase in the creep compliance and considerable decrease in the relaxation modulus of the irradiated cement paste compared to control samples. Substantial drop was observed in the measured E_r and the degree of the percentage loss increased with increasing porosity of the sample. Contrary to previous research, the study's findings suggest that neutron and gamma radiations have a negative effect on the creep and stress relaxation behavior of cement paste. Irradiation produced a profound impact on nanomechanical properties for the samples studied at dose levels much lower than the nominal thresholds for damage (10^{18} N/cm^2 & 10^{19} Grays). To further understand and characterize the viscoelastic behavior of irradiated cement paste, it is important to differentiate between fast and thermal neutron dose effects. Additional experiments with varying gamma and neutron dose along with lower dose rates should be studied.

The key to understanding concrete structures' vulnerability to degradation and how that affects their ability to perform safety functions is studying relevant aging mechanisms and their possible effects on those structures. This knowledge also helps to decide on the necessary and best repair and remedial measures. Investigating the time-dependent viscoelastic behavior of cement paste is therefore coupled to the selection of an appropriate constitutive equation that will properly anticipate long term performance of the concrete structures under time-dependent displacement or loading. Aging mechanism in concrete is directly related to the changes in the microstructure of the cement paste. Thus, in this study, nanoindentation based creep tests were performed on the cement paste with water to cement ratio of 0.35. The samples of various ages were prepared by arresting the hydration of the cement paste using solvent exchange and freeze-drying method. Two analytical constitutive models: time shift and solidification theory are employed to predict the aging creep of cement paste. The reduced modulus values recorded for the samples at different age implies that the hydration of samples was successfully arrested at

time of interest. The maximum displacement recorded during the creep test suggests that the solvent exchange approach, which has been shown to cause negligible damage to the pore structure, should be selected as freeze drying fails to retain the microstructure of the cement paste. The time shift approach which relates shift factors to the age is utilized to characterize the aging creep. The model was able to predict the creep behavior of the cement paste sample at later ages in comparison with the early. This is because the model simply shifts the compliance functions horizontally and fails to consider the intrinsic change in the microstructure with time due to solidification, dissolution or possible polymerization of C-S-H. As only the formation of new hydration phases is considered as part of the aging process, the well-known solidification theory that is used to model the aging creep of concrete at the macroscale is unable to account for the aging viscoelasticity of the material. This is because the theory ignores the response of other unhydrated phases to stress histories. This disadvantage was addressed by arresting the hydration of cement paste and the predicted compliance curves show better agreement with the measured data compared to time shift approach. Thus, the results recommends that it is important to freeze the hydration of cement paste using solvent exchange method and model the aging creep by solidification theory to study the viscoelastic aging behavior of cement paste. The study highlighted the effectiveness of nanoscale characterization of time dependent properties. Further, the accuracy of the models under study should be verified for cement paste samples with varying water to cement ratio. There is need to develop advanced model to predict the aging viscoelasticity of cement paste, accounting for various aging process including dissolution and polymerization of hydration phases. To understand the viscoelastic deformation properties and control microcracking, multiscale modeling of cement paste blended with alternative or supplemental cementitious materials is necessary.

References

1. Sanchez, F. and K. Sobolev, *Nanotechnology in Concrete – a Review.* Construction and Building Materials, 2010. **24**(11): p. 2060-2071.
2. Scrivener, K.L. *Nanotechnology and Cementitious Materials*. in *Nanotechnology in Construction 3*. 2009. Berlin, Heidelberg: Springer Berlin Heidelberg.
3. Gagg, C.R., *Cement and Concrete as an Engineering Material: An Historic Appraisal and Case Study Analysis.* Engineering Failure Analysis, 2014. **40**: p. 114-140.
4. Double, D.D., A. Hellawell, and S.J. Perry, *The Hydration of Portland Cement.* Proceedings of the Royal Society of London. Series A, Mathematical and Physical Sciences, 1978. **359**(1699): p. 435-451.
5. Sasmal, S. and M.B. Anoop, *Nanoindentation for Evaluation of Properties of Cement Hydration Products*, in *Nanotechnology in Eco-Efficient Construction*. 2019. p. 141-161.
6. Corr, D. and S.P. Shah, *Concrete Materials Science at the Nanoscale*, in *Applications of Nanotechnology in Concrete Design*. p. 2-12.
7. Trtik, P., B. Münch, and P. Lura, *A Critical Examination of Statistical Nanoindentation on Model Materials and Hardened Cement Pastes Based on Virtual Experiments.* Cement and Concrete Composites, 2009. **31**(10): p. 705-714.
8. Velez, K., S. Maximilien, D. Damidot, G. Fantozzi, and F. Sorrentino, *Determination by Nanoindentation of Elastic Modulus and Hardness of Pure Constituents of Portland Cement Clinker.* Cement and Concrete Research, 2001. **31**(4): p. 555-561.
9. Němeček, J., *Creep Effects in Nanoindentation of Hydrated Phases of Cement Pastes.* Materials Characterization - Mater Charact, 2009. **60**: p. 1028-1034.
10. Jones, C.A. and Z.C. Grasley, *Short-Term Creep of Cement Paste During Nanoindentation.* Cement and Concrete Composites, 2011. **33**(1): p. 12-18.
11. Zanjani Zadeh, V. and C.P. Bobko, *Nano-Mechanical Properties of Internally Cured Kenaf Fiber Reinforced Concrete Using Nanoindentation.* Cement and Concrete Composites, 2014. **52**: p. 9-17.
12. Lee, H., V. Vimonsatit, P. Chindaprasirt, T. Ngo, and P. Mendis, *Creep Properties of Cement and Alkali Activated Fly Ash Materials Using Nanoindentation Technique.* Construction and Building Materials, 2018. **168**: p. 547-555.
13. Gautham, S. and S. Sasmal, *Determination of Fracture Toughness of Nano-Scale Cement Composites Using Simulated Nanoindentation Technique.* Theoretical and Applied Fracture Mechanics, 2019. **103**: p. 102275.
14. Brown, L., P.G. Allison, and F. Sanchez, *Use of Nanoindentation Phase Characterization and Homogenization to Estimate the Elastic Modulus of Heterogeneously Decalcified Cement Pastes.* Materials & Design, 2018. **142**: p. 308-318.
15. Mondal, P., S.P. Shah, and L. Marks, *A Reliable Technique to Determine the Local Mechanical Properties at the Nanoscale for Cementitious Materials.* Cement and Concrete Research, 2007. **37**(10): p. 1440-1444.
16. Oliver, W.C. and G.M. Pharr, *An Improved Technique for Determining Hardness and Elastic Modulus Using Load and Displacement Sensing Indentation Experiments.* Journal of Materials Research, 1992. **7**(6): p. 1564-1583.
17. Davydov, D. and M. Jirásek. *Modeling of Nanoindentation by a Visco-Elastic Porous Model with Application to Cement Paste*. in *Nanotechnology in Construction 3*. 2009. Berlin, Heidelberg: Springer Berlin Heidelberg.

18. Fu, Z., H. Su, and Z. Wen, *Multi-Scale Numerical Analysis for Linear Elastic Behavior of Clay Concrete.* International Journal of Solids and Structures, 2020. **203**: p. 23-45.
19. Akl, A., M. Saiidi, and A. Vosooghi, *Deflection of in-Span Hinges in Prestressed Concrete Box Girder Bridges During Construction.* Engineering Structures, 2016. **131**.
20. Mencík, J., *Uncertainties and Errors in Nanoindentation*. 2012: Nanoindentation in Materials Science.
21. Gautham, S. and S. Sasmal, *Recent Advances in Evaluation of Intrinsic Mechanical Properties of Cementitious Composites Using Nanoindentation Technique.* Construction and Building Materials, 2019. **223**: p. 883-897.
22. Lukovic, M., E. Schlangen, B. Savija, G. Ye, and O. Çopuroglu, *Using Nano-Indentation and Microscopy to Obtain Mechanical Properties.* EMABM 2015: Proceedings of the 15th Euroseminar on Microscopy Applied to Building Materials, Delft, The Netherlands, 17-19 June 2015, 2015.
23. Miller, M., C. Bobko, M. Vandamme, and F.-J. Ulm, *Surface Roughness Criteria for Cement Paste Nanoindentation.* Cement and Concrete Research, 2008. **38**: p. 467-476.
24. Davydov, D., M. Jirásek, and L. Kopecký, *Critical Aspects of Nano-Indentation Technique in Application to Hardened Cement Paste.* Cement and Concrete Research, 2011. **41**(1): p. 20-29.
25. Constantinides, G. and F.-J. Ulm, *The Nanogranular Nature of C–S–H.* Journal of the Mechanics and Physics of Solids, 2007. **55**(1): p. 64-90.
26. Constantinides, G., K.S. Ravi Chandran, F.J. Ulm, and K.J. Van Vliet, *Grid Indentation Analysis of Composite Microstructure and Mechanics: Principles and Validation.* Materials Science and Engineering: A, 2006. **430**(1-2): p. 189-202.
27. Sorelli, L., G. Constantinides, F.-J. Ulm, and F. Toutlemonde, *The Nano-Mechanical Signature of Ultra High Performance Concrete by Statistical Nanoindentation Techniques.* Cement and Concrete Research, 2008. **38**(12): p. 1447-1456.
28. Wang, X.H., S. Jacobsen, J.Y. He, Z.L. Zhang, S.F. Lee, and H.L. Lein, *Application of Nanoindentation Testing to Study of the Interfacial Transition Zone in Steel Fiber Reinforced Mortar.* Cement and Concrete Research, 2009. **39**(8): p. 701-715.
29. Guillonneau, G., G. Kermouche, S. Bec, and J.-L. Loubet, *Determination of Mechanical Properties by Nanoindentation Independently of Indentation Depth Measurement.* Journal of Materials Research, 2012. **27**(19): p. 2551-2560.
30. da Silva, W.R.L., J. Němeček, and P. Štemberk, *Application of Multiscale Elastic Homogenization Based on Nanoindentation for High Performance Concrete.* Advances in Engineering Software, 2013. **62-63**: p. 109-118.
31. Nežerka, V., J. Němeček, Z. Slížková, and P. Tesárek, *Investigation of Crushed Brick-Matrix Interface in Lime-Based Ancient Mortar by Microscopy and Nanoindentation.* Cement and Concrete Composites, 2015. **55**: p. 122-128.
32. Zhu, W., M.T.J. Fonteyn, J. Hughes, and C. Pearce. *Nanoindentation Study of Resin Impregnated Sandstone and Early-Age Cement Paste Specimens*. in *Nanotechnology in Construction 3*. 2009. Berlin, Heidelberg: Springer Berlin Heidelberg.
33. ISO-14577-1, *Metallic Materials - Instrumented Indentation Test for Hardness and Materials Parameters - Part 1: Test Method.* Geneva, Switzerland, 2015.
34. Miller, M., C. Bobko, M. Vandamme, and F.-J. Ulm, *Surface Roughness Criteria for Cement Paste Nanoindentation.* Cement and Concrete Research, 2008. **38**(4): p. 467-476.

35. Trtik, P., J. Dual, B. Muench, and L. Holzer, *Limitation in Obtainable Surface Roughness of Hardened Cement Paste: 'Virtual' Topographic Experiment Based on Focussed Ion Beam Nanotomography Datasets.* Journal of Microscopy, 2008. **232**(2): p. 200-206.
36. Constantinides, G. and F.-J. Ulm, *The Effect of Two Types of C-S-H on the Elasticity of Cement-Based Materials: Results from Nanoindentation and Micromechanical Modeling.* Cement and Concrete Research, 2004. **34**(1): p. 67-80.
37. Chen, J.J., L. Sorelli, M. Vandamme, F.-J. Ulm, and G. Chanvillard, *A Coupled Nanoindentation/Sem-Eds Study on Low Water/Cement Ratio Portland Cement Paste: Evidence for C–S–H/Ca(Oh)2 Nanocomposites.* Journal of the American Ceramic Society, 2010. **93**(5): p. 1484-1493.
38. Han, J., G. Pan, W. Sun, C. Wang, and D. Cui, *Application of Nanoindentation to Investigate Chemomechanical Properties Change of Cement Paste in the Carbonation Reaction.* Science China Technological Sciences, 2012. **55**(3): p. 616-622.
39. Xu, J., D.J. Corr, and S.P. Shah, *Nanomechanical Properties of C-S-H Gel/Cement Grain Interface by Using Nanoindentation and Modulus Mapping.* Journal of Zhejiang University-SCIENCE A, 2015. **16**(1): p. 38-46.
40. Ma, R., L. Guo, W. Sun, J. Liu, and J. Zong, *Strength-Enhanced Ecological Ultra-High Performance Fibre-Reinforced Cementitious Composites with Nano-Silica.* Materials and Structures, 2017. **50**(2): p. 166.
41. Vandamme, M., F.-J. Ulm, and P. Fonollosa, *Nanogranular Packing of C–S–H at Substochiometric Conditions.* Cement and Concrete Research, 2010. **40**(1): p. 14-26.
42. Kim, J.J., M.K. Rahman, and M.M. Reda Taha, *Examining Microstructural Composition of Hardened Cement Paste Cured under High Temperature and Pressure Using Nanoindentation and 29si Mas Nmr.* Applied Nanoscience, 2012. **2**(4): p. 445-456.
43. Jha, K.K., N. Suksawang, D. Lahiri, and A. Agarwal, *Energy-Based Analysis of Nanoindentation Curves for Cementitious Materials.* ACI Materials Journal, 2012. **109**(1).
44. Hu, C., Y. Gao, Y. Zhang, and Z. Li, *Statistical Nanoindentation Technique in Application to Hardened Cement Pastes: Influences of Material Microstructure and Analysis Method.* Construction and Building Materials, 2016. **113**: p. 306-316.
45. Zhu, W., J.J. Hughes, N. Bicanic, and C.J. Pearce, *Nanoindentation Mapping of Mechanical Properties of Cement Paste and Natural Rocks.* Materials Characterization, 2007. **58**(11-12): p. 1189-1198.
46. Mondal, P., S.P. Shah, and L.D. Marks, *Nanoscale Characterization of Cementitious Materials.* ACI Materials Journal, 2008. **105**(2): p. 174-179.
47. E3-11, A.I., *Astm International. E3-11 Standard Guide for Preparation of Metallographic Specimens*. 2017, West Conshohocken, PA; ASTM International, 2017. .
48. *Ti Premier User Manual*. 2014.
49. Ley-Hernandez, A.M., J. Lapeyre, R. Cook, A. Kumar, and D. Feys, *Elucidating the Effect of Water-to-Cement Ratio on the Hydration Mechanisms of Cement.* ACS Omega, 2018. **3**(5): p. 5092-5105.
50. Ghabezloo, S., *Association of Macroscopic Laboratory Testing and Micromechanics Modelling for the Evaluation of the Poroelastic Parameters of a Hardened Cement Paste.* Cement and Concrete Research, 2010. **40**(8): p. 1197-1210.
51. Xie, R. and B. Tang, *Influence of Surface Roughness on Concrete Nanoindentation.* European Journal of Environmental and Civil Engineering, 2020: p. 1-14.

52. Calabri, L., N. Pugno, C. Menozzi, and S. Valeri, *Afm Nanoindentation: Tip Shape and Tip Radius of Curvature Effect on the Hardness Measurement.* Journal of Physics: Condensed Matter, 2008. **20**(47): p. 474208.
53. Lura, P., P. Trtik, and B. Münch, *Validity of Recent Approaches for Statistical Nanoindentation of Cement Pastes.* Cement and Concrete Composites, 2011. **33**(4): p. 457-465.
54. Touati, D. and G. Cederbaum, *Stress Relaxation of Nonlinear Thermoviscoelastic Materials Predicted from Known Creep.* Mechanics of Time-Dependent Materials, 1997. **1**(3): p. 321-330.
55. Patil, P. and K. Kapali, *High Strength Concrete without Using Cementitious Admixtures.* international journal of engineering research and, 2018. **7**(1).
56. Atienza Jose, M. and M. Elices, *Role of Residual Stresses in Stress Relaxation of Prestressed Concrete Wires.* Journal of Materials in Civil Engineering, 2007. **19**(8): p. 703-708.
57. Hamed, E., *Relaxation Behavior of Concrete under Sustained Uniaxial Compressive Deformation.* Journal of Materials in Civil Engineering, 2016. **28**(6): p. 06016007.
58. Bentur, A., N.B. Milestone, and J.F. Young, *Creep and Drying Shrinkage of Calcium Silicate Pastes Ii. Induced Microstructural and Chemical Changes.* Cement and Concrete Research, 1978. **8**(6): p. 721-732.
59. Bažant, Z.P., A.B. Hauggaard, S. Baweja, and F.J. Ulm, *Microprestress-Solidification Theory for Concrete Creep. I: Aging and Drying Effects.* Journal of Engineering Mechanics, 1997. **123**(11): p. 1188-1194.
60. Acker, P., *Micromechanical Analysis of Creep and Shrinkage Mechanisms.* British Library Conference Proceedings, 2001: p. 15-26.
61. Xiao, J., Y. Fan, and V.W.Y. Tam, *On Creep Characteristics of Cement Paste, Mortar and Recycled Aggregate Concrete.* European Journal of Environmental and Civil Engineering, 2015. **19**(10): p. 1234-1252.
62. Do, Q.H., S. Bishnoi, and K.L. Scrivener, *Microstructural Modeling of Early-Age Creep in Hydrating Cement Paste.* Journal of Engineering Mechanics, 2016. **142**(11): p. 04016086.
63. Magura, D.D., M. Sozen, and C.P. Siess, *A Study of Stress Relaxation in Prestressing Reinforcement.* Pci Journal, 1964. **9**: p. 13-57.
64. Venkovic, N., *Nanoindentation Relaxation Study and Micromechanics of Cement-Based Materials*, in *Civil Engineering*. 2016, Laval University: Québec, Canada. p. 158.
65. Brooks, J.J. and P. Forsyth, *Relaxation of Concrete and Its Relation to Creep under Uniaxial Cyclic Compression at Various Frequencies.* Magazine of Concrete Research, 1986. **38**(137): p. 175-182.
66. Bažant, Z.P., M.H. Hubler, and M. Jirásek, *Improved Estimation of Long-Term Relaxation Function from Compliance Function of Aging Concrete.* Journal of Engineering Mechanics, 2013. **139**(2): p. 146-152.
67. Van Breugel, K., *Relaxation of Young Concrete*. 1980, Delft University of Technology: Delft, Netherlands. p. 144.
68. Vandamme, M. and F.J. Ulm, *Nanoindentation Investigation of Creep Properties of Calcium Silicate Hydrates.* Cement and Concrete Research, 2013. **52**: p. 38–52.
69. Hilloulin, B., M. Robira, and A. Loukili, *Coupling Statistical Indentation and Microscopy to Evaluate Micromechanical Properties of Materials: Application to*

Viscoelastic Behavior of Irradiated Mortars. Cement and Concrete Composites, 2018. **94**: p. 153-165.
70. Hunnicutt, W., E.T. Rodriguez, P. Mondal, and Y.L. Pape, *Examination of Gamma-Irradiated Calcium Silicate Hydrates. Part Ii: Mechanical Properties.* Journal of Advanced Concrete Technology, 2020. **18**(10): p. 558-570.
71. Park, S.W. and R.A. Schapery, *Methods of Interconversion between Linear Viscoelastic Material Functions. Part I—a Numerical Method Based on Prony Series.* International Journal of Solids and Structures, 1999. **36**(11): p. 1653-1675.
72. Oza, A., R. Phd, and R. Lakes, *Interrelation of Creep and Relaxation for Nonlinearly Viscoelastic Materials: Application to Ligament and Metal.* Rheologica Acta, 2003. **42**: p. 557-568.
73. Sassone, M. and M.A. Chiorino, *Design Aids for the Evaluation of Creep Induced Structural Effects.* Shrinkage and creep of concrete, 2005: p. 239-259.
74. Cheng, Y.-T. and F. Yang, *Obtaining Shear Relaxation Modulus and Creep Compliance of Linear Viscoelastic Materials from Instrumented Indentation Using Axisymmetric Indenters of Power-Law Profiles.* Journal of Materials Research, 2009. **24**: p. 3013-3017.
75. Lin, C.-Y., *Alternative Form of Standard Linear Solid Model for Characterizing Stress Relaxation and Creep: Including a Novel Parameter for Quantifying the Ratio of Fluids to Solids of a Viscoelastic Solid.* Frontiers in Materials, 2020. **7**(11).
76. Brooks, J.J. and A.M. Neville, *Relaxation of Stress in Concrete and Its Relation to Creep.* ACI Journal Proceedings, 1976. **73**(4).
77. Kizito, N., H. Beushausen, P. Moyo, and P. Arito, *An Experimental Study on the Creep and Relaxation Behaviour of Concrete*, in *2nd International Conference on Advances in Cement and Concrete Technology in Africa*. 2016: Dar es Salaam, Tanzania. p. 485-495.
78. Zhang, C.Y., Y.W. Zhang, K.Y. Zeng, L. Shen, and Y.Y. Wang, *Extracting the Elastic and Viscoelastic Properties of a Polymeric Film Using a Sharp Indentation Relaxation Test.* Journal of Materials Research, 2006. **21**(12): p. 2991-3000.
79. Sun, Y., Z. Gu, J. Wang, and X. Yuan, *Research of Method for Solving Relaxation Modulus Based on Three-Point Bending Creep Test.* Materials (Basel), 2019. **12**(12).
80. Shimizu, S., T. Yanagimoto, and M. Sakai, *Pyramidal Indentation Load–Depth Curve of Viscoelastic Materials.* Journal of Materials Research, 1999. **14**(10): p. 4075-4086.
81. Sakai, M., *Mechanical Probe for Micro-/Nano-Characterization*. 2003. p. 351-383.
82. Meyer, E., *Investigations of Hardness Testing and Hardness.* Phys. Z, 1908. **9**(66): p. 18.
83. Bartier, O., X. Hernot, and G. Mauvoisin, *Theoretical and Experimental Analysis of Contact Radius for Spherical Indentation.* Mechanics of Materials - Mech Mater, 2010. **42**: p. 640-656.
84. Douglas, R.W., W.L. Armstrong, J.P. Edward, and D. Hall, *A Penetration Viscometer.* Glass Technol., 1965. **6**(2): p. 52-55.
85. Chu, S.N.G. and J.C.M. Li, *Impression Creep; a New Creep Test.* Journal of Materials Science, 1977. **12**(11): p. 2200-2208.
86. Raman, V. and R. Berriche, *An Investigation of the Creep Processes in Tin and Aluminum Using a Depth-Sensing Indentation Technique.* Journal of Materials Research, 1992. **7**(3): p. 627-638.
87. Radok, J.R.M., *Visco-Elastic Stress Analysis.* Quarterly of Applied Mathematics, 1957. **15**: p. 198-202.

88. Lee, E.H. and J.R.M. Radok, *The Contact Problem for Viscoelastic Bodies.* Journal of Applied Mechanics, 1960. **27**: p. 438.
89. Vandamme, M. and F.-J. Ulm, *Viscoelastic Solutions for Conical Indentation.* International Journal of Solids and Structures, 2006. **43**(10): p. 3142-3165.
90. Sneddon, I.N., *The Relation between Load and Penetration in the Axisymmetric Boussinesq Problem for a Punch of Arbitrary Profile.* International Journal of Engineering Science, 1965. **3**(1): p. 47-57.
91. Patil, P. and C. Jones, *Reducing Uncertainties in Nanoindentation Experiments for Cementitious Materials.* Transportation Research Record, 2022: p. 03611981221101033.
92. Li, X., Z. Grasley, E.J. Garboczi, and J. Bullard, *Modeling the Apparent and Intrinsic Viscoelastic Relaxation of Hydrating Cement Paste.* Cement and Concrete Composites, 2015. **55**.
93. Lee-Sullivan, P., D. Dykeman, and Q. Shao, *Mechanical Relaxations in Heat-Aged Polycarbonate. Part I: Comparison between Two Molecular Weights.* Polymer Engineering and Science, 2003. **43**: p. 369+.
94. Neville, A.M. and J.J. Brooks, *Concrete Technology*. 2010: Prentice Hall.
95. Bamonte, P. and P.G. Gambarova, *Properties of Concrete Required in Nuclear Power Plants*, in *Infrastructure Systems for Nuclear Energy*. 2014. p. 407-438.
96. William, K., Y. Xi, and D. Naus, *A Review of the Effects of Radiation on Microstructure and Properties of Concretes Used in Nuclear Power Plants*, O.R.N.L. U.S. Nuclear Regulatory Commission. Office of Nuclear Regulatory Research, Editor. 2013.
97. Herman Graves, Y.L.P., Dan Naus, Joseph Rashid, Victor Saouma, Abdul Sheikh, James Wall, *Expanded Materials Degradation Assessment (Emda): Aging of Concrete Andcivil Structures (Nureg/Cr-7153, Volume 4)*, U.S.N.R. Commission, Editor. 2014, Office of Nuclear Regulatory Research, U.S. Nuclear Regulatory Commission: Washington, DC.
98. Khmurovska, Y., P. Štemberk, S. Sikorin, J. Němeček, D. Jóźwiak-Niedźwiedzka, M. Doleželová, Y. Kaladkevich, E. Pavalanski, and V. Fatseyeu, *Effects of Gamma-Ray Irradiation on Hardened Cement Mortar.* International Journal of Concrete Structures and Materials, 2021. **15**(1): p. 17.
99. Hilsdorf, H.K., J. Kropp, and H.J. Koch. *The Effects of Nuclear Radiation on the Mechanical Properties of Concrete*. 1978.
100. Field, K.G., I. Remec, and Y.L. Pape, *Radiation Effects in Concrete for Nuclear Power Plants – Part I: Quantification of Radiation Exposure and Radiation Effects.* Nuclear Engineering and Design, 2015. **282**: p. 126-143.
101. Li, X., *Modeling of the Aging Viscoelastic Properties of Cement Paste Using Computational Methods* in *Civil Engineering*. 2012, Texas A&M University.
102. Grasley, Z.C. and D.A. Lange, *Constitutive Modeling of the Aging Viscoelastic Properties of Portland Cement Paste.* Mechanics of Time-Dependent Materials, 2007. **11**: p. 175.
103. Rosseel, T.M., I. Maruyama, Y. Le Pape, O. Kontani, A.B. Giorla, I. Remec, J.J. Wall, M. Sircar, C. Andrade, and M. Ordonez, *Review of the Current State of Knowledge on the Effects of Radiation on Concrete.* Journal of Advanced Concrete Technology, 2016. **14**(7): p. 368-383.
104. Khmurovska, Y., P. Štemberg, J. Žák, S. Sikorin, Y. Khaladkevich, E. Pavalanski, and V. Fatseyeu, *Cement Mortar Creep under Exposure to Gamma-Ray Irradiation.* Journal of Nuclear Research and Development, 2019(18): p. 24-28.

105. Giorla, A., M. Vaitová, Y. Le Pape, and P. Štemberk, *Meso-Scale Modeling of Irradiated Concrete in Test Reactor.* Nuclear Engineering and Design, 2015. **295**: p. 59-73.
106. Le Pape, Y., K.G. Field, and I. Remec, *Radiation Effects in Concrete for Nuclear Power Plants, Part Ii: Perspective from Micromechanical Modeling.* Nuclear Engineering and Design, 2015. **282**: p. 144-157.
107. Robira, M., B. Hilloulin, A. Loukili, G. Potin, X. Bourbon, and A. Abdelouas, *Multi-Scale Investigation of the Effect of Γ Irradiations on the Mechanical Properties of Cementitious Materials.* Construction and Building Materials, 2018. **186**: p. 484-494.
108. Tajuelo, R., Elena, W. Hunnicutt, P. Mondal, and Y. Le Pape, *Examination of Gamma-Irradiated Calcium Silicate Hydrates. Part I: Chemical-Structural Properties.* Journal of the American Ceramic Society, 2019. **103**.
109. Tajuelo, R., Elena, W.A. Hunnicutt, P. Mondal, and Y. Le Pape, *Assessing the Effects of Gamma Irradiation in Concrete*, in *ANS Annual Meeting, Embedded Topical: Nuclear Fules & Structural Materials for Next Generation Nuclear Reactors*. 2018, American Nuclear Society: United States. p. 1649 to 1649.
110. McDowall, D., *The Effect of Gamma Irradiation on the Creep Properties of Concrete.* Comm. of the European Communities, 1971: p. 55-69.
111. Gray, B.S., *The Effects of Reactor Radiation on Cements and Concrete*. 1972: Commission of the European Communities (CEC).
112. Aslam, M., *Introducing Kolmogorov-Smirnov Tests under Uncertainty: An Application to Radioactive Data.* ACS omega, 2019. **5**(1): p. 914-917.
113. Hart, A., *Mann-Whitney Test Is Not Just a Test of Medians: Differences in Spread Can Be Important.* BMJ (Clinical research ed.), 2001. **323**(7309): p. 391-393.
114. Fillmore, D.L., *Literature Review of the Effects of Radiation and Temperature on the Aging of Concrete*. 2004, University of North Texas Libraries: Idaho Falls, Idaho. p. 26.
115. Abdo, A.E.S. and E. Amin, *Distribution of Temperature Rise in Biological Shield Due to Thermal Neutrons.* Annals of Nuclear Energy, 2001: p. 275-283.
116. Kontani, O., Y. Ichikawa, A. Ishizawa, M. Takizawa, and O. Sato, *Irradiation Effects on Concrete Structures.* Int. Symp. On the Ageing Manag. of Nucl. P. P, 2012. **4**: p. 173-182.
117. Giorla, A.B., Y.L. Pape, and C.F. Dunant, *Computing Creep-Damage Interactions in Irradiated Concrete.* Journal of Nanomechanics and Micromechanics, 2017. **7**(2): p. 04017001.
118. Galitz, C.L., *The Effects of Early-Age Stress on the Elastic and Viscoelastic Behavior of Cement Paste*, in *Civil and Environmental Engineering*. 2015, Virginia Polytechnic Institute and State University: Blacksburg, VA.
119. Honorio, T., B. Bary, and F. Benboudjema, *Multiscale Estimation of Ageing Viscoelastic Properties of Cement-Based Materials: A Combined Analytical and Numerical Approach to Estimate the Behaviour at Early Age.* Cement and Concrete Research, 2016. **85**: p. 137-155.
120. Bazant, Z.P. and S. Prasannan, *Solidification Theory for Concrete Creep. Ii: Verification and Application.* Journal of Engineering Mechanics, 1989. **115**(8): p. 1704-1725.
121. Bažant, Z.P. and S. Prasannan, *Solidification Theory for Concrete Creep. I: Formulation.* Journal of Engineering Mechanics, 1989. **115**(8): p. 1691-1703.
122. Alan S. Wineman, K.R.R., *Mechanical Response of Polymers: An Introduction*. 2000, Cambridge, United Kingdom: Cambridge University Press.

123. Carol, I. and Z.P. Bažant, *Viscoelasticity with Aging Caused by Solidification of Nonaging Constituent.* Journal of Engineering Mechanics, 1993. **119**(11): p. 2252-2269.
124. Grasley, Z., *Closed-Form Solutions for Uniaxial Passive Restraint Experiments*, in *American Concrete Institute*. 2010, American Concrete Institute, ACI Special Publication. p. 17-31.
125. Struik, L.C.E., *Physical Aging in Amorphous Polymers and Other Materials*, in *Applied Sciences*. 1977, Delft University of Technology. p. 249.
126. Morland, L.W. and E.H. Lee, *Stress Analysis for Linear Viscoelastic Materials with Temperature Variation.* Transactions of the Society of Rheology, 1960. **4**(1): p. 233-263.
127. Vichit-Vadakan, W. and G.W. Scherer, *Measuring Permeability and Stress Relaxation of Young Cement Paste by Beam Bending.* Cement and Concrete Research, 2003. **33**(12): p. 1925-1932.
128. Zhang, J. and G.W. Scherer, *Comparison of Methods for Arresting Hydration of Cement.* Cement and Concrete Research, 2011. **41**(10): p. 1024-1036.
129. Beaudoin, J.J. and J. Marchand, *14 - Pore Structure*, in *Handbook of Analytical Techniques in Concrete Science and Technology*, V.S. Ramachandran and J.J. Beaudoin, Editors. 2001, William Andrew Publishing: Norwich, NY. p. 528-628.
130. Korpa, A. and R. Trettin, *The Influence of Different Drying Methods on Cement Paste Microstructures as Reflected by Gas Adsorption: Comparison between Freeze-Drying (F-Drying), D-Drying, P-Drying and Oven-Drying Methods.* Cement and Concrete Research, 2006. **36**(4): p. 634-649.
131. Knapen, E., Ö. Cizer, K. Van Balen, D. Van Gemert, J. Marchand, B. Bissonnette, R. Gagne, M. Jolin, and F. Paradis. *Comparison of Solvent Exchange and Vacuum Drying Techniques to Remove Free Water from Early Age Cement-Based Materials*. in *2nd International RILEM Symposium on Advances in Concrete through Science and Engineering*. 2006. Quebec, Canada: Rilem Publications S.A.R.L.; France.
132. Scrivener, K., R. Snellings, and B. Lothenbach, *A Practical Guide to Microstructural Analysis of Cementitious Materials*. 2016, Boca Raton: CRC Press.
133. Canut, M.M.C., *Pore Structure in Blended Cement Pastes*, in *Department of Civil Engineering*. 2011, Technical University of Denmark: Kgs. Lyngby, Denmark. p. 346.
134. Gallé, C., *Effect of Drying on Cement-Based Materials Pore Structure as Identified by Mercury Intrusion Porosimetry: A Comparative Study between Oven-, Vacuum-, and Freeze-Drying.* Cement and Concrete Research, 2001. **31**(10): p. 1467-1477.
135. Zhang, L. and F.P. Glasser, *Critical Examination of Drying Damage to Cement Pastes.* Advances in Cement Research, 2000. **12**(2): p. 79-88.
136. Scherer, G.W., *Freezing Gels.* Journal of Non-Crystalline Solids, 1993. **155**(1): p. 1-25.
137. Collier, N., J. Sharp, N. Milestone, J. Hill, and H. Godfrey, *The Influence of Water Removal Techniques on the Composition and Microstructure of Hardened Cement Pastes.* Cement and Concrete Research, 2008. **38**: p. 737-744.
138. Scherer, G.W. and J. Valenza, *Mechanisms of Frost Damage.* Materials Science of Concrete, 2005. **7**: p. 209-246.

Appendix A - Load Functions and Fit Parameters

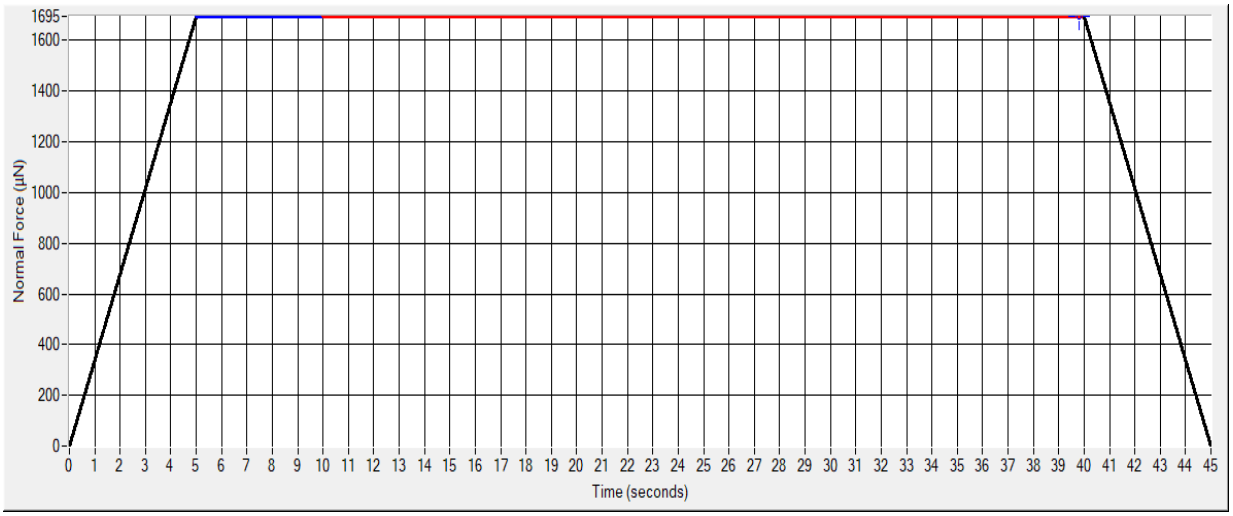

Figure A 1 Reference creep load function with reference segment of 5 seconds and maximum load of 1695 µN.

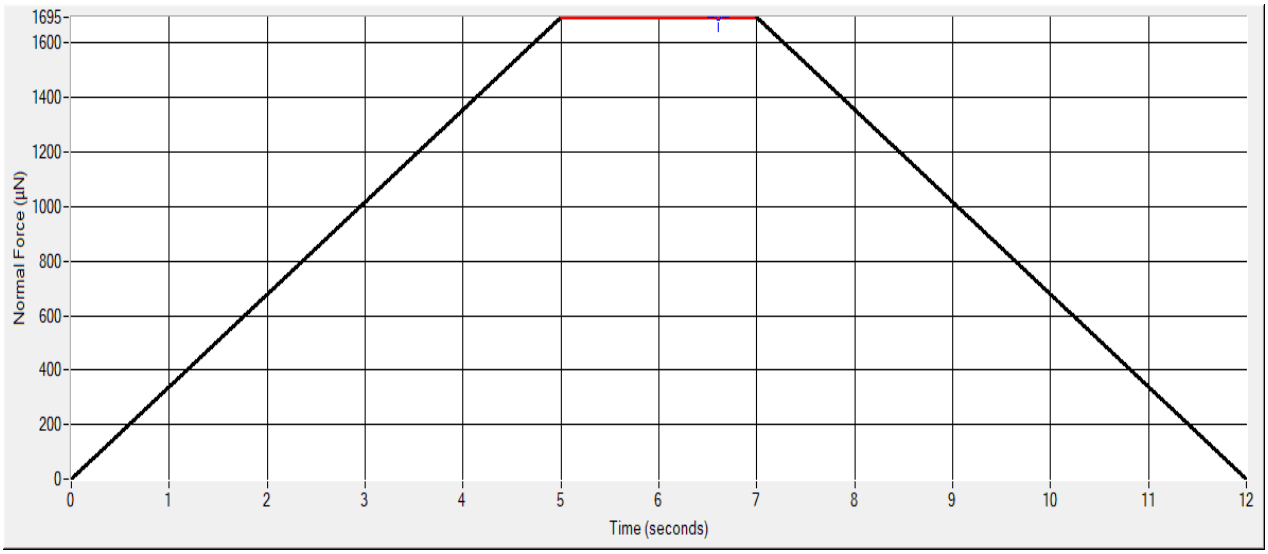

Figure A 2 Basic elastic step load function for 0.35w/c sample.

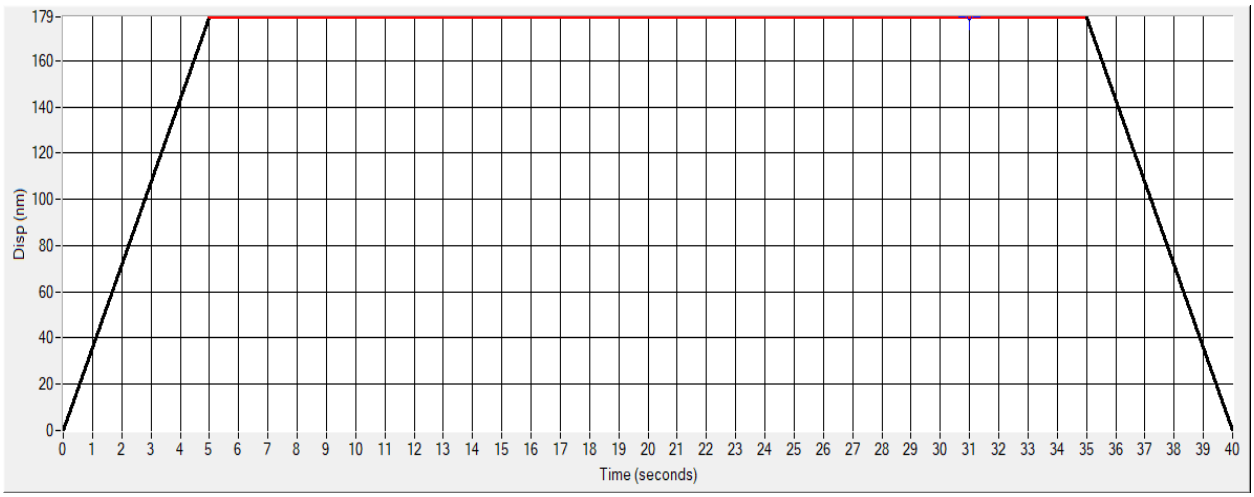

Figure A 3 Basic quasi static trapezoid load function in displacement-controlled feedback mode and maximum depth of 180 nm.

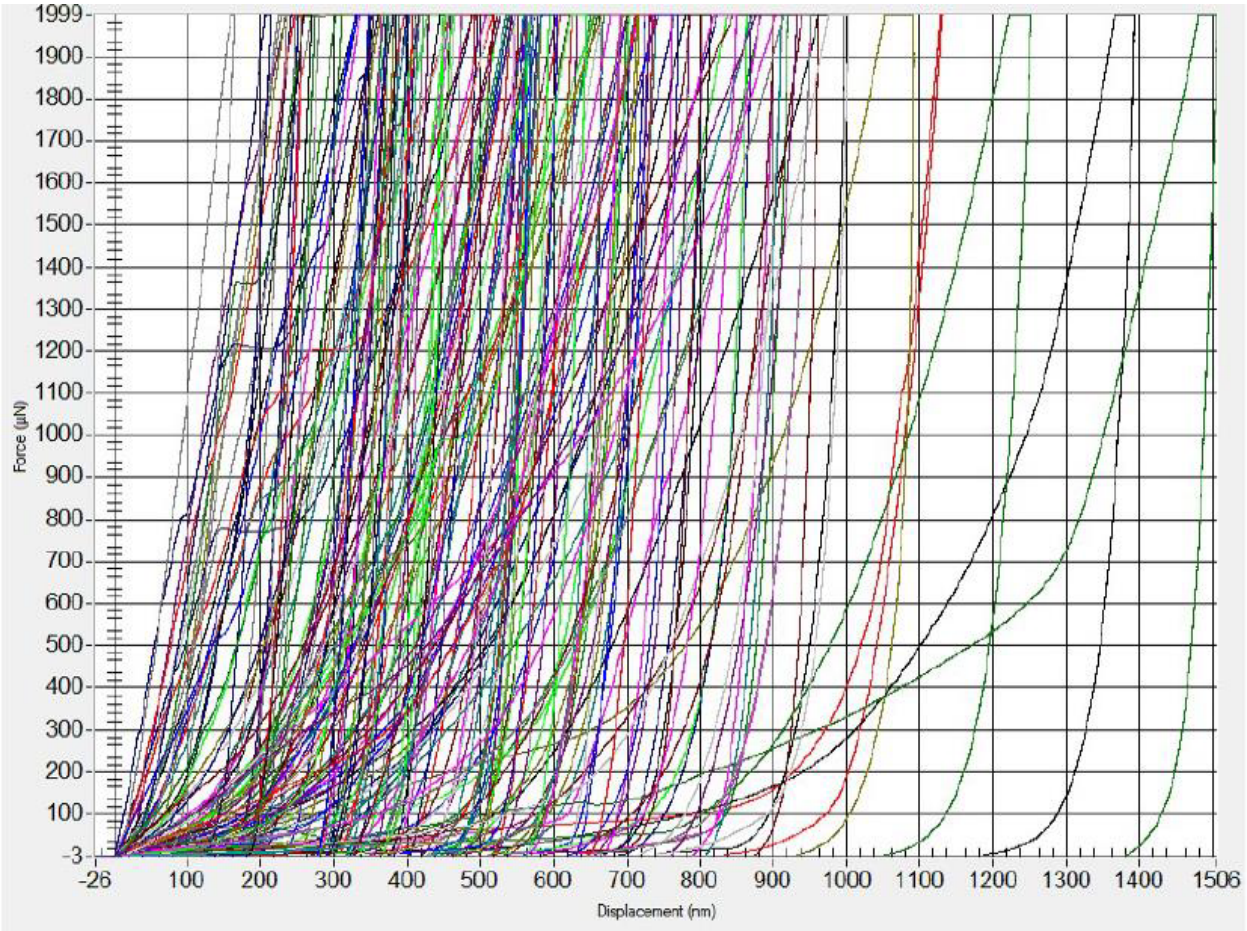

Figure A 4 Sample load–indentation depth curves from grid nanoindentation based creep test.

Table A 1 Average fit parameters for all age cement paste samples with 0.35 w/c.

Age of the sample	Hydration Freeze Method	Average Fit Parameters (GPa)			
		E_0	E_1	E_2	E_3
0.25 days	Solvent Exchange	2.305	482.300	163.572	47.944
	Freeze Drying	0.726	32.510	12.424	9.527
0.5 days	Solvent Exchange	3.327	486.975	78.963	53.135
	Freeze Drying	0.772	60.497	17.595	7.117
1 days	Solvent Exchange	4.818	191.011	80.981	74.997
	Freeze Drying	3.615	281.916	102.096	152.233
2 days	Solvent Exchange	5.441	204.786	124.559	96.516
	Freeze Drying	7.301	321.142	253.659	111.928
3 days	Solvent Exchange	5.725	162.889	163.933	39.619
	Freeze Drying	5.567	316.927	121.084	78.933
7 days	Solvent Exchange	5.782	289.996	93.959	76.567
	Freeze Drying	6.024	247.023	63.438	37.968
28 days	Solvent Exchange	6.665	288.951	119.746	105.514
	Freeze Drying	7.383	327.814	165.382	112.346

Appendix B - Raw Data for Nanoindentation Based Creep and Stress Relaxation Test

1. Relaxation tests (file://BRKR-MJ05V9VE/Users/ENGG autoCE1077/OneDrive/Relaxation%20tests)
2. Creep tests (file://BRKR-MJ05V9VE/Users/ENGG auto CE1077/OneDrive/Relaxation%20tests/Creep%20tests)
3. Solvent exchange (file://BRKR-MJ05V9VE/Users/ENGG autoCE1077/OneDrive/Solvent%20exchange)
4. Freeze Drying (file://BRKR-MJ05V9VE/Users/ENGG autoCE1077/OneDrive/Freeze%20Drying)
5. Irradiated samples (file://BRKR-MJ05V9VE/Users/ENGG autoCE1077/OneDrive/Nuclear%20samples)